ISAS - INTERNATIONAL SCHOOL FOR ADVANCED STUDIES

HIGH-ENERGY PHYSICS SECTOR

MATTER EFFECTS ON CONVERSION OF NEUTRINOS FROM SUPERNOVAE AND COSMOLOGICAL SOURCES

a PhD thesis by Cecilia Lunardini

Advisor:

Prof. Alexei Yu. Smirnov

External advisor:

Prof. G. Raffelt

Academic Year 2000 - 2001

SISSA - SCUOLA INTERNAZIONALE SUPERIORE DI STUDI AVANZATI

TRIESTE
Via Beirut 2-4

TRIESTE

INTERNATIONAL SCHOOL OF ADVANCED STUDIES
SCUOLA INTERNAZIONALE DI STUDI SUPERIORI AVANZATI

HIGH-ENERGY PHYSICS SECTOR

MATTER EFFECTS ON CONVERSION OF NEUTRINOS FROM SUPERNOVAE AND COSMOLOGICAL SOURCES

a PhD thesis by Cecilia Lunardini

Advisor:

Prof. Alexei Yu. Smirnov

External advisor:

Prof. G. Raffelt

Academic Year 2000 - 2001

Introduction

The idea of neutrinos oscillations was born in 1957, when Pontecorvo suggested that neutrino–antineutrino mixing, and therefore $\nu \leftrightarrow \bar{\nu}$ oscillations could take place in analogy to the mixing and oscillations of a K^0-$\bar{K}^0$ system [1]. Only one type of neutrino, the electron neutrino ν_e, was known at that time.

Five years later, after the discovery of the muon neutrino ν_μ [2], Maki, Nakagawa and Sakata proposed the mixing of ν_e and ν_μ and studied its implications, including the possibility of ν_e-ν_μ transitions [3].

Flavour oscillations, $\nu_e \leftrightarrow \nu_\mu$, were discussed by Pontecorvo in 1967 [4]. In the same paper it is argued, for the first time, that oscillation effects could be tested by solar neutrino observations. Following this suggestion, vacuum oscillations were studied [5] as a possible explanation of the anomalously low counting rate of solar neutrinos in the ^{37}Cl experiment at Homestake [6].

In 1978 Wolfenstein pointed out [7] that neutrino oscillations are modified by matter due to the effect of forward elastic scattering. The idea was developed by Mikheev and Smirnov [8], who found that resonant conversion may occur in media with varying density. The Mikheev-Smirnov-Wolfenstein (MSW) effect had important applications to solar neutrinos [8], providing a very attractive solution of the solar neutrino problem, and to neutrinos from collapsing stars [9]. The interest in matter effects increased – leading to extensive and detailed studies – in parallel with the developments of experiments, which gave more and more solid indications of anomalies in the rates of solar and atmospheric neutrinos .

Presently, after the results from SuperKamiokande in 1998 [10] and from SNO in 2001 [11], the neutrino oscillations appear to be the most convincing solution of these anomalies.

The MSW effect played an important role in the study of the neutrino signal from a supernova (SN1987A) observed in 1987 by the Kamiokande and IMB experiments [12, 13]. The effects of resonant conversion in the star [14, 15, 16, 17] and of regeneration of electron neutrinos and antineutrinos in the matter of the Earth [18, 19, 20, 21] were investigated. It was found [14, 22] that resonant conversion inside the star produces the appearance of an high energy tail in the $\bar{\nu}_e$ spectra, which contradicts observations [22], leading to the exclusion of some range

of large mixing angles. The resulting bounds, however, are much weaker in the region $\Delta m^2 \sim 10^{-5}$ eV^2, in which matter effects in the Earth are important. Further detailed analyses of the SN1987A data confirmed these results [23].

The regeneration inside the Earth of $\bar{\nu}_e$ with large mixing was considered as a possible explanation of the difference of the energy spectra observed in the Kamiokande and IMB detectors [24]. In the light of the recent results of solar neutrino experiments, which favour large ν_e - ν_μ / ν_τ mixings, the interpretation of SN1987A data has been revisited, with particular attention to the implications on the solution of the solar neutrino problem and on the neutrino mass hierarchy [25, 26, 27, 28].

The SN1987A event is the first and – up to now – only case of detection of neutrinos from a source outside the solar system. The great success of this observation produced interest in the study of neutrino signals from distant sources. While attention was devoted to the physics potential of future supernova neutrino detections (see e.g. [29]), the observation of gamma ray bursts [30] and of ultra-high energy cosmic rays [31] – which are supposed to have extragalactic origin – suggested that highly energetic neutrinos could be produced copiously by very distant (cosmological) objects like Active Galactic Nuclei (AGN) [32, 33, 34, 35, 36], topological defects [37, 38, 39, 40] and by the Gamma Ray Bursters (GRBs) themselves [41, 42, 43].

Neutrino telescopes, devoted to the observation of supernova neutrinos and high-energy cosmic neutrinos, are in their infancy: besides the smaller scale underground experiments which are already operating (e.g. LVD [44] dedicated to supernova neutrinos), large telescopes have been realized in the anctartic ice [45] and in the mediterranean sea [46, 47], as prototypes of kilometer-size detectors [49]. Large airshower experiments are now under construction [48], while other projects are being proposed [50, 51].

The purpose of the study of extragalactic neutrinos is twofold: first, to get information on the physics of the sources – now still largely unknown –, second, to test neutrino physics, and in particular neutrino oscillations, with unprecedented scales of energy and base-lines. It was marked [52] that oscillations lead to the appearance of tau neutrinos in the flux of high-energy cosmic neutrinos. Moreover, the study of oscillation effects opens the possibility to probe neutrino mixings and distinguish between different mass spectra [53]. Matter effects on oscillations of high-energy neutrinos were found to be significant in a largely CP-asymmetric relic neutrino background for neutrinos crossing cosmological distances [54].

This thesis collects in a unitary presentation the results of a series of papers [25, 54, 55, 56] in which we studied the effects of matter on oscillations of cosmic neutrinos from various sources.

After a first introductory chapter, in chapter 2 we consider the conditions for significant matter effect; in particular we show that a minimum width of medium is required, independently of the neutrino oscillation parameters and energy, and

of the matter density profile. In chapter 3 this condition is applied to high-energy neutrinos propagating across the universe: we find that substantial effect is produced by the relic neutrino background provided that it has a large CP-asymmetry and the neutrino source is at cosmological distance. The effect and its observability are discussed in detail. The chapters 4-6 are devoted to supernova neutrinos and their regeneration in the matter of the Earth. A detailed description of the Earth matter effect is presented in chapter 4, and in chapter 5 we give an application to the neutrino signal from SN1987A. We find that the Earth effect could reconcile the difference in the energy spectra of the Kamiokande and IMB data. In chapter 6 we consider future supernova neutrino detections: we show that the Earth matter effect is observable and has important implications on the reconstruction of the neutrino mixing scheme and mass spectrum. The discussion is completed by three appendices.

Chapter 1

Oscillations of mixed neutrinos in matter

How does the matter affect neutrino propagation? Essentially, the interaction with the matter constituents has two effects:

(i) the neutrinos are absorbed or undergo inelastic scattering, changing their momentum and energy. This causes a deviation of the neutrino state from coherence. The probability of absorption or inelastic scattering is proportional to the square of the Fermi constant G_F, thus being typically very small. As a consequence, in most of the realistic cases the effect of these processes can be neglected.

(ii) The neutrinos experience forward scattering, in which their momentum is not changed. This process is coherent and produces a neutrino-matter potential which is proportional to G_F. Under certain conditions this refraction potential strongly modifies the neutrino vacuum oscillations; the effect depends on the properties of the medium (chemical composition, density profile, etc.) and on the neutrino oscillation parameters (masses and mixings).

In this chapter we discuss briefly the main aspects of neutrino oscillations and conversion in matter. The discussion is intended as an introduction and starting point of the material in the chapters 2-6, with no expectations of completeness. For exhaustive and detailed reviews on the subject we address to refs. [57, 58, 59, 60].

1.1 Neutrino potentials in matter

Let us discuss the refraction potential of neutrinos in matter. To start with, we consider the charged current forward scattering of ν_e on electrons. At low energies, this process is described by the effective four-fermion Hamiltonian:

$$H_{CC} = \frac{G_F}{\sqrt{2}} [\bar{e}\gamma_\mu(1-\gamma_5)\nu_e][\bar{\nu}_e\gamma^\mu(1-\gamma_5)e] = \frac{G_F}{\sqrt{2}} [\bar{e}\gamma_\mu(1-\gamma_5)e][\bar{\nu}_e\gamma^\mu(1-\gamma_5)\nu_e] \,, \quad (1.1)$$

after the Fierz transformation. The matter-induced potential on ν_e is obtained from (1.1) by integrating over the degrees of freedom of the electron. The result contains the following terms:

$$\langle \bar{e}\gamma_0 e\rangle = \langle e^\dagger e\rangle = n_e\,, \qquad \langle \bar{e}\gamma e\rangle = \langle \mathbf{v}_e\rangle\,, \quad \langle \bar{e}\gamma_0\gamma_5 e\rangle = \langle \frac{\boldsymbol{\sigma}_e\cdot \mathbf{p}_e}{E_e}\rangle\,, \quad \langle \bar{e}\gamma\gamma_5 e\rangle = \langle \boldsymbol{\sigma}_e\rangle\,, \tag{1.2}$$

where $\mathbf{v}_e$, $\mathbf{p}_e$, σ_e, E_e are the velocity, momentum, spin and energy of the electrons. We denoted by n_e the number density of electrons in the medium. If the medium is unpolarized and has zero total momentum only the first term in (1.2) differs from zero, and we get the effective hamiltonian:

$$H_{eff}(\nu_e) = \langle H_{CC}\rangle \equiv \nu_e^\dagger (V_e)_{CC}\nu_e \tag{1.3}$$

$$(V_e)_{CC} = \sqrt{2}\,G_F n_e\,. \tag{1.4}$$

The contribution of the neutral current interaction to the neutrino-matter potential can be found in a similar way and is the same for all the neutrino flavours. The same argument which leads to the result (1.4) can can be applied to the neutrino scattering on nucleons. For ordinary matter made by electrons, protons and neutrons, under the assumption of electrically neutral medium (equal concentrations of protons and electrons) one finds the potentials:

$$V_e = \sqrt{2}\,G_F\left(n_e - \frac{n_n}{2}\right)\,, \qquad V_\mu = V_\tau = \sqrt{2}\,G_F\left(-\frac{n_n}{2}\right)\,, \tag{1.5}$$

where n_n is the number density of neutrons in the medium. In the expressions (1.5) the contribution of the neutrino-proton scattering cancels with the one from neutral current scattering on electrons.

The matter potentials for neutrinos are related to the ones of their antineutrinos by a change of sign: $V_\alpha = -V_{\bar{\alpha}}$.

Some remarks are in order. If the chemical composition and physical characteristics of the medium are different from the ones we considered here the neutrino-matter potential receives additional contributions with respect to the forms (1.5). This is the case if the matter is polarized [61] or contains neutrinos (see chapter 3). Moreover, at high energies the propagator corrections to the Hamiltonian (1.1) need to be taken into account, and the potentials (1.5) are modified accordingly (see e.g.[62]).

1.2 The evolution equation

Let us consider a system of flavour neutrino states $\nu_f = (\nu_e, \nu_\mu, \nu_\tau ...)$ mixed by mass terms (vacuum mixing). In the ultrarelativistic limit the propagation of these neutrinos is described by the evolution equation [7, 8]:

$$i\frac{d\nu_f}{dt} = H\nu_f, \quad H \simeq \frac{M^2}{2E} + V_f\,, \tag{1.6}$$

where E is the neutrino energy, M is the neutrino mass matrix in the flavour basis and V_f represents the matrix of potentials describing the interaction with the medium. The eigenstates ν_i of M are related to the flavour states by the mixing matrix U such that, defining $\nu = (\nu_1, \nu_2, \nu_3, ...)$, we have:

$$\begin{aligned} M &= U\, diag(m_1, m_2, m_3, ...)\, U^\dagger \ , \\ \nu_f &= U\nu \ . \end{aligned} \tag{1.7}$$

According to the Standard Model the matrix of potentials is flavour diagonal:

$$V_f = diag(V_e, V_\mu, V_\tau) \ , \tag{1.8}$$

with V_e, V_μ and V_τ given in eq. (1.5).

In the case of two neutrinos, *e.g.* (ν_e, ν_μ) – which we will consider from now on – the mixing matrix can be written in terms of a single angle θ:

$$U = \begin{pmatrix} \cos\theta & \sin\theta \\ -\sin\theta & \cos\theta \end{pmatrix} . \tag{1.9}$$

From eqs. (1.6), (1.8) and (1.9) we find the equation which describes $\nu_e \leftrightarrow \nu_\mu$ oscillations in matter:

$$i\frac{d}{dt}\begin{pmatrix} \nu_e \\ \nu_\mu \end{pmatrix} = \begin{pmatrix} -\frac{\Delta m^2}{4E}\cos 2\theta + V & \frac{\Delta m^2}{4E}\sin 2\theta \\ \frac{\Delta m^2}{4E}\sin 2\theta & \frac{\Delta m^2}{4E}\cos 2\theta \end{pmatrix}\begin{pmatrix} \nu_e \\ \nu_\mu \end{pmatrix} . \tag{1.10}$$

where (see eq. (1.5)):

$$V \equiv V_e - V_\mu = \sqrt{2}\, G_F n_e \ , \tag{1.11}$$

and $\Delta m^2 \equiv m_2^2 - m_1^2$. In eq. (1.10) we omitted terms which are proportional to the identity in the flavour basis and are irrelevant to the description of neutrino oscillations.

In general, the electron density n_e of the medium depends on the coordinate along the neutrino trajectory or, equivalently, on the time t describing the evolution: $n_e = n_e(t)$. Therefore, the effective Hamiltonian H_{fl} defined by eq. (1.10) is time-dependent and the evolution equation does not have a general analytical solution.

At any instant of time H_{fl} can be diagonalized by a unitary transformation:

$$\nu_{fl} = U_m(t)\nu_m \ , \qquad U_m(t)^\dagger H_{fl}(t) U_m(t) = diag(E_{1m}(t),\, E_{2m}(t)) \ , \tag{1.12}$$

where $\nu_m = (\nu_{1m}, \nu_{2m})$ are the Hamiltonian eigenstates corresponding to the eigenenergies:

$$\begin{aligned} E_{1m} &= \frac{V}{2} - \frac{\Delta m^2}{4E}\sqrt{\left(\frac{2EV}{\Delta m^2} - \cos 2\theta\right)^2 + \sin^2 2\theta} \ , \\ E_{2m} &= \frac{V}{2} + \frac{\Delta m^2}{4E}\sqrt{\left(\frac{2EV}{\Delta m^2} - \cos 2\theta\right)^2 + \sin^2 2\theta} \ . \end{aligned} \tag{1.13}$$

The mixing matrix U_m equals:

$$U_m = \begin{pmatrix} \cos\theta_m & \sin\theta_m \\ -\sin\theta_m & \cos\theta_m \end{pmatrix}, \tag{1.14}$$

where mixing angle $\theta_m(t)$ in matter is given by:

$$\tan 2\theta_m = \frac{\sin 2\theta}{\cos 2\theta - 2V(t)E/\Delta m^2}. \tag{1.15}$$

In the basis of the instantaneous eigenstates ν_m the equation (1.10) takes the form:

$$i\frac{d}{dt}\begin{pmatrix} \nu_{1m} \\ \nu_{2m} \end{pmatrix} = \begin{pmatrix} E_{1m}(t) & -i\dot{\theta}_m(t) \\ i\dot{\theta}_m(t) & E_{2m}(t) \end{pmatrix}\begin{pmatrix} \nu_{1m} \\ \nu_{2m} \end{pmatrix}, \tag{1.16}$$

where $\dot{\theta}_m \equiv d\theta_m/dt$.

In the following sections we will consider some solutions of the eqs. (1.10) and (1.16) corresponding to certain density profiles of the medium and discuss their properties.

1.3 Constant density case

If the density n_e of the medium is constant along the neutrino trajectory, $n_e = const$, we have that in eq. (1.16) $\dot{\theta}_m = 0$ and the eigenenergies E_{1m} and E_{2m} do not depend on time. In this case the evolution of the neutrino system follows straightforwardly from eq. (1.16). Given the distance L travelled by the neutrinos in the medium one finds the $\nu_e \leftrightarrow \nu_\mu$ oscillation probability:

$$P(\nu_e \to \nu_\mu;\, L) = \sin^2 2\theta_m \sin^2\left(\pi\frac{L}{l_m}\right), \tag{1.17}$$

where the oscillation amplitude and length take the form:

$$\sin^2 2\theta_m = \frac{\sin^2 2\theta}{\left(\frac{2EV}{\Delta m^2} - \cos 2\theta\right)^2 + \sin^2 2\theta} \tag{1.18}$$

$$l_m = \frac{2\pi}{E_{2m} - E_{1m}} = \frac{4\pi E}{\Delta m^2}\frac{1}{\sqrt{\left(\frac{2EV}{\Delta m^2} - \cos 2\theta\right)^2 + \sin^2 2\theta}}. \tag{1.19}$$

In absence of matter, $V = 0$, the eqs. (1.17)-(1.19) give the well known expressions which describe vacuum oscillations (see e.g. [58]).

Let us comment on the oscillation probability (1.17). From eqs. (1.18)-(1.19) it follows that both the oscillation length and depth are modified by matter and

have a characteristic resonance form. The depth (1.18) is maximal, $\sin^2 2\theta_m = 1$ ($\theta_m = \pi/4$), when the *resonance condition*

$$\frac{2EV}{\Delta m^2} = \cos 2\theta \tag{1.20}$$

is fulfilled. From eq. (1.11) we find that the condition (1.20) corresponds to the resonance density

$$n_e^{res} = \frac{\Delta m^2}{2E}\frac{\cos 2\theta}{\sqrt{2}G_F} \,. \tag{1.21}$$

As the expression (1.19) shows, the oscillation length l_m takes its maximum value at resonance:

$$l_m(n_e = n_e^{res}) \equiv l^{res} = \frac{4\pi E}{\Delta m^2 \sin 2\theta} \,. \tag{1.22}$$

In contrast with vacuum oscillations, where the conversion probability can not exceed $\sin^2 2\theta$, in presence of matter we can have a large mixing, and therefore large conversion probability, even for very small values of the vacuum mixing angle θ.

From eq. (1.18) it follows that the depth of oscillations is larger than 1/2 if the matter density is in the interval $[n_e^{res} - \Delta n_e, n_e^{res} + \Delta n_e]$, with

$$\Delta n_e = n_e^{res} \tan 2\theta \,. \tag{1.23}$$

The expression (1.18) also shows that the resonant enhancement of the mixing is possible if

$$\frac{\Delta m^2}{V}\cos 2\theta = \frac{m_2^2 - m_1^2}{V}(\cos^2\theta - \sin^2\theta) > 0 \,. \tag{1.24}$$

If $V > 0$, as it is for a ν_e-ν_μ system, the condition (1.24) is equivalent to the requirement that the lower mass eigenstate has the larger ν_e component. In the case of $\bar{\nu}_e$-$\bar{\nu}_\mu$ oscillations we have $V < 0$ and the condition (1.24) requires a larger $\bar{\nu}_e$ component in the heavier state. Clearly, the enhancement of mixing is possible in one – ν_e or $\bar{\nu}_e$ – channel only: if the ν_e mixing is enhanced, the mixing of $\bar{\nu}_e$ is suppressed and vice versa.

1.4 Media with varying density: adiabatic approximation

We now consider the case in which the density n_e changes (e.g. decreases) on the way of the neutrinos, and suppose that the density variation is slow enough so that

$$|\dot{\theta}_m| \ll |E_{2m} - E_{1m}| \,. \tag{1.25}$$

The condition (1.25), called the *adiabaticity condition*, is often expressed in terms of the adiabaticity parameter χ:

$$\chi \gg 1 \,, \tag{1.26}$$

$$\chi \equiv \frac{|E_{2m} - E_{1m}|}{2|\dot{\theta}_m|} \,. \tag{1.27}$$

The condition of adiabaticity corresponds to the requirement that the probability P' of transitions between the states ν_{1m} and ν_{2m} is very small: $P' \ll 1$. As a consequence, if the adiabaticity condition is fulfilled the states ν_{1m} and ν_{2m} evolve independently: the only effect of the density variation is the slow change of the flavour composition of these states due to the change of the mixing angle θ_m.

Let us consider the propagation of neutrinos in a medium with varying density from the initial time t_i to the final time t_f and denote by θ_i and θ_f the corresponding mixing angles in matter. In the adiabatic approximation (1.25) one can neglect the $\dot{\theta}_m$ terms in the equation (1.16) and find the conversion probability:

$$P(\nu_e \to \nu_\mu) = \frac{1}{2} - \frac{1}{2}\cos 2\theta_i \cos 2\theta_f - \frac{1}{2}\sin 2\theta_i \sin 2\theta_f \cos\Phi \,, \tag{1.28}$$

where the oscillation phase Φ equals:

$$\Phi = \int_{t_i}^{t_f} (E_{2m}(t') - E_{1m}(t'))dt' \,. \tag{1.29}$$

Consider, e.g., the case in which $\sin^2 2\theta \ll 1$ and the initial and final matter densities, n_i and n_f, are far above and far below the resonance value: $n_i \gg n_e^{res}$ and $n_f \ll n_e^{res}$. From eq. (1.15) it follows that $\cos 2\theta_i \simeq -1$ and $\cos 2\theta_f \simeq 1$; moreover $\sin 2\theta_i \simeq \sin 2\theta_f \simeq 0$. Thus, eq. (1.28) gives a large conversion probability: $P \simeq 1$. Notice that the third term in the expression (1.28), which describes oscillations, is suppressed, so that, essentially, non-oscillatory conversion takes place. We mark that, as it appears in (1.28), once the conversion occurs adiabatically, the conversion probability P is independent of the details of the density profile of the medium, but is determined only by the initial and final values of the density.

In general the conversion probability (1.28) is large ($P(\nu_e \to \nu_\mu) \gtrsim 1/2$) if $n_i > n_e^{res}$ and $n_f < n_e^{res}$, i.e. if the layer of the medium with resonance density is crossed during the neutrino propagation.

The analysis that led to the result (1.28) can be generalized to include the effect of $\nu_{1m} \leftrightarrow \nu_{2m}$ transitions and gives the expression [63]:

$$P(\nu_e \to \nu_\mu) \simeq \frac{1}{2} - \frac{1}{2}\cos 2\theta_i \cos 2\theta_f (1 - 2P') \,, \tag{1.30}$$

where we have omitted oscillating terms which average to zero in many cases. If $P' = 0$ the adiabatic result (1.28) is recovered. For strong breaking of adiabaticity,

$|\dot{\theta}_m| \gg |E_{2m} - E_{1m}|$, we have $P' \simeq 1$ and the conversion and survival probability interchange. As a consequence, in the case in which $\cos 2\theta_i \simeq -1$ and $\cos 2\theta_f \simeq 1$ we get a very small conversion probability, $P(\nu_e \to \nu_\mu) \simeq 0$. In general, the breaking of adiabaticity weakens the conversion effect.

For moderate violation of adiabaticity the transition probability P' is well described by the Landau-Zener form [63, 64]:

$$P' \simeq P_{LZ} = e^{-\frac{\pi}{2}\chi_R}\,, \tag{1.31}$$

where χ_R is the adiabaticity parameter taken at the MSW resonance point: $\chi_R \equiv \chi(n_e = n_e^{res})$.

Let us comment on the adiabaticity condition, eq (1.25). Since the difference of the eigenenergies reaches its minimum – equal to $(\Delta m^2/2E)\sin 2\theta$ (see eq. (1.13)) – at the MSW resonance, the adiabaticity is more critical at the resonance point: if the conversion is adiabatic in the resonance it is also adiabatic away from it [1]. From eqs. (1.11), (1.27), (1.13) and (1.15) we find the expression of the adiabaticity parameter at resonance:

$$\chi_R = \frac{\sin^2 2\theta}{\cos 2\theta}\frac{\Delta m^2}{2E}\left|\frac{dn_e}{dt}\frac{1}{n_e}\right|^{-1}_{n_e=n_e^{res}}\,. \tag{1.32}$$

The expression (1.32) has a simple physical interpretation. Let us define the length Δr corresponding to a variation of the density Δn_e, with Δn_e given in eq. (1.23), from the resonance value n_e^{res}. It is easy to obtain:

$$\Delta r = \tan 2\theta \left|\frac{dn_e}{dt}\frac{1}{n_e}\right|^{-1}_{n_e=n_e^{res}}\,. \tag{1.33}$$

In terms of Δr and of the oscillation length at resonance l_{res}, eq. (1.22), the parameter χ_R writes:

$$\chi_R = 2\pi\frac{\Delta r}{l^{res}}\,. \tag{1.34}$$

Thus, the adiabaticity condition $\chi_R \gg 1$ is equivalent to the requirement that the matter density changes over length scales Δr much larger than the oscillation length.

Besides the cases discussed here, there are other situations of physical interest for which the evolution equation (1.10) can be solved analytically. This is the case, e.g. if the density profile is a periodic or quasi-periodic series of layers of matter with constant density (step-like and "castle-wall" profile). For neutrino propagation in these media parametric effects may occur; for their illustration we refer to the dedicated literature [65] (see also chapter 2).

[1] Assuming that the matter density n_e does not have strong gradients outside the resonance region.

1.5 A graphical representation

As an illustration of the results of secs. 1.3-1.4, we discuss a graphic representation of the evolution of a neutrino system in matter [66, 67, 68].

Let us introduce the vectors:

$$\vec{\nu} = \left(\mathrm{Re}\nu_e^\dagger\nu_\mu,\ \ \mathrm{Im}\nu_e^\dagger\nu_\mu,\ \ \nu_e^\dagger\nu_e - 1/2\right)\ , \tag{1.35}$$

$$\vec{B} \equiv \frac{2\pi}{l_m}(\sin 2\theta_m,\ \ 0,\ \ \cos 2\theta_m)\ , \tag{1.36}$$

where ν_α, $(\alpha = \mu, e)$ are the neutrino wave functions; notice that the components of the vector $\vec{\nu}$ are the elements of the density matrix.

It is possible to check that the evolution equation (1.6) can be written in terms of $\vec{\nu}$ and $\vec{B}$ as:

$$\frac{d\vec{\nu}}{dt} = \left(\vec{B} \times \vec{\nu}\right)\ , \tag{1.37}$$

which is analogous to the equation describing the behaviour of the spin of an electron in a magnetic field. This analogy provides a pictorial interpretation of the evolution of the neutrino system: the vector $\vec{\nu}$ moves on the surface of a cone with axis $\vec{B}$ (see fig. 1.1) and the rotation phase ϕ corresponds to the phase of oscillations (see eq. (1.29)). When the neutrino is in a pure flavour state the vector $\vec{\nu}$ is aligned with the z-axis. The direction of the axis $\vec{B}$ is determined by $2\theta_m$ (eq. (1.36)); the angle of the cone equals $2\theta_a$ where θ_a describes the admixtures of the eigenstates ν_{1m} and ν_{2m} in the instantaneous neutrino state: $\nu(t) = \cos\theta_a\nu_{1m} + \sin\theta_a\nu_{2m}e^{i\phi}$. The angle θ_a depends on the initial conditions and in general changes during the evolution.

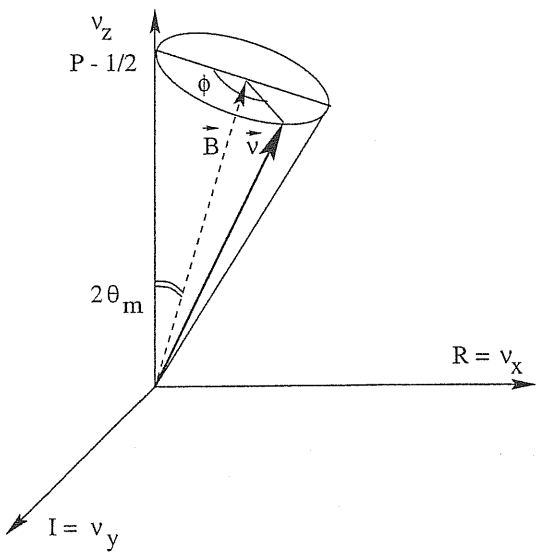

Figure 1.1: Graphic representation of the neutrino oscillations in the uniform medium (from [69]).

The projection of the vector $\vec{\nu}$ on the z-axis, ν_z, gives the probability to find ν_e in the state $\nu(t)$:

$$P \equiv \nu_e^\dagger\nu_e = \nu_z + \frac{1}{2}\ . \tag{1.38}$$

Let us now discuss the dynamics described by eq. (1.37) for the cases presented in secs. 1.3-1.4.

(1) In the constant density case (fig. 1.1) the mixing angle θ_m is constant, thus $\vec{B}$ is fixed (its direction does not change with time) and the vector $\vec{\nu}$ precesses about it with constant angular velocity and the

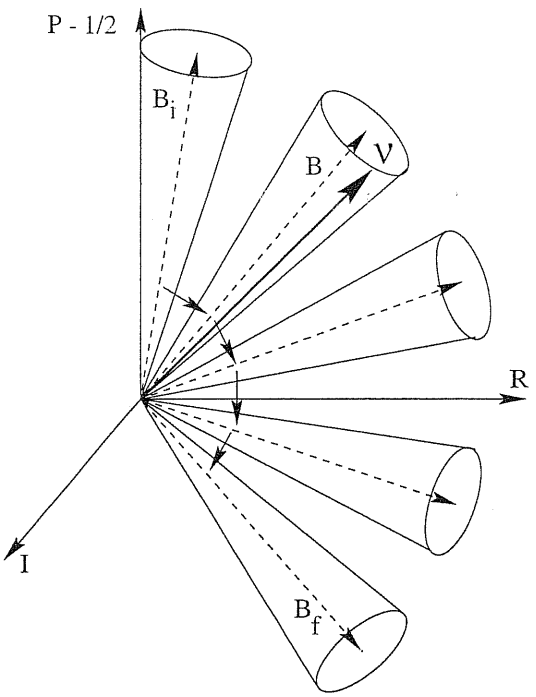

Figure 1.2: Graphic representation of the neutrino adiabatic conversion (from [69]).

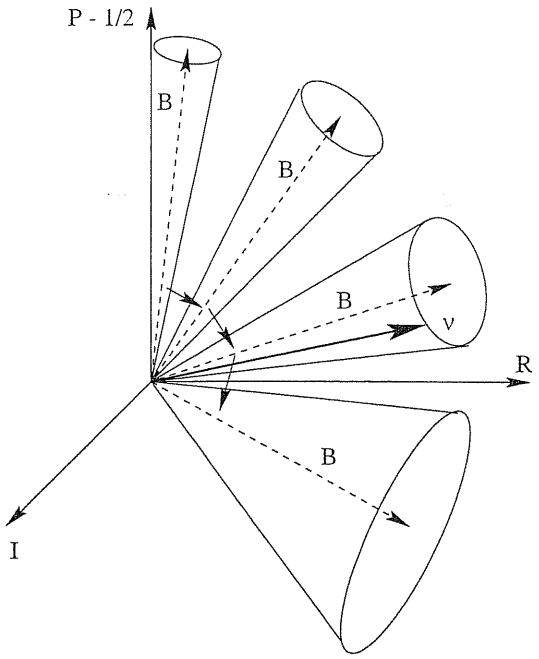

Figure 1.3: Graphic representation of the non-adiabatic neutrino conversion (from [69]).

cone amplitude $2\theta_a$ remains constant. As follows from eq. (1.35), if the neutrino is initially in a flavour state, the corresponding vector $\vec{\nu}$ lies on the z-axis (fig. 1.1). The evolution has the character of oscillations described in eq. (1.17).

(2) If the matter density varies, the vector $\vec{B}$ moves according to the change of the mixing angle (see eq. (1.15)). If the density variation is slow enough so that the adiabaticity condition (1.25) is fulfilled, the angle θ_a is constant: the admixtures of the eigenstates are conserved. The vector $\vec{\nu}$ precesses about the instantaneous direction of the $\vec{B}$ vector, as shown in fig. 1.2. Qualitatively, $\vec{B}$ moves so slowly that $\vec{\nu}$ has time enough to adjust itself to the change of direction of $\vec{B}$ and thus follow its motion.

(3) If the adiabaticity is broken, the transitions $\nu_{1m} \leftrightarrow \nu_{2m}$ become essential. This implies that the admixtures of the eigenstates in a given state change or, equivalently, θ_a is no longer a constant. Thus, the vector $\vec{\nu}$ rotates about $\vec{B}$ with varying cone angle (fig. 1.3); in other words the neutrino state can not completely adjust itself to the change of direction of $\vec{B}$.

1.6 Generalization to three neutrinos

For a system of three neutrinos, ν_e, ν_μ and ν_τ, the evolution equation describing oscillations in matter is:

$$i\frac{d}{dt}\begin{pmatrix}\nu_e\\ \nu_\mu\\ \nu_\tau\end{pmatrix} = \left[\frac{1}{2E}U\begin{pmatrix}m_1^2 & 0 & 0\\ 0 & m_2^2 & 0\\ 0 & 0 & m_3^2\end{pmatrix}U^\dagger + \begin{pmatrix}V & 0 & 0\\ 0 & 0 & 0\\ 0 & 0 & 0\end{pmatrix}\right]\begin{pmatrix}\nu_e\\ \nu_\mu\\ \nu_\tau\end{pmatrix}, \quad (1.39)$$

analogously to eq. (1.10). The 3-flavour mixing matrix U can be written in the general form (see e.g. [70]):

$$U = V_{23}W_{13}V_{12}D\,, \quad (1.40)$$

where

$$V_{12} = \begin{pmatrix}c_{12} & s_{12} & 0\\ -s_{12} & c_{12} & 0\\ 0 & 0 & 1\end{pmatrix}, \quad W_{13} = \begin{pmatrix}c_{13} & 0 & s_{13}\,e^{-i\delta}\\ 0 & 1 & 0\\ -s_{13}\,e^{i\delta} & 0 & c_{13}\end{pmatrix}, \quad V_{23} = \begin{pmatrix}1 & 0 & 0\\ 0 & c_{23} & s_{23}\\ 0 & -s_{23} & c_{23}\end{pmatrix}, \quad (1.41)$$

and $D = diag(e^{-i\varphi_1}, 1, e^{-i\varphi_2})$. Here $c_{ij} \equiv \cos\theta_{ij}$ and $s_{ij} \equiv \sin\theta_{ij}$. The phase δ in W_{13} is the usual Dirac-type CP violating phase, whereas the phases φ_1 and φ_2 are present only in the Majorana case. It immediately follows from eq. (1.39) that the Majorana phases have no effect on neutrino oscillations, therefore the factor D in eq. (1.40) will be omitted from here on.

In general, the analytical study of eq. (1.39) is rather difficult. However in certain realistic situations the problem can be reduced to the study of a two-neutrino system. In what follows we will focus on these particular cases.

Let us consider a 3-ν system with the hierarchical mass spectrum:

$$\Delta m_{12}^2 \ll \Delta m_{23}^2 \approx \Delta m_{13}^2\,, \quad (1.42)$$

as suggested by the interpretation of the results of solar and atmospheric neutrino experiments [10, 71, 72]. Under the assumption (1.42) the dynamics of propagation reduces to the 2-ν case in the following circumstances:

(i) The source - detector distance L is much smaller than the oscillation length associated with smallest mass splitting:

$$L \ll l_{12} = \frac{4\pi E}{\Delta m_{12}^2}\,. \quad (1.43)$$

This implies that the oscillation phase between the states ν_1 and ν_2 is very small, i.e. there is no evolution of the ν_1-ν_2 subsystem. This allows one to neglect the quantity

Δm^2_{12} and put $m^2_1 = m^2_2$ in eq. (1.39). Under this approximation the matrix V_{12} commutes with the mass matrix M and thus cancels in (1.39). Furthermore, one can go to a new basis $\tilde{\nu}$ defined by $\nu = V_{23}\tilde{\nu}$ and get the equation:

$$i\frac{d}{dt}\begin{pmatrix}\tilde{\nu}_1\\ \tilde{\nu}_2\\ \tilde{\nu}_3\end{pmatrix} = \begin{pmatrix} -\frac{\Delta m^2_{31}}{4E}\cos 2\theta_{13} + V & 0 & \frac{\Delta m^2_{31}}{4E}\sin 2\theta_{13} \\ 0 & 0 & 0 \\ \frac{\Delta m^2_{31}}{4E}\sin 2\theta_{13} & 0 & \frac{\Delta m^2_{31}}{4E}\cos 2\theta_{13}\end{pmatrix}\begin{pmatrix}\tilde{\nu}_1\\ \tilde{\nu}_2\\ \tilde{\nu}_3\end{pmatrix}, \qquad (1.44)$$

i.e. the problem is reduced to a 2-flavour problem of oscillations between $\tilde{\nu}_1 = \nu_e$ and $\tilde{\nu}_3 = s_{23}\,\nu_\mu + c_{23}\,\nu_\tau$. These oscillations are governed by the large mass squared difference Δm^2_{31} and mixing angle θ_{13}; they can be studied according to the discussion in secs. 1.3-1.5. In (1.44) we have omitted the phase δ since under the condition (1.43) the CP-violating effects induced by this phase are unobservable.

(ii) The heavier mass splitting dominates over the level splitting induced by the matter potential, $\Delta m^2_{23}/2E \gg V$, and the source-detector distance is much larger than the oscillation length associated with the largest mass splitting:

$$L \gg l_{23} = \frac{4\pi E}{\Delta m^2_{23}}. \qquad (1.45)$$

In this case oscillations due to Δm^2_{23} are usually averaged out or/and the coherence of the ν_3 with the rest of system is lost. The state ν_3 decouples, leading to the averaged vacuum oscillation result. Once this is taken into account one easily finds the survival probability:

$$P(\nu_e \to \nu_e) \simeq c^4_{13} P(\Delta m^2_{12}, \theta_{12}) + s^4_{13}\,, \qquad (1.46)$$

where $P(\Delta m^2_{12}, \theta_{12})$ is the two-flavour survival probability given by the evolution equation (1.10) with $\Delta m = \Delta m_{12}$, $\theta = \theta_{12}$ and the replacement $V \to c^2_{13}\,V$ [73].

Chapter 2

The minimum width condition

As discussed in the previous chapter, strong flavour conversion of neutrinos can be realized as a consequence of the interaction with matter. Depending on the neutrino energy, mixing, mass squared difference and density profile of the medium, the character of conversion is different, ranging from oscillations with enhanced depth in uniform media to adiabatic conversion in media with varying density or parametric effects in quasi-periodic or periodic matter profiles.

It is intuitively clear that to have a significant matter effect a sufficiently large amount of matter is needed. Let us define the width of the medium as the integrated number density of scatterers along the path travelled by the neutrino in the matter:

$$d = \int n(L)dL \ , \tag{2.1}$$

which is frequently named "column density" in astrophysical context. Since in ordinary matter the effective neutrino potential is determined by the concentration of electrons, n_e (see eq. (1.11)), we will take $n = n_e$ in eq. (2.1).

In this chapter we show that there exists a minimum value d_{min} for the width d below which it is not possible to have significant neutrino conversion. This lower bound is independent of the density profile and of the neutrino energy and mass. That allows us to make conclusions on the relevance of matter effect in various situations without knowledge of the density distribution.

2.1 Density profiles and widths

In this section we consider various mechanisms of matter enhancement of neutrino flavour conversion. For each of them we work out the minimum width of the medium needed to have significant conversion probability, showing that a lower bound for the width exists and is realized in the case of uniform medium with resonance density.

2.1.1 The absolute minimum width: constant resonance density

Let us consider a system of two mixed flavour states[1], ν_e and ν_μ (ν_τ), characterized by vacuum mixing angle θ and mass squared difference Δm^2. We assume that the vacuum mixing is small, so that vacuum oscillations effects are negligible ($P^{vac}_{\nu_e \to \nu_\mu} \ll 1$) and a strong transition in medium, i.e. $P_{\nu_e \to \nu_\mu} = O(1)$, is essentially due to matter effect. For definitness, we choose the condition of significant conversion to be

$$P_{\nu_e \to \nu_\mu} \geq \frac{1}{2} \,. \tag{2.2}$$

Let us consider a uniform medium with resonance density $n_e = n_e^{res}$, with n_e^{res} given in eq. (1.21). In this case the neutrino oscillate in matter with maximal depth: $D = \sin^2 2\theta_m = 1$, and the oscillation length takes the maximal value l^{res}, eq. (1.22).

According to eq. (1.17) the condition (2.2) starts to be satisfied when the neutrinos have travelled a distance $L = l^{res}/4$,corresponding to the width:

$$d_{min} = \frac{1}{4} n_e^{res} l^{res} . \tag{2.3}$$

Inserting the expressions of n_e^{res} and l^{res} given in (1.21) and (1.22), we get:

$$d_{min} = \frac{\pi}{2\sqrt{2} G_F \tan 2\theta} = \frac{d_0}{\tan 2\theta} \,, \tag{2.4}$$

where

$$d_0 = \frac{\pi}{2\sqrt{2} G_F} \simeq \frac{1.11}{G_F} \,. \tag{2.5}$$

We will call d_0 the refraction width. Numerically,

$$d_0 = 2.45 \cdot 10^{32} \mathrm{cm}^{-2} = 4.08 \cdot 10^8 \, \mathrm{A\,cm}^{-2} \,, \tag{2.6}$$

where $A = 6 \cdot 10^{23}$ is the Avogadro number[2].

[1] The arguments remain the same for three neutrinos.

[2] It can be checked that different choices of the condition (2.2) lead to analogous results. For instance, taking $P_{\nu_e \to \nu_\mu} \geq \frac{3}{4}$ we find

$$d_0^{3/4} = \frac{4}{3} d_0 = \frac{2\pi}{3\sqrt{2} G_F} = 5.41 \cdot 10^8 \, \mathrm{A\,cm}^{-2},$$

and, for $P_{\nu_e \to \nu_\mu} \geq \frac{1}{4}$:

$$d_0^{1/4} = \frac{2}{3} d_0 = \frac{\pi}{3\sqrt{2} G_F} = 2.7 \cdot 10^8 \, \mathrm{A\,cm}^{-2}.$$

The widths d_{min} and d_0 have a simple physical interpretation. The refraction width d_0 is a universal quantity: it is determined only by the Fermi coupling constant, and does not depend on the neutrino parameters at all. Using the definition of refraction length

$$l_0 \equiv \frac{2\pi}{V} = \frac{2\pi}{\sqrt{2} n_e G_F} \tag{2.7}$$

we can write:

$$\frac{d_0}{n_e} = \frac{l_0}{4} \,. \tag{2.8}$$

It appears that d_0 corresponds to the distance at which the matter-induced phase difference between the flavour states equals $\pi/2$. This can be considered as the definition of refraction width, which by eq. (2.7) can be written in the general form:

$$d_0 \equiv \frac{\pi}{2} \frac{n_m}{V_m} \,, \tag{2.9}$$

where V_m is the neutrino-medium potential and n_m is the concentration of the relevant scatterers in the medium.

The minimum width, d_{min}, is inversely proportional to $\tan 2\theta$, which represents properties (the mixing) of the neutrino system itself. The smaller the mixing θ, the larger is the width d_{min} needed for strong transition.

The condition (2.2) can be generalized. It corresponds to the case of initial state coinciding with a pure flavour state. In general one can require that the change of the probability to detect a given flavour α is larger than $1/2$:

$$\Delta P \equiv P_f(\nu_\alpha) - P_i(\nu_\alpha) \geq \frac{1}{2} \,, \tag{2.10}$$

where P_i and P_f are the initial and final probabilities. The condition (2.2) corresponds to $P_i(\nu_\mu) = 0$, so that $P_f(\nu_\alpha) = P_{\nu_e \to \nu_\mu}$. Taking $P_i = 1/4$ and $P_f = 3/4$, we get in a similar way:

$$d_{1/2} = \frac{2}{3} d_{min} = \frac{\pi}{3\sqrt{2} G_F \tan 2\theta} \,. \tag{2.11}$$

This $d_{1/2}$ is the extreme value, however for most practical situations the condition (2.2) is more relevant, and from here on we will use the the width d_{min} determined in (2.4).

In what follows we will show that for all the other density profiles the width $d_{1/2}$ required by the condition (2.2) is larger than d_{min}.

2.1.2 Uniform medium with density out of resonance

For $n_e \neq n_e^{res}$ the inequality (2.2) can be satisfied only if $\sin^2 2\theta_m \geq \frac{1}{2}$, which means that the density is required to be in the resonance interval: $n_e^{res}(1 - \tan 2\theta) \leq n_e \leq n_e^{res}(1 + \tan 2\theta)$ (see chapter 1). At the edges of the interval we get the width

$$d_{1/2} = \frac{\pi}{2G_F}\left(\frac{1}{\tan 2\theta} \pm 1\right) \simeq \sqrt{2} d_{min} \ , \tag{2.12}$$

which is larger than d_{min}. For other values of the density in the resonance interval we have $d_{min} < d_{1/2} < \sqrt{2} d_{min}$[3].

2.1.3 Medium with varying density

In general the neutrino propagation has a character of interplay of resonance conversion and oscillations. As shown in chapter 1, strong transition requires the fulfillment of the resonance condition (1.20) and of the adiabaticity condition, eq. (1.25). Notice that both these conditions are local, and can be fulfilled for arbitrarily small widths of the medium. Clearly, they are not sufficient to assure a significant conversion, and a third condition of large enough matter width is needed.

Let us consider a linear density profile with length $2L$ and average density equal to the resonance one, so that $n_{max} = n_e^{res} + \Delta n$ and $n_{min} = n_e^{res} - \Delta n$. We denote θ_{1m} and θ_{2m} the mixings in the initial and final points, and define $\gamma \equiv \chi_R^{-1}$ with χ_R the adiabaticity parameter at resonance (1.32). In the first order of adiabatic perturbation theory one gets that the conversion probability is given by:

$$\begin{aligned} P_{\nu_e \to \nu_\mu}(L) &= \frac{1}{2} - \frac{1}{2}\cos 2\theta_{1m} \cos 2\theta_{2m} \\ &- \frac{1}{2}\sin 2\theta_{1m} \sin 2\theta_{2m} \cos\left[\frac{1}{\gamma} f(x)\right] \\ &- 2\sin(2\theta_{1m} - 2\theta_{2m})\alpha(x) \cos\left[\frac{1}{2\gamma} f(x)\right] \ , \end{aligned} \tag{2.13}$$

where

$$\begin{aligned} x &= 2\pi\gamma \frac{L}{l^{res}} \ , \\ f(x) &= \ln(x + \sqrt{1 + x^2}) + x\sqrt{1 + x^2} \ , \\ \alpha(x) &= \int_0^x \frac{dy}{1 + y^2} \cos\left[\frac{1}{2\gamma} f(y)\right] \ . \end{aligned} \tag{2.14}$$

[3]It can be checked that the width $d_{1/2}$ in eq. (2.12) is larger than d_{min} for small mixing: $\sin 2\theta \lesssim 0.3$. We will use this condition as criterion of smallness of the mixing.

In the adiabatic approximation, $\gamma \ll 1$, we get from eqs. (2.13) and (2.14):

$$d_{1/2} = d_{min}\left[1 + \left(1 - \frac{\pi}{8}\right)\gamma^2\right]. \tag{2.15}$$

This expression shows that for the adiabatic case $d_{1/2} \simeq d_{min}$ and for weak violation of adiabaticity the minimum width increases quadratically with γ. We remark that in this case the effect is dominated by oscillations with large (close to maximal) depth. The change of density gives only small corrections.

Let us consider now a situation in which the resonance adiabatic conversion is the main mechanism of flavour transition. A pure conversion effect is realized if the initial neutrino state that enters the medium coincides with one of the eigenstates of the Hamiltonian in matter, and the propagation in matter is adiabatic. In this case no phase effect, and therefore no oscillations occur. Let us denote n_i and n_f the initial and final densities of the medium, and suppose the initial state is $\nu_i = \nu_{2m} = \sin\theta_m \nu_e + \cos\theta_m \nu_\mu$. The probability to find a ν_μ in this state is $P_i(\nu_\mu) = \cos^2\theta_m(n_i)$. The state evolves following the change of density, so that it remains an eigenstate of the Hamiltonian, and the probability to find ν_μ in the final state is $P_f(\nu_\mu) = \cos^2\theta_m(n_f)$. Since the initial state ν_i does not coincide with a pure flavour state we will use the condition (2.10) as criterion of strong matter effect. Inserting P_i and P_f in (2.10), we get the condition for $d_{1/2}$:

$$\cos 2\theta_m(n_f) - \cos 2\theta_m(n_i) = 1\ . \tag{2.16}$$

Taking the initial and final values of the density as $n_i = n_e^{res} + \Delta n$ and $n_f = n_e^{res} - \Delta n$ ($\Delta n \geq 0$), and using the definition (1.19) we find that the equality (2.16) leads to

$$\Delta n = n_e^{res}\frac{1}{\sqrt{3}}\tan 2\theta\ . \tag{2.17}$$

Clearly, for a given Δn the size of the layer, and therefore its width, depend on the gradient of the density which can be expressed in terms of the parameter γ. We get:

$$n_e(L)dL = \frac{2E\cos 2\theta}{\Delta m^2 \sin^2 2\theta}\frac{1}{\gamma}dn_e\ , \tag{2.18}$$

and then integrating this equation we obtain:

$$d = \frac{2E\cos 2\theta}{\Delta m^2 \sin^2 2\theta}\frac{1}{\gamma}\Delta n\ . \tag{2.19}$$

Finally, inserting the expressions (2.17) and (1.20) in eq. (2.19) we find:

$$d_{1/2} = \frac{4}{\pi\sqrt{3}}\frac{1}{\gamma}d_{min}\ . \tag{2.20}$$

Let us comment on this result. As far as the adiabaticity condition is satisfied, the change of probability does not depend on the density distribution; it is a function of the initial and final densities only. If Δn is fixed, the decrease of the width means the decrease of the length L of the layer, and therefore increase of the gradient of the density. This will lead eventually to violation of the adiabaticity condition. Thus, the minimal width corresponds to the maximal γ for which the adiabaticity is not broken substantially.

For strong adiabaticity violation an increase of $d_{1/2}$ is expected, due to the increase of the minimum Δn required by the condition (2.10), and therefore of the corresponding length. This can be seen if we consider the previous argument taking into account the effect of the adiabaticity breaking from the beginning. Using the Landau-Zener level crossing probability $P_{LZ} = \exp(-\pi/2\gamma)$, which describes the transition between two eigenstates, we get, instead of (2.16):

$$(1 - 2P_{LZ})(\cos 2\theta_m(n_f) - \cos 2\theta_m(n_i)) = 1 \ , \tag{2.21}$$

where we have averaged out the interference terms. Then instead of eq. (2.17) we get

$$\Delta n = n_e^{res} \frac{1}{\sqrt{16P_{LZ}^2 - 16P_{LZ} + 3}} \tan 2\theta \ . \tag{2.22}$$

Finally, the condition for $d_{1/2}$ can be written as:

$$d_{1/2} = \frac{4}{\pi\gamma\sqrt{16P_{LZ}^2 - 16P_{LZ} + 3}} d_{min} \ . \tag{2.23}$$

For $\gamma \to 0$ eq. (2.23) gives $d_{1/2} \to \infty$, according to the fact that the density changes very slowly and therefore the width needed to have significant conversion increases. With the increase of γ the width $d_{1/2}$ decreases and has a minimum at $\gamma \simeq 0.7$, for which we find $d_{1/2} \simeq 1.5\, d_{min}$. With further increase of γ ($\gamma \gtrsim 0.7$) the width $d_{1/2}$ increases rapidly. According to (2.23) it diverges for $P \to 1/4$, when $\gamma \to \pi/(4 \ln 2) \simeq 1.13$. This value corresponds to the case in which the adiabaticity violation is so strong that even an infinite amount of matter is not enough to satisfy the condition (2.10). Thus, we have found that also in this case $d_{1/2} > d_{min}$.

2.1.4 Step-like and castle-wall profile

As an extreme case of strong adiabaticity violation, let us consider the profile consisting of two layers of matter, having densities $n_1 = n_e^{res} + \Delta n$ and $n_2 = n_e^{res} - \Delta n$ ($\Delta n \geq 0$), and equal lengths $L_1 = L_2 = L$. At the border between the layers the density has a jump of size $2\Delta n$. We fix $L = l^{res}/8$, so that $d = d_{min}$. The result for the conversion probability can be computed exactly:

$$P^{step}_{\nu_e \to \nu_\mu} = s^2 \sin^2\left(\frac{\pi}{4s}\right) + s^2 c^2 \left[1 - \cos\left(\frac{\pi}{4s}\right)\right]^2 \ , \tag{2.24}$$

where we denote the mixing parameters in the two layers as $\sin 2\theta_{2m} = \sin 2\theta_{1m} \equiv s$, $\cos 2\theta_{2m} = -\cos 2\theta_{1m} \equiv c$. In absence of the step ($\Delta n = 0$), $P^{step}_{\nu_e \to \nu_\mu}$ equals $1/2$, recovering the case $n_e = n_e^{res} = \text{const}$. The probability (2.24) decreases monotonically as Δn increases. Expanding in $\delta = (\Delta n / n_e^{res} \tan 2\theta)^2$ we get[4]:

$$P^{step}_{\nu_e \to \nu_\mu} \simeq \frac{1}{2} - (\sqrt{2} - 1 - \frac{\pi}{8})\delta \simeq \frac{1}{2} - 0.02\,\delta \ . \tag{2.25}$$

According to (2.25), for $d = d_0$ we have $P^{step}_{\nu_e \to \nu_\mu} < 1/2$. This implies that, to have $P^{step}_{\nu_e \to \nu_\mu} = 1/2$ one needs $d_{1/2} > d_{min}$.

A generalization of the step-like profile is given by the castle-wall profile. This consists of a periodical sequence of alternate layers of matter, having two different densities n_1 and n_2. We denote the corresponding mixing angles as θ_{1m} and θ_{2m}. In this case, a strong transformation requires certain conditions on the oscillation phases acquired by neutrinos in the layers[74]; therefore the transformation is a consequence of the specific density profile, rather than of an enhancement of the mixing. Suppose $n_1 \ll n_e^{res}$ and $n_2 = 0$, and take the width of each layer to be equal to half oscillation length, so that the oscillation phase acquired in each layer is π. It can be shown[75] that for small θ this is the condition under which the conversion probability increases most rapidly with the distance. As a function of the number N of periods (a period corresponds to two layers), the probability is given by[76, 75]:

$$P_{\nu_e \to \nu_\mu}(N) = \sin^2(2N\Delta\theta) \ , \tag{2.26}$$

where $\Delta\theta \equiv \theta_{1m} - \theta_{2m} = \theta_{1m} - \theta$. Using the approximation $2\theta_{1m} - 2\theta \simeq \sin 2\theta_{1m} - \sin 2\theta$, and expanding $\sin 2\theta_{1m}$ in n_1, we get:

$$d_{1/2} = \frac{\pi^2}{2\sqrt{2}G_F} \frac{1}{\sin 2\theta} \simeq \pi d_{min} \ . \tag{2.27}$$

Again, we find that $d_{1/2} \geq d_{min}$.

Thus, for all the known mechanisms of matter enhancement of flavour transition (resonant oscillations, adiabatic conversion, parametric effects), we have found that the width $d_{1/2}$ is larger than d_{min}, which is realized for the case of uniform medium with resonance density. In fact the constant profile with resonance density could be expected from the beginning to represent an extreme case: this profile is singled out, since it is the simplest distribution with the density fixed at the unique value n_e^{res}.

[4]This approximation proves to be very good (relative error $\leq 0.5\%$) for $0 \leq \delta \leq 1$, i.e. for n_1 and n_2 in the resonance interval.

It is worthwile to introduce also the total nucleon width. Let us consider a medium made of electrons, protons and neutrons with number densities n_e, n_p and n_n. Defining the number of electrons per nucleon as $Y_e \equiv n_e/(n_n + n_p)$, we can write the total nucleon width that corresponds to d_0 as:

$$d_{0N} \equiv \frac{d_0}{Y_e} \ . \tag{2.28}$$

We can also introduce the total mass width d_ρ:

$$d_\rho \equiv m_N d_{0N} = \frac{m_N d_0}{Y_e} \ . \tag{2.29}$$

For electrically and isotopically neutral medium ($n_e = n_n = n_p$), eq. (2.28) gives:

$$d_{0N} = 2d_0 \ , \tag{2.30}$$

and numerically:

$$d_{0N} = 4.9 \cdot 10^{32} \mathrm{cm}^{-2} \ , \qquad d_\rho = 8.16 \cdot 10^8 \ \mathrm{g} \cdot \mathrm{cm}^{-2} \ . \tag{2.31}$$

Several generalizations of the arguments of this section are possible. In particular, we refer to [25] for the derivation of the minimum width required for active-sterile coversion, neutrino oscillations induced by flavour changing interactions and the conversion of high-energy neutrinos, in which propagator corrections are important. The case of neutrinos propagating in a neutrino background is discussed in refs. [25, 54] and in the chapter 3.

2.2 The minimum width condition and some applications

2.2.1 Minimum width and bounds on the mixing

As follows from the analysis in section 2.1, a significant neutrino conversion in matter requires the fulfilment of the minimum width condition[5]:

$$d \geq d_{min} = \frac{d_0}{\tan 2\theta} \ , \tag{2.32}$$

[5]This condition refers to the requirement of conversion probability larger than 1/2, eq. (2.2). In some circumstances, however, even a small effect, with conversion probability $P \ll 1/2$ can be important.

and therefore of the less stringent bound:

$$r \equiv \frac{d}{d_0} \geq 1 \ . \tag{2.33}$$

These conditions are independent of the density distribution, and therefore of the specific matter effect involved. Thus the knowledge of the width d allows one to conclude about the significance of the matter effect even if the density profile is unknown. This is the case of some astrophysical objects for which estimates or bounds on d can be obtained directly by observational data with no assumption on their internal structure.

In the Table 2.1 we show the parameters of interest of some objects, toghether with the values of the ratio r. For $r \gtrsim 1$, (eq. 2.33), the condition (2.32) can be fulfilled and gives the bound on the mixing:

$$\sin 2\theta \gtrsim \frac{1}{r} = \frac{d_0}{d} \ . \tag{2.34}$$

Notice that our analysis holds for small mixings: $\sin 2\theta \ll 1$. For applications we assume $\sin 2\theta \lesssim 0.3$, for which we find from eq. (2.34) that the minimum width condition is satisfied for $r \gtrsim 3$.

The inequality (2.34) can be considered as the sensitivity limit for the mixing angle that can be achieved by studies of neutrino conversion in a layer of given width d. The real sensitivity can be however much lower than the absolute limit given by the condition (2.34). This is related to the fact that in the case of varying density only part of the total amount of matter effectively contributes to the conversion. Introducing the corresponding width d^{conv} we have the condition:

$$\sin 2\theta \gtrsim \frac{d_0}{d^{conv}} \ , \tag{2.35}$$

instead of the (2.34).

Let us find the expression of d^{conv} for a medium with monotonically varying density. As discussed in section 2.3, the transition occurs mainly in the resonance layer. Using the result (2.17) we get:

$$d^{conv} = n_e^{res} \frac{dL}{dn} 2\Delta n = \frac{2}{\sqrt{3}} n_e^{res} l_n \tan 2\theta \ , \tag{2.36}$$

where $l_n \equiv |(\frac{dn}{dL})^{-1}|_{res} n_e^{res}$. Inserting the expression (2.36) in the condition (2.35), we find:

$$\sin^2 2\theta \gtrsim \frac{\sqrt{3} d_0}{2 n_e^{res} l_n} \ . \tag{2.37}$$

Clearly, d^{conv} could be much smaller than the total width d of the object, so that the condition (2.37) on the mixing could be much stronger than (2.34). Notice that the

bound (2.37) is quadratic in $\sin 2\theta$. Using the definition (1.32) of the adiabaticity parameter, $\chi_R = \gamma^{-1}$, the condition (2.37) can be written as $\gamma \leq 4/(\pi\sqrt{3})$, which corresponds to the adiabaticity condition close to its limit of validity.

Another important issue is that the maximal sensitivity for the mixing θ can be achieved for particular values of $\Delta m^2/E$, which depend on the specific density profile. As follows from (2.37), for constant (or slowly varying with the distance) l_n the smallest $\sin^2 2\theta$ corresponds to the largest n_e^{res}, and therefore to the largest values of $\Delta m^2/E$. This is the case of exponential density profile. For power-law profile, $n_e \sim L^{-k}$, we get $|l_n| = L/k$, so that $\sin^2 2\theta \sim L^{k-1}$. Taking $k > 1$, fulfilled by practically all the realistic profiles, we find that the smallest θ is achieved for the smallest L, and consequently the highest values of n_e and $\Delta m^2/E$.

Notice that d^{conv} is a local property which depends on the derivative in l_n. Of course, the description given by d^{conv} is not correct when the density profile is close to the constant one, so that $l_n \to \infty$. In this case d^{conv} can be even larger than the total width d. Thus, the correct condition on the mixing can be written as:

$$\sin 2\theta \gtrsim \frac{d_0}{min\,[d, d^{conv}]} \,. \tag{2.38}$$

2.2.2 The Sun, the Earth, the Moon and supernovae

For neutrinos crossing the Earth we consider two types of trajectories, corresponding to different values of the zenith angle θ_z. For $\cos\theta_z$=1 neutrinos travel along the diameter of the Earth, crossing the core and the two layers of the mantle. We get r =13.6, and therefore according to (2.34) we could expect significant matter conversion for $\sin^2 2\theta \gtrsim 5 \cdot 10^{-3}$. However this maximal sensitivity, which would be achieved for uniform density distribution, is not realized for the Earth profile. For small mixing, the difference between the densities in the core and in the mantle is larger than the resonance interval. As a result, the oscillations are resonantly enhanced either in the mantle or in the core, and only one of the two parts effectively contributes to the effect. At the same time, for certain ranges of $\Delta m^2/E$, different from both the resonance values in the core and in the mantle, parametric enhancement of oscillations occurs. Numerical calculations (see e.g. [57]) give $\sin^2 2\theta \gtrsim 2 \cdot 10^{-2}$ as best sensitivity.

For $\cos\theta_z$=0.81 the trajectory is tangential to the core, and therefore it represents the path of maximal length in the mantle. In this case we find r $\simeq$6.4 and the sensitivity limit $\sin^2 2\theta \gtrsim 2.5 \cdot 10^{-2}$. Since this case realizes approximatively the optimal condition of uniform medium, we have good agreement with the results of exact calculations.

In the case of the Moon, r =1.4, and therefore a large mixing is required: $\sin^2 2\theta \gtrsim$0.5.

object	density (cm^{-3})	size (cm)	$r = d/d_0$
Earth:			
$\cos\theta_z = 1$	$2.6 \cdot 10^{24}$	$1.26 \cdot 10^9$	13.6
$\cos\theta_z = 0.81$	$1.5 \cdot 10^{24}$	10^9	6.4
Sun	$\sim 7 \cdot 10^{24}$	$6.96 \cdot 10^{10}$	2600
Moon	$\sim 10^{24}$	$3.48 \cdot 10^8$	1.4
Supernova	$3 \cdot 10^{33}$	10^7	10^9
Universe			
$(n_\nu = n_{\bar{\nu}})$	$1.5 \cdot 10^4$	10^{27}	$3 \cdot 10^{-2}$
Universe			
$(n_\nu \gg n_{\bar{\nu}})$	$\sim 10^5$	10^{27}	0.3
AGN		$d \simeq 10^{22} \div 10^{23}\mathrm{cm}^{-2}$	$10^{-10} \div 10^{-9}$
GRB	$10^{10} \div 10^{12}$	$< 5 \cdot 10^{15}$	$< 10^{-5}$

Table 2.1: The density, the size and the matter width in units of refraction width, $r = d/d_0$, for various physical objects. The values given for the densities are averaged along the trajectories of the neutrinos. We quote the number density of electrons for objects made of usual matter, and the concentration of the neutrino background for the universe [25]. For the Earth the results are given for two trajectories with different zenith angle θ_z. The results for the universe correspond to redshift $z = 5$ for the cases of $\nu_\alpha - \nu_s$ and $\bar{\nu}_\alpha - \bar{\nu}_s$ in CP-symmetric and strongly CP-asymmetric neutrino background with $\eta_\nu \simeq 1$ [25].

A numerical integration of the density profile of the Sun[77] gives $d \simeq 1.5 \cdot 10^{12}\mathrm{g} \cdot \mathrm{cm}^{-2}$. Dividing this result by $d_\rho = m_N d_{0N}$, with $Y_e = 0.7$, we find $r \simeq 2600$. From the condition (2.34) we get then $\sin^2 2\theta \gtrsim 1.5 \cdot 10^{-7}$. This bound is remarkably weaker than the one obtained from the condition (2.37): taking $n_e^{res} \simeq 50 A\,\mathrm{cm}^{-3}$ and $l_n \simeq 0.3 R_\odot$, we get $\sin^2 2\theta \simeq 2.4 \cdot 10^{-4}$, in good agreement with the results of exact computations[8, 57].

For supernovae the total width of the matter above the neutrinosphere gives $r \simeq 10^9$, for which the condition (2.34) would lead to $\sin^2 2\theta \gtrsim 10^{-18}$. Using the density profile $n_e = n_e^0 (R_0/R)^3$[21], with $R_0 = 10^7$ cm and $n_e^0 \simeq 10^{34}\mathrm{cm}^{-3}$, from (2.37) we find $\sin^2 2\theta \gtrsim 10^{-8}$, which agrees well with the results of numerical calculations[57].

As shown in the previous examples, the maximal sensitivity for $\sin^2 2\theta$, given by the total width d, can be achieved in the case of uniform medium at $\Delta m^2/E$ corresponding to the resonance density. Such a situation is realized for neutrinos crossing the mantle of the Earth. In the case of substantial deviations from the constant density, like in the Sun or in supernovae, the sensitivity is much lower. The stronger the deviation from constant density, the smaller d^{conv}, and therefore the lower is the sensitivity.

2.2.3 AGN, GRBs and integalactic medium

Let us now turn to high energy neutrinos from Active Galactic Nuclei (AGN) and Gamma Ray Bursters (GRBs).

In AGN, neutrinos are considered to be produced by the interaction of accelerated protons with a photon or proton background[32, 34, 33].

The width of matter crossed by neutrinos in an AGN can be estimated on the basis of the existing data on the X-ray emission of these objects. The variability of the spectra suggests that the X-radiation is emitted very close to the AGN core[78]. The proton acceleration and therefore the neutrino production are supposed to happen in the same region. For this reason the width of matter crossed by neutrinos equals approximatively the one crossed by the X-radiation. For the later the experimental data[79, 80, 81] give the value $d_{AGN} \simeq (10^{-2} \div 10^{-1})\ A\ \mathrm{cm}^{-2}$, therefore significant neutrino conversion in AGN is excluded[6] (for a short discussion, see also ref.[82]).

A rather successful description of the origin of GRB is provided by the fireball model[83], in which neutrino production is predicted to happen in an analogous way as in AGN[41, 42, 43]. A fireball can emit protons, detected as high-energy cosmic rays on Earth, accompanied by a flux of neutrinos. The requirement that the fireball should be transparent to protons gives an estimate of the width of the object: $d_{GRB} \leq d_{abs}$, where $d_{abs} = 10 \div 100\ A\,\mathrm{cm}^{-2}$ is the total absorption width for the protons. It is possible to evaluate the width in a different way. An estimate of the electron number density in the fireball is given in ref.[41]: $n_{GRB} \simeq (10^{10} \div 10^{12})$ cm^{-3}. Using this value, and taking the fireball mass in the range of star-like objects, $M = (1 \div 10)\, M_{\odot}$, we can get the radius of the object, $R_{GRB} = 5 \cdot (10^{14} \div 10^{15})$ cm, and then the width: $d_{GRB} = 10 \div 10^{4}\ A\ \mathrm{cm}^{-2}$. In agreement with the first argument, we see, then, that also in GRBs the matter effect on neutrino conversion is negligible.

Besides the matter of the source, high energy neutrinos from extragalactic objects cross the intergalactic medium and the dark matter halos of galaxies or clusters of galaxies. In these media the dominant contribution to matter effects is given by the background of relic neutrinos. For dark matter halos the minimum width condition can be satisfied only in the extreme case of very large clusters of galaxies [25] and will not be presented in this work. The propagation in the neutrino background of the intergalactic medium has interesting aspects and will be discussed in detail in the next chapter.

[6] In the present discussion we have considered radial propagation of neutrinos from the inner to the external regions of the object. We have not considered neutrinos travelling through the core of the AGN. In this case a significant matter-induced conversion could occur, however neutrinos crossing the core are supposed to be a small fraction of the total neutrino flux produced.

Chapter 3

High-energy neutrino conversion and the lepton asymmetry in the universe

In this chapter we study the possible matter effects on oscillations of high energy cosmic neutrinos. Applying the criterion given in the previous chapter, we find that the only type of matter which can produce significant effect is a strongly CP-asymmetric neutrino background, provided that the source of the high energy neutrino flux is at cosmological distances. The dynamics of the propagation of high energy neutrinos in the neutrino background is studied in detail and the possibility of observing the matter effect is discussed.

3.1 Neutrinos in the Universe

3.1.1 The relic neutrino background: CP asymmetry

Let us describe the relic neutrino gas by the number densities of the various flavours, n_α ($\alpha = e, \bar{e}, \mu$, etc.), and by the CP-asymmetry η_ν defined as:

$$\eta_\nu \equiv (n_\alpha - n_{\bar{\alpha}})/n_\gamma \ , \tag{3.1}$$

where n_γ is the concentration of photons.

The Big Bang Nucleosynthesis (BBN) and structure formation [84, 85] admit large CP-asymmetries for muon and tau neutrinos, while the asymmetry for the electron neutrino is strongly constrained:

$$|\eta_{\mu,\tau}| \lesssim 10 \ , \qquad -0.01 \lesssim \eta_e \lesssim 0.3 \ . \tag{3.2}$$

Large asymmetries have also important implications on the properties of the spectrum of the cosmic microwave background radiation (CMBR) [85]. The recent results

on the second acoustic peak of the CMBR from BOOMERANG and MAXIMA-1 experiments [86] seem to favour a large lepton asymmetry, $\eta_\nu \sim 1$ [87, 88, 89, 90]. In particular, a satisfactory interpretation of the data requires [88, 90]:

$$|\eta_{\mu,\tau}| \lesssim 1.1 \ , \qquad -2.5 \cdot 10^{-3} \lesssim \eta_e \lesssim 0.06 \ , \tag{3.3}$$

thus providing a stronger restriction of the allowed values of η_e, η_μ and η_τ with respect to (3.2). In our discussion we will consider asymmetries η_μ and η_τ as large as $|\eta_{\mu,\tau}| \sim 1$, according to the upper limit (3.3); however results will be given also for larger values, allowed by the less stringent bound (3.2).

We want to underline here that the realization of large CP-asymmetries in the individual lepton flavours is consistent with zero lepton asymmetry. This corresponds to:

$$\eta_e + \eta_\mu + \eta_\tau = 0 \ , \tag{3.4}$$

that is, to zero total lepton number. Large lepton asymmetry, in contrast, implies large CP-asymmetry.

In the presence of neutrino masses and mixing the flavour composition of the neutrino background changes with time, so that one expects the present values of the CP-asymmetries in the various flavours to be different from those at the epoch of BBN which are constrained by the bounds (3.2). For the discussion of the flavour evolution of the relic neutrino gas we refer to the Appendix A; in the following of the chapter we consider neutrinos produced in relatively recent epochs, with redshift $z \lesssim 50$, when the concentrations of neutrinos of the various flavours in the background have already settled down to the present values and do not change with time.

3.1.2 High-energy neutrinos across the universe: minimum width condition

Let us consider the interactions of high-energy neutrinos propagating from cosmological sources to the Earth. These neutrinos cross layers of matter in the source itself, then interact with particles in the interstellar and intergalactic media, and finally interact in the matter of our cluster of galaxies and of our galaxy.

In what follows we will discuss interactions in the intergalactic medium. The effects of the matter of the sources can be neglected [25]. As we will show later, for neutrino oscillation parameters and energies relevant for this discussion also the effect of the galactic halo and of the halo of the cluster of galaxies are very small [25].

As shown in chapter 2, the necessary condition for significant matter effect is the minimum width condition, eq. (2.33), which involves the refraction width d_0, eq. (2.5), and the width d of the medium, eq. (2.1).

Let us find the width of matter crossed by a beam of neutrino produced in the universe at the epoch t and propagating to the present epoch $t_0 \sim 10^{18}$ s. Using the scaling of the concentration of the medium, $n(t) \propto t^{-2}$, eq. (2.1) gives [25]:

$$d(t) = d_U \left[\frac{t_0}{t} - 1\right] \simeq d_U \left[(1+z)^{\frac{3}{2}} - 1\right] , \tag{3.5}$$

$$d_U \equiv t_0 n_0 , \tag{3.6}$$

where n_0 is the present concentration of the background and we have introduced the redshift $z \equiv (t_0/t)^{2/3} - 1$.

Let us evaluate the ratio $r \equiv d/d_0$ for different components of the intergalactic medium and study the fulfillment of the condition (2.33) .

1). Due to the very small concentration of nucleons and electrons, the width of these components is extremely small, $d_B/d_0 \ll 1$, even for neutrinos produced at cosmological distances. Indeed, the baryon concentration can be estimated as $n_B = n_\gamma \eta_B$ where $\eta_B = 10^{-10} - 10^{-9}$ is the baryon asymmetry of the universe and n_γ the photon concentration. At present time $n_\gamma = n_\gamma^0 \simeq 412$ cm^{-3}. Taking, e.g., production epoch $z \simeq 1$ we find from eqs. (3.5)-(2.5) that for baryons $r \equiv r_B \sim 10^{-11}$.

2). The scattering on the electromagnetic background has negligible effect due to the smallness of interaction. The neutrino-photon potential is of the second order in the Fermi constant and depends on the energy of the neutrino beam and on the temperature and concentration of the photon gas [91, 92]. Using the results of ref. [92] (see also the discussion in [93]) we find from eqs. (3.5)-(2.5) $r_\gamma \lesssim 10^{-8}$ for neutrino energy $E \lesssim 10^{21}$ eV and production epoch $z \simeq 1$.

3). The effect of the scattering on the neutrino background can produce significant effect if the background has large CP-asymmetry[1]. Indeed, for asymmetry $\eta_\nu \sim 1$ we get $d_\nu \sim d_0$. Clearly, if the lepton asymmetry is of the order of the baryon one, $\eta_\nu \simeq \eta_B$, the width is negligibly small: $d_\nu \sim d_B \ll d_0$.

Let us consider the minimum width condition for neutrino background in more detail. The effective potential due to the scattering of neutrinos on the relic neutrino

[1]For CP-symmetric background significant effects can appear at large temperature, $T \gtrsim 1$ MeV, due to thermal effects [62], or at extremely high neutrino energies, due to neutrino-antineutrino scattering in the resonant Z^0 channel [25].

background can be written as

$$V = F\eta_\nu \sqrt{2} G_F n_\gamma \ , \tag{3.7}$$

where F is a constant of order 1 which depends on the specific conversion channel (see sections 3.2 and 3.3). With the potential (3.7), eqs. (3.5), (2.33) and (2.5) give the condition:

$$r(z) = 1.6 \cdot 10^{-2} |F| \eta_\nu \left[(z+1)^{\frac{3}{2}} - 1 \right] \geq 1 \ . \tag{3.8}$$

For neutrinos produced in the present epoch, $z \simeq 0$ and values of η_ν allowed by the bounds (3.2)-(3.3) the condition (3.8) is not satisfied: $r(z \sim 0) \ll 1$. From (3.8) we can define the epoch z_d which corresponds to $r = 1$:

$$1 + z_d = \left[1 + \frac{1}{1.6 \cdot 10^{-2} |F| \eta_\nu} \right]^{\frac{2}{3}} \ , \tag{3.9}$$

so that for neutrinos produced at $z \geq z_d$ the minimum width condition is fulfilled. Taking for instance $\eta_\nu = 1$ and $F = 2$ we get $z_d \simeq 9$; by requiring $r \simeq 0.3$ (which corresponds to 10% matter effect [25]) we find $z_d \simeq 3.7$.

The following remark is in order. As discussed in chapter 2 the condition (2.33) is necessary but not sufficient to have significant matter effects. In particular the width needed to have conversion probability larger than 1/2 is $d_{min} > d_0$, with d_{min} given in eq. 2.4, for uniform media (and small mixing angle, $\sin 2\theta \lesssim 0.3$), and larger than d_{min} for media with varying density.

We conclude, then, that the only component of the intergalactic medium which can produce a significant matter effect is a strongly CP-asymmetric neutrino background, with $\eta_\nu \gtrsim 1$. Moreover, cosmological epochs of neutrino production are required: $z \gtrsim 3$.

3.2 High energy neutrino conversion: the active-active case

Let us consider three mixed active neutrinos, ν_e, ν_μ, ν_τ, and find the potential for a beam of high energy neutrinos ("beam neutrinos") due to the interaction with the relic neutrino background ("background neutrinos").

3.2.1 The refraction potential

As we discuss in Appendix A, the decoherence due to the spread of wavepackets implies that the background neutrinos are in mass eigenstates. As a consequence,

the matrix of potentials, V_ν, for the beam neutrinos propagating in this background is not diagonal in the flavour basis, $(\nu_e, \nu_\mu, \nu_\tau)$. It is possible to check [94] that V_ν becomes diagonal in the basis of the mass eigenstates, (ν_1, ν_2, ν_3), where it can be written as:

$$\begin{aligned} V_\nu &= \sqrt{2}G_F\left[(n_1 - n_{\bar{1}}) + (n_2 - n_{\bar{2}}) + (n_3 - n_{\bar{3}})\right] \\ &+ \sqrt{2}G_F \begin{pmatrix} n_1 f(-s_Z^{(1)}) - n_{\bar{1}} f(s_Z^{(1)}) & 0 & 0 \\ 0 & n_2 f(-s_Z^{(2)}) - n_{\bar{2}} f(s_Z^{(2)}) & 0 \\ 0 & 0 & n_3 f(-s_Z^{(3)}) - n_{\bar{3}} f(s_Z^{(3)}) \end{pmatrix} , \end{aligned} \tag{3.10}$$

where n_i ($n_{\bar{i}}$) denotes the concentration of the mass state ν_i ($\bar{\nu}_i$) in the background and $f(s_Z^{(i)})$ is the Z-boson propagator function:

$$f(s_Z^{(i)}) \equiv \frac{1 - s_Z^{(i)}}{(1 - s_Z^{(i)})^2 + \gamma_Z^2} \, . \tag{3.11}$$

Here γ_Z and $s_Z^{(i)}$ are the normalized width of the Z-boson and total energy squared in the $\nu_i - \nu_i$ center of mass for non-relativistic background neutrinos:

$$s_Z^{(i)} \simeq \frac{2Em_i}{M_Z^2} \simeq 2.4 \cdot 10^{-2} \left(\frac{E}{10^{20}\text{eV}}\right)\left(\frac{m_i}{1\text{ eV}}\right) \, , \qquad \gamma_Z \equiv \frac{\Gamma_Z}{M_Z} \, , \tag{3.12}$$

with m_i being the mass of the neutrino ν_i and E the energy of the beam neutrino.

The terms in the first line of eq. (3.10) are due to neutral current $\nu - \nu$ scattering in the t-channel. The terms in the second line of eq. (3.10) represent the contributions of $\nu_i - \nu_i$ scattering with Z-boson exchange in the u-channel, and of $\nu_i - \bar{\nu}_i$ annihilation processes.

For $E \lesssim 10^{20}$eV and $m_i \lesssim 1$ eV the energy in the $\nu_i - \nu_i$ center of mass is much below the Z-boson resonance: $s_Z \lesssim 0.03$. In this case the propagator function (3.11) reduces to unity: $f(s_Z^{(i)}) \simeq f(-s_Z^{(i)}) \simeq 1$, and the neutrino-neutrino potential (3.10) becomes energy-independent.

For extremely high energies, $E \simeq 10^{21} - 10^{22}$eV, and neutrino mass of order 1 eV the propagator corrections become important. However, in this range of energies the absorption effects of the neutrino background are strong (see chapter 2). Therefore, the neutrino fluxes at Earth are largely suppressed. In what follows we will concentrate on the low energy limit, $s_Z^{(i)} \ll 1$, which is mainly relevant for applications.

For a beam of antineutrinos propagating in a neutrino background the potential $V_{\bar{\nu}}$ is given by eq. (3.10) with the replacement $n_i \to n_{\bar{i}}$ and vice-versa for all the ν_i states.

The fact that the neutrino-neutrino potential matrix, eq. (3.10), is diagonal in the basis of mass eigenstates has a straightforward consequence: the effect of refraction consists in a modification of the neutrino effective masses only. In terms of the present CP-asymmetries η_i^0 for the mass states ν_i of the background we find (for $s_Z^{(i)} \ll 1$) the following corrections:

$$\frac{\Delta m_{21}^2}{2E} \to \mathcal{E}_{21} \equiv \frac{\Delta m_{21}^2}{2E} + \sqrt{2} G_F n_\gamma (\eta_2^0 - \eta_1^0) \ ,$$
$$\frac{\Delta m_{32}^2}{2E} \to \mathcal{E}_{32} \equiv \frac{\Delta m_{32}^2}{2E} + \sqrt{2} G_F n_\gamma (\eta_3^0 - \eta_2^0) \ . \tag{3.13}$$

As it is shown in the Appendix A, the present composition of the neutrino background is determined by the initial flavour asymmetries, η_e, η_μ and η_τ, and by the mixing matrix U of the neutrino system. The expressions of $\mathcal{E}_{21}$ and $\mathcal{E}_{32}$ in terms of these quantities can be found from the results of the Appendix A (see section A.0.2). In particular, with the asymmetries (A.13) eq. (3.13) gives:

$$\mathcal{E}_{ji} = \frac{\Delta m_{ji}^2}{2E} + V_{ji}, \tag{3.14}$$
$$V_{ji} \equiv F_{ji} \eta \sqrt{2} G_F n_\gamma \ , \tag{3.15}$$
$$F_{21} = \cos 2\theta \ , \qquad F_{32} = \sin^2 \theta \ . \tag{3.16}$$

Here we denote as η the maximal flavour asymmetry, $\eta \equiv Max\{\eta_\mu, \eta_\tau, \eta_e\}$, which is realized in the background at the epoch of nucleosynthesis, $T \simeq T_{BBN}$; thus η is constrained by the bounds (3.2).

In eqs. (3.14)-(3.15) the information on the specific mixing matrix and initial composition of the background are encoded in the F factors. The dependence of F_{ji} on the mixing angle in eq. (3.16) is a consequence of expressing the potential (3.15) is terms of the flavour asymmetry η, while the background neutrinos are in mass eigenstates. For simplicity in what follows we will drop the indexes j, i from the quantities $\mathcal{E}$, V and F in the expressions (3.14)-(3.16).

3.2.2 The conversion probability

From the fact that the potential V modifies the effective mass eigenvalues, eqs. (3.14)-(3.16), it follows that the interaction with the neutrino background does not change the mixing matrix of the neutrino system, which remains the same as in vacuum. Conversely, the phase of oscillations is affected by the medium, so that the dynamics of the neutrino propagation consists in oscillations with constant depth, given by the vacuum mixing angle, and varying oscillation length. The probability P of conversion between two active neutrinos, ν_α, ν_β, with mixing angle θ equals:

$$P(t, t_i) = \sin^2 2\theta \sin^2 \left(\frac{\Phi}{2} \right) \ , \tag{3.17}$$

and the oscillation phase Φ is given by:

$$\Phi(t, t_i) = \int_{t_i}^{t} \mathcal{E}(\tau) d\tau \ . \tag{3.18}$$

We denote as t_i, t the initial and final time of the evolution of the system; $\mathcal{E}$ is given in eq. (3.14). Using the scaling relations:

$$E = E_0 (t_0/t)^{2/3} = E_0 (1+z) \ , \quad V = V_0 (t_0/t)^2 = V_0 (1+z)^3 \ , \tag{3.19}$$

where E_0 and V_0 are the energy and the potential at the present epoch, $z = 0$, we get:

$$\Phi = \Phi_{vac} + \Phi_{matt} \ , \tag{3.20}$$

with the following expressions for the vacuum oscillation phase, Φ_{vac}, and the matter contribution Φ_{matt}:

$$\Phi_{vac}(x, x_i) = \frac{3}{10} \frac{\Delta m^2 t_0}{E_0} \left(x^{\frac{5}{3}} - x_i^{\frac{5}{3}} \right) \ , \tag{3.21}$$

$$\Phi_{matt}(x, x_i) = V_0 t_0 \left(\frac{1}{x_i} - \frac{1}{x} \right) \ . \tag{3.22}$$

We defined $x \equiv t/t_0$ and $x_i \equiv t_i/t_0$.

The matter induced phase, Φ_{matt}, depends only on the characteristics of the background and on the initial and final moments of time. In particular for early production epochs, $x_i \ll 1$, one gets:

$$\Phi_{matt} \simeq V_0 t_0 \frac{1}{x_i} \ , \tag{3.23}$$

which shows that the phase Φ_{matt} is accumulated mainly at the production time.

Being independent of $E_0/\Delta m^2$, the phase Φ_{matt} becomes comparable or even larger than the vacuum oscillation phase, Φ_{vac}, at very high energies, $E_0/\Delta m^2 \gtrsim 10^{32}$ eV^{-1}. Taking $x_i = 0.125$, corresponding to production at redshift $z \simeq 3$, and $x = 1$ we have $\Phi_{vac} \simeq 0.23\pi$ for $E_0/\Delta m^2 \simeq 10^{32}$ eV^{-1}. This is comparable to the matter phase, $\Phi_{matt} \simeq 0.29\pi$ given by eqs. (3.22) and (3.15) with $F\eta \simeq 10$. As $E_0/\Delta m^2$ increases the vacuum phase Φ_{vac} decreases and the total oscillation phase is dominated by the matter contribution Φ_{matt}. From eqs. (3.17) and (3.22) we find the asymptotic value of the conversion probability[2]:

$$P(E_0/\Delta m^2 \to \infty) = \sin^2 2\theta \sin^2 \left(\frac{1}{2} V_0 t_0 \left(\frac{1}{x_i} - \frac{1}{x} \right) \right) \ . \tag{3.24}$$

[2]Even though eq. (3.24) gives a a non-zero value for the conversion probability in the limit $\Delta m^2 \to 0$, the matter effect we are describing requires massive non-degenerate neutrinos: $\Delta m^2 \neq 0$. This condition is necessary for our starting point (section 3.2.1, see eq. (3.10)) that the neutrinos in the background are in mass eigenstates (different from the flavour ones), produced from flavour states by the spread of the wavepackets during the evolution of the universe. Thus, the expression (3.24) should be intended as the high-energy limit of the conversion probability for a given (non-zero) value of Δm^2.

Notice that the expression (3.24) is insensitive to the change of sign of the potential V_0 (i.e. of the product $F\eta$): this implies that in the limit of very high energies a beam of neutrinos and one of antineutrinos will experience the same matter effect.

In fig. 3.1 we show the survival probability, $1 - P$, as a function of $E_0/\Delta m^2$ for neutrinos produced at $z = 3$ and arriving at Earth at the present epoch, with $\sin^2 2\theta = 0.5$ and various values of the product $F\eta$. The figure was produced by averaging the conversion probability, eq. (3.17), over the interval $\Delta E_0 \simeq E_0$, keeping in mind the finite accuracy in the reconstruction of the neutrino energy in the detector:

$$P(E_0) = \frac{1}{\Delta E_0} \int_{E_0/2}^{3E_0/2} dE' P(E') \ . \tag{3.25}$$

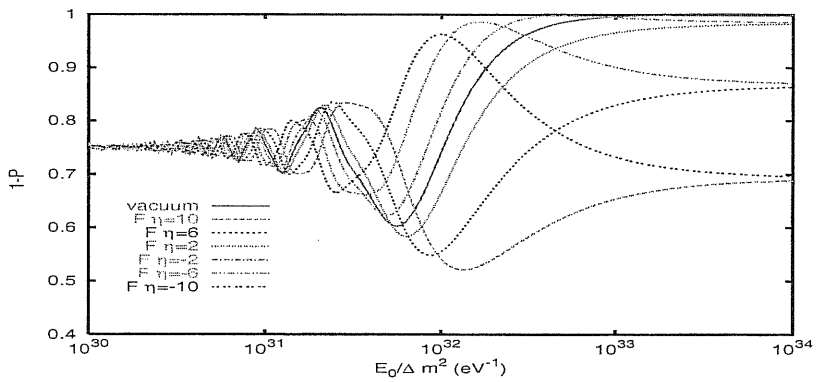

Figure 3.1: The survival probability $1 - P(\nu_\alpha \to \nu_\beta)$ as a function of the ratio $E_0/\Delta m^2$ for various values of $F\eta$. We have taken $\sin^2 2\theta = 0.5$ and production epoch $z = 3$.

Let us comment on the figure 3.1. In absence of asymmetry, $F\eta = 0$, the conversion is given by vacuum oscillations ($\Phi_{matt} = 0$). For $E_0/\Delta m^2 \gtrsim 10^{32}$ eV^{-1} the vacuum oscillation phase Φ_{vac} is very small, thus the conversion probability approaches the unity.

For strongly CP-asymmetric neutrino background the matter induced phase Φ_{matt} is sizeable. In consequence, the deviation of the survival probability $1 - P$ from the value given by vacuum oscillations can be as large as $\sim 30\%$. Clearly, as it follows from eq. (3.17), a strong effect requires a large mixing angle: if $\sin^2 2\theta \ll 1$ the effect of matter on the oscillation phase will be unobservable due to the very small amplitude of oscillations. At extremely high energies, $E_0/\Delta m^2 \gtrsim 10^{33}$ eV^{-1}, the deviation is constant and independent of the sign of $F\eta$, according to eq. (3.24).

3.3 High energy neutrino conversion: the active-sterile case

Let us consider the case in which a sterile neutrino ν_s is mixed with the active flavours, ν_α. We discuss here two-neutrino mixing; a generalization to a four-neutrino framework will be given in section 3.5.

3.3.1 The refraction potential

In contrast to the active-active conversion studied in section 3.2, for an active-sterile neutrino system the matrix of the refraction potentials is diagonal in the flavour basis (ν_α, ν_s):

$$V_\nu = \begin{pmatrix} V_\alpha & 0 \\ 0 & 0 \end{pmatrix} . \tag{3.26}$$

In the low energy limit, $s_Z \ll 1$, the potential V_α depends on the flavour asymmetries η_e^0, η_μ^0 and η_τ^0 as follows:

$$V_\alpha = \sqrt{2} G_F n_\gamma \left[\eta_\alpha^0 + \sum_{\beta=e,\mu,\tau} \eta_\beta^0 \right] . \tag{3.27}$$

The potential (3.27) can be written in the same general form as eq. (3.15):

$$V = F \eta \sqrt{2} G_F n_\gamma , \tag{3.28}$$

with the same definition of η as the maximal flavour asymmetry in the background at the epoch of nucleosynthesis, $\eta \equiv Max\{\eta_\mu, \eta_\tau, \eta_e\}$. The factor F depends on the specific conversion channel and the flavour content of the background:

$$F \equiv \frac{1}{\eta} \left[\eta_\alpha^0 + \sum_{\beta=e,\mu,\tau} \eta_\beta^0 \right] , \qquad \text{for } \nu_\alpha - \nu_s \text{ channel} . \tag{3.29}$$

Let us consider for instance the conversion of ν_e to ν_s. Using the results for the present flavour asymmetries given in the Appendix A (eqs. (A.20) and (A.22)) we get:

$$F = 2 \left(1 + \frac{\eta_e}{\eta} \sin^2 \theta \right) , \tag{3.30}$$

for the case in which the $\nu_e - \nu_s$ conversion in the background occurred in the resonance channel. Here we considered $\eta_\mu, \eta_\tau \geq \eta_e$. If the $\nu_e - \nu_s$ conversion in the background proceeded in the non-resonant channel (see eq. (A.21) of the Appendix A) one finds a form for the factor F analogous to eq. (3.30) with the replacement $\sin^2 \theta \to \cos^2 \theta$.

For conversion of antineutrinos the $\bar{\nu} - \nu$ potential has opposite sign: $V_{\bar{\nu}} = -V_\nu$. Thus the expression (3.28) holds with the replacement $F \to -F$.

3.3.2 The dynamics of neutrino conversion

Due to the expansion of the universe the cosmological neutrinos experience a potential which changes with time. In contrast with the active-active case, the effect of medium changes both the oscillation length and the mixing angle θ. The dynamics of the flavour transition is determined by the resonance and adiabaticity conditions, eqs. (1.20) and (1.25).

Using eq. (3.28) and the scaling relations (3.19), from the resonance condition (1.20) we get the following relations:

- The present energy of neutrinos which cross the resonance at the epoch z equals:

$$E_0 = 10^{20}\text{eV}\left(\frac{\Delta m^2}{10^{-10}\text{eV}^2}\right)\frac{10^4\cos 2\theta}{F\eta(1+z)^4}\ . \tag{3.31}$$

- For a given E_0 and Δm^2 the redshift z_R at which the resonance condition was realized is given by:

$$1+z_R = 10\left[\frac{\cos 2\theta}{F\eta\,(10^{-10}\text{eV}^2/\Delta m^2)\,(E_0/10^{20}\text{eV})}\right]^{\frac{1}{4}}\ . \tag{3.32}$$

- Neutrinos produced at a distance z undergo resonance if their present energy is in the interval:

$$E_0 = 10^{20}\text{eV}\left(\frac{\Delta m^2}{10^{-10}\text{eV}^2}\right)\frac{10^4\cos 2\theta}{F\eta}\left[\frac{1}{(1+z)^4}\ ,\ 1\right]\ . \tag{3.33}$$

  Taking $F\eta = 10$, $\cos 2\theta \simeq 1$, $\Delta m^2 = 10^{-10}\text{eV}^2$ and $z = 3$ from eq. (3.33) we find $E_0 \simeq 4\cdot 10^{20} - 10^{23}\text{eV}$. With the same values of the parameters and $E_0 = 10^{20}\text{eV}$ we get that the resonance condition (3.31) is satisfied at $z_R \simeq 4.6$.

The adiabaticity condition involves the time variation of both the neutrino energy and the concentration of the neutrino background. In terms of the adiabaticity parameter at resonance, χ_R, it is written as:

$$\begin{aligned}&\chi_R \gg 1\\ &\chi_R \equiv \frac{(\Delta m^2)^2}{4E}\sin^2 2\theta\left[\frac{d}{dt}(EV)\right]^{-1}\Bigg|_{res}\ ,\end{aligned} \tag{3.34}$$

where the subscript "*res*" indicates that the various quantities are evaluated at resonance, i.e. when the condition (1.20) is fulfilled. With the potential (3.28), using the scalings (3.19) and the resonance condition (1.20), we find:

$$\chi_R \simeq 10^{-2}F\eta\tan^2 2\theta(1+z_R)^{\frac{3}{2}}\ . \tag{3.35}$$

For $F\eta \lesssim 10$, $\tan^2 2\theta = 1$ and $z_R \lesssim 5$ one finds $\chi_R \lesssim 1.4$. Thus, for neutrinos produced at epochs $z < 5$, we expect breaking of the adiabaticity. Notice that χ_R does not depend explicitly on the neutrino energy and mass squared difference; it increases with η and z_R.

From eq. (3.35) we get the redshift z_a corresponding to $\chi_R = 2\pi \gg 1$:

$$1 + z_a \equiv \left[\frac{2\pi \cdot 10^2}{F\eta \tan^2 2\theta}\right]^{\frac{2}{3}} . \tag{3.36}$$

If the resonance condition is fulfilled at $z \geq z_a$ the level crossing (resonance) proceeds adiabatically. Taking $F\eta = 10$ and $\tan 2\theta = 1$ we find $z_a \simeq 15$.

For $\eta \gtrsim 1$ and $\tan 2\theta \leq 1$ we have $z_a \geq z_d$. Thus, we can define three epochs of neutrino production, corresponding to different characters of the evolution of the neutrino beam:

(i) Earlier epoch: $z > z_a$, when both adiabaticity and the minimum width conditions are satisfied. If also the resonance condition is fulfilled at $z_R > z_a$ the neutrinos will undergo strong resonance conversion. Otherwise, if the resonance condition is not realized (e.g., due to a large value of $\Delta m^2/E$) the matter effect can be small.

(ii) Intermediate epoch: $z_a > z > z_d$. The adiabaticity at resonance is not satisfied (if $z_a > z_R > z_d$). At the same time the matter width can be large enough to induce significant matter effect.

Two remarks are in order. (1) The propagation still can be adiabatic in the part of the interval $[z_d, z_a]$ outside the resonance, and in the whole of it if the resonance condition is never satisfied in this time interval. (2) In monotonously varying density the condition for strong matter effect reduces to the adiabaticity condition [25]. Therefore, in spite of the fulfillment of the minimum width condition, the matter effect can be small for neutrinos produced in the most part of the interval $[z_d, z_a]$.

(iii) Later epoch: $z < z_d$. For neutrinos produced in this epoch the matter effects are expected to be small.

The fig. 3.2 shows the minimum width, resonance and adiabaticity conditions in the z - $F\eta$ plane. The minimum width condition (3.8) is fulfilled in the shadowed region. The lower border of this area corresponds to the curve $z = z_d(F\eta)$ (eq. (3.9)). For values of $F\eta$ and of z in this region one may expect significant matter effect.

The dashed lines show the values of z and $F\eta$ for which the resonance condition (1.20) is satisfied for neutrinos with a given $E_0/(\Delta m^2 \cos 2\theta)$ (iso-contours of resonance).

The solid lines are iso-contours of the adiabaticity parameter: they are contours of constant ratio $\chi_R/\tan^2 2\theta$ (see eq. (3.35)). The upper curve corresponds to $\chi_R/\tan^2 2\theta = 2\pi$, that is, to $z = z_a$ for $\tan^2 2\theta = 1$. For values of neutrino production epoch z and $F\eta$ above this contour one would expect resonant adiabatic conversion as dominating mechanism of neutrino transformation. For a given $F\eta$ and z the adiabaticity iso-contour gives the value of $\chi_R/\tan^2 2\theta$ for neutrinos produced at the epoch $z_i \geq z$ and having the resonance at z. In turn, the resonance at z and $F\eta$ can be satisfied for certain values of $E_0/(\Delta m^2 \cos 2\theta)$. It is clear from the figure that strong adiabatic conversion occurs for large production epochs, $z \gtrsim 10$, large asymmetry, $F\eta \gtrsim 10$ and large mixing $\tan^2 2\theta \sim O(1)$. For $F\eta \sim 2$ the minimal width condition is fulfilled for large production epochs, $z \gtrsim 8$, and some effects of adiabatic conversion may be seen at $z \gtrsim 15$.

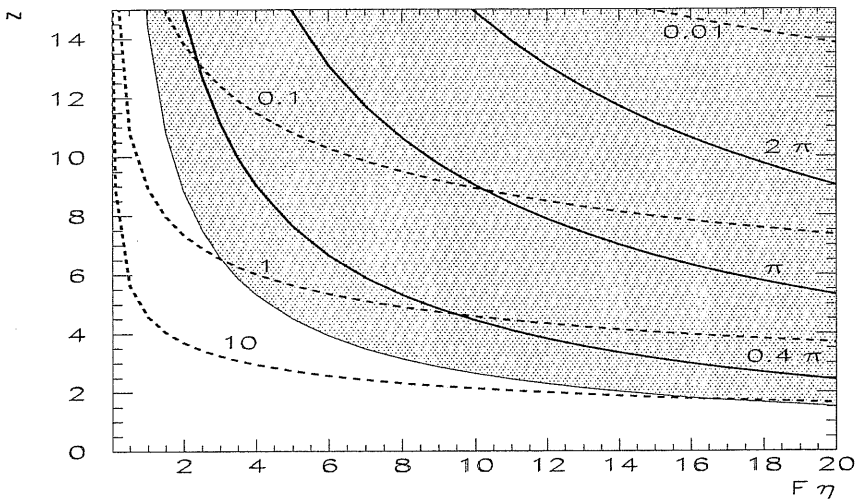

Figure 3.2: The minimum width, resonance and adiabaticity conditions in the z-$F\eta$ plane for $\nu_\alpha - \nu_s$ conversion. The solid lines are iso-contours of adiabaticity, i.e. of the quantity $\chi_R/\tan^2 2\theta$ (numbers on the curves). The dashed lines are iso-contours of resonance, i.e. of the ratio $E_0/(\Delta m^2 \cos 2\theta)$; the values are given on the curves in units of 10^{30} eV^{-1}. The minimum width condition is satisfied in the shadowed region.

From the above considerations it appears that for realistic parameters a flavour transition of neutrinos occurs either due to vacuum oscillations modified by matter effect or by an interplay of oscillations and non-adiabatic conversion.

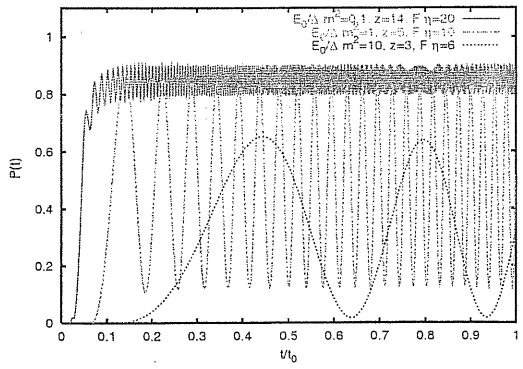

Figure 3.3: The $\nu_\alpha - \nu_s$ conversion probability $P(t)$ as a function of time. We have taken $\sin^2 2\theta = 0.5$ and three different choices of $E_0/\Delta m^2$ (in units of 10^{30} eV^{-1}), production epoch z and $F\eta$. The time t is given in units of the age of the universe, t_0.

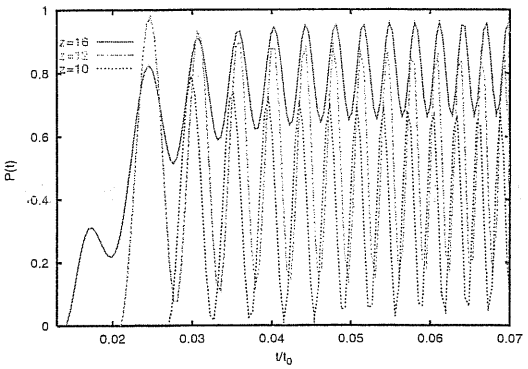

Figure 3.4: The $\nu_\alpha - \nu_s$ conversion probability $P(t)$ as a function of time in the regime of good adiabaticity (see fig. 3.2).We have taken production epochs z earlier, simultaneous and later than the resonance epoch z_R. Here $\sin^2 2\theta = 0.5$, $F\eta = 14$ and $E_0/\Delta m^2 = 1.8 \cdot 10^{28}$ eV^{-1}. The time t is given in units of the age of the universe, t_0.

3.3.3 The conversion probability

Let us consider neutrinos produced at a given epoch z with a certain flavour ν_α and propagating in the expanding universe with a given constant asymmetry η.

We find the $\nu_\alpha - \nu_s$ conversion probability by numerical solution of the evolution equation for two neutrino species with the Hamiltonian in the flavour basis (ν_α, ν_s):

$$H = \begin{pmatrix} -\frac{\Delta m^2}{2E(z)}\cos 2\theta + V(z) & \frac{\Delta m^2}{4E(z)}\sin 2\theta \\ \frac{\Delta m^2}{4E(z)}\sin 2\theta & 0 \end{pmatrix}, \tag{3.37}$$

where $E(z)$ and $V(z)$ scale according to eq. (3.19). As discussed in sect. 3.3.2 (see fig. 3.2), the dynamics of flavour transformation depends on the production epoch z, the resonance epoch, z_R, which depends on $E_0/\Delta m^2$, and on the value of the adiabaticity parameter at resonance, χ_R. The figure 3.3 illustrates the real time evolution of the neutrino states for $\sin^2 2\theta = 0.5$ and different z, z_R, χ_R, which represent different regimes of conversion.

The solid curve corresponds to production much before the resonance epoch: $z > z_R = 6.8$ and weak adiabaticity breaking in the resonance, $\chi_R \simeq 4.3$. The dominating process is the adiabatic conversion which occurs in the resonance epoch, $t_R/t_0 \simeq 0.05$. The averaged transition probability is close to what one would expect for the pure adiabatic case: $P_{ad} = 1 - \sin^2\theta = 0.85$. Weak adiabaticity violation leads to the appearance of oscillations at $t > t_R$.

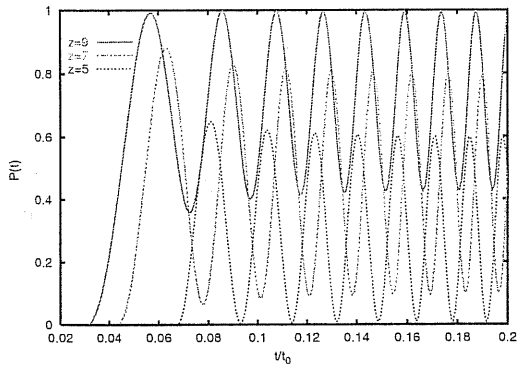

Figure 3.5: The same as fig. 3.4 for the regime of moderate breaking of adiabaticity. Here $\sin^2 2\theta = 0.5$, $F\eta = 10$ and $E_0/\Delta m^2 = 1.73 \cdot 10^{29}$ eV^{-1}.

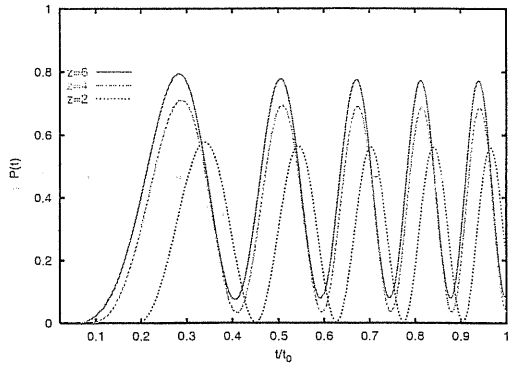

Figure 3.6: The same as fig. 3.4 for the regime of strong breaking of adiabaticity. Here $\sin^2 2\theta = 0.5$, $F\eta = 6$ and $E_0/\Delta m^2 = 4.6 \cdot 10^{30}$ eV^{-1}.

The dashed curve corresponds to production close to resonance $z \gtrsim z_R = 4.2$ and strong adiabaticity violation in the resonance: $\chi_R \simeq 1.2$. The dominating process is oscillations in matter with resonance density. At production the mixing is almost maximally enhanced, $\sin^2 2\theta_m \simeq 1$. The change of matter density leads to slight increase of the average conversion probability with respect to $\sin^2 2\theta_m/2$. The decrease of density is fast: the typical scale of density change is smaller than the oscillation length, so that maximal depth oscillations do not have time to develop.

The dotted line shows the same type of regime with stronger adiabaticity violation in resonance. The depth D of oscillations is smaller, and the average conversion probability is close to $D/2$. For further illustration, in fig. 3.4 we show the evolution in the case of good adiabaticity. Different curves correspond to different production epochs: (i) before resonance, $z > z_R$, (ii) at resonance, $z = z_R$, (iii) after resonance, $z < z_R$.

The figures 3.5-3.6 show similar sets of curves in the cases of moderate and strong violation of adiabaticity.

Let us consider the properties of the conversion probability $P(\nu_\alpha \to \nu_s)$ for neutrinos produced at epoch z and arriving at Earth at the present epoch, $z = 0$. The probability P depends on z, on the product $F\eta$, on the energy and mass squared difference in the ratio $E_0/\Delta m^2$, and on the mixing angle θ: $P = P(z, F\eta, E_0/\Delta m^2, \theta)$. As follows from figs. 3.3-3.6 the probability is a rapidly oscillating function of z, and also of $E_0/\Delta m^2$. We averaged P over the energy resolution interval $\Delta E_0 \simeq E_0$ according to eq. (3.25). The interpretation of the numerical results can be easily given using the z - $F\eta$ diagram of fig. 3.2.

In fig. 3.7 we show the dependence of the conversion probability on the production epoch z for different values of $F\eta$ and fixed $E_0/\Delta m^2$ and $\sin^2 2\theta$. The

curves with $F\eta > 0$ represent the resonance channel. For $z \lesssim 1$ both vacuum oscillations and matter conversion probabilities have oscillating behaviour. For $z \gtrsim 2$ oscillations are averaged out, so that the vacuum oscillation probability converges to $\sin^2 2\theta/2$ [3]. A substantial ($\sim 10\%$) deviation from the vacuum oscillation probability due to matter effect starts at $z \simeq 1$ for $F\eta \simeq 10$ and at $z \simeq 3$ for $F\eta \simeq 2$.

For $F\eta \simeq 6 - 10$ and $z \simeq 4 - 5$ neutrinos are produced at densities much higher than the resonance density and they cross the resonance at $z = 2 - 2.5$. The adiabaticity is broken in the resonance, however above the resonance the propagation can be adiabatic. For higher asymmetry, $F\eta \gtrsim 10$, the adiabaticity starts to be broken near the resonance, so that the original flavour state $\nu_\alpha \simeq \nu_{2m}$ will evolve to $\nu_{2m}^R \simeq (\nu_\alpha + \nu_s)/\sqrt{2}$. Thus, we have $P \simeq 1/2$. With the decrease of z the initial state will deviate from ν_{2m} and the conversion probability becomes smaller. With the decrease of $F\eta$ the adiabaticity starts to be violated earlier (before resonance), so that the transition probability decreases.

For negative values of $F\eta$ (or for antineutrinos) the matter effect suppresses the mixing and, in consequence, the conversion effect. However, the suppression effect is weaker than the enhancement in the resonant channel.

Notice that for $F\eta \simeq 10$ and $z \simeq 5$ the matter effect can change the vacuum oscillation probability P_v by a factor of 2:

$$(P - P_v)/P_v \simeq 1 \ . \tag{3.38}$$

For $z \simeq 2$ and $F\eta \simeq 10$ the deviation can reach $\sim 40\%$ and it equals $\sim 20\%$ for $F\eta \simeq 2$.

In fig. 3.8 we show the dependence of the survival probability, $1 - P$, on $E_0/\Delta m^2$ for production epoch $z = 3$, $\sin^2 2\theta = 0.5$ and various values of $F\eta$. Oscillations are averaged for $E_0/\Delta m^2 \lesssim 3 \cdot 10^{30}$ eV^{-1}; the averaging disappears at $E_0/\Delta m^2 \sim 10^{32}$ eV^{-1}, when the oscillation length approaches the size of the horizon (see also sect. 3.2.2 and fig. 3.1).

The matter effect increases with $E_0/\Delta m^2$. For $E_0/\Delta m^2 \lesssim 5 \cdot 10^{30}$ eV^{-1} the resonance epoch z_R (see eq. (3.32)) is earlier than the production epoch of the neutrinos. Thus the neutrinos do not cross the resonance and the matter effects is realized mainly in the epoch of neutrino production, when the potential (3.28) was larger (see fig. 3.3). The value of the effect is determined by the mixing in matter at the production time. With the increase of $E_0/\Delta m^2$ the resonance epoch z_R approaches the production epoch (see fig. 3.2). As a consequence the mixing at production, and therefore the matter effect, increase. The maximal matter effect is achieved at energies for which the resonance condition is fulfilled at production

[3] Notice that partial averaging exists already at small z due to our integration over ΔE_0. For this reason P does not reach its maximal possible value $P_{max} = \sin^2 2\theta$.

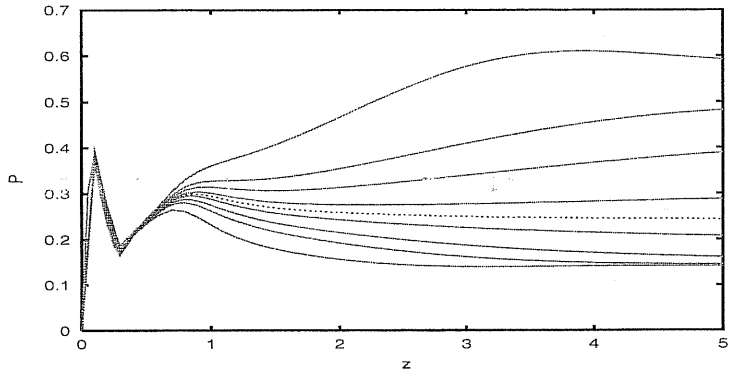

Figure 3.7: The $\nu_\alpha - \nu_s$ conversion probability P as a function of the production epoch z for various values of $F\eta$. From the upper to the lower curve: $F\eta = 20, 10, 6, 2, 0, -2, -6, -10, -20$; the dotted line represents the vacuum oscillations probability ($F\eta = 0$). We have taken $\sin^2 2\theta = 0.5$ and $E_0/\Delta m^2 = 10^{31}$ eV^{-1}.

epoch or slightly later (notice that the adiabaticity is strongly broken at resonance). For $z \simeq 3$ this occurs in the interval $E_0/\Delta m^2 \simeq 10^{31} - 10^{32}$ eV^{-1}. For $z \simeq 5$ maximal matter effect is realized at $E_0/\Delta m^2 \simeq (5-7) \cdot 10^{30}$ eV^{-1} (fig. 3.9).

In fig. 3.10 we show the dependence of the matter effect, i.e. the difference $P - P_v$, on the quantity $F\eta$ for various values of the mixing angle. For the parameters used in the plot the neutrinos are produced close to the resonance and the adiabaticity is strongly violated in the resonance. The matter effect can be estimated as the deviation of the jump probability from 1:

$$1 - P_{LZ} \simeq 1 - \exp(-\pi\chi_R/2) \ . \tag{3.39}$$

In our case $\chi_R \ll 1$, so that the matter effect is proportional to $F\eta$:

$$P - P_v \simeq \frac{\pi}{2}\chi_R \propto F\eta \tan^2 2\theta \ , \tag{3.40}$$

according to eq. (3.35). This explains the linear increase of the matter effect with η and F.

In fig. 3.11 we show the dependence of $P - P_v$ on the mixing parameter $\sin^2 2\theta$ for different values of the ratio $E_0/\Delta m^2$ and fixed production epoch $z = 3$ and $F\eta = 6$. The neutrinos are produced in the resonance epoch or after it depending on their energy. For small mixing the matter effect is proportional to the mixing parameter $\sin^2 2\theta_m$ at the production time. This explains the linear increase of the effect with $\sin^2 2\theta$ ($\sin^2 2\theta_m \propto \sin^2 2\theta$) and with $E_0/\Delta m^2$ (for $E_0/\Delta m^2 \sim 10^{31}$ eV^{-1} the

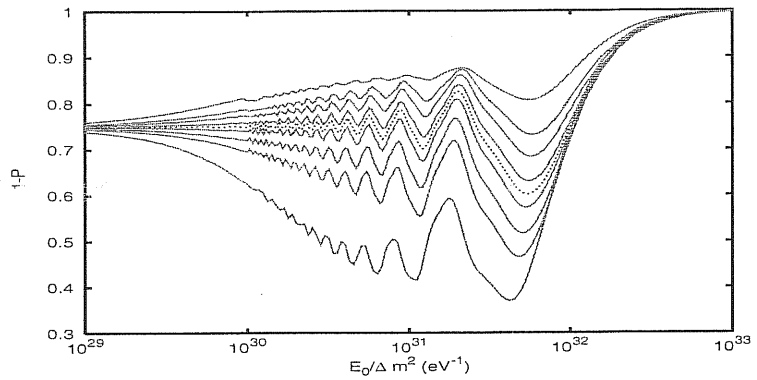

Figure 3.8: The survival probability $1 - P(\nu_\alpha - \nu_s)$ as a function of the ratio $E_0/\Delta m^2$ for various values of $F\eta$. From the upper to the lower curve: $F\eta = -20, -10, -6, -2, 0, 2, 6, 10, 20$; the dotted line represents the effect of vacuum oscillations ($F\eta = 0$). We have taken $\sin^2 2\theta = 0.5$ and production epoch $z = 3$.

production epoch coincides with the resonance one). For maximal mixing, $\sin^2 2\theta = 1$, the average probability takes the value $P = 1/2$ independently on adiabaticity violation [95]. Therefore in this case $P - P_v = 0$. The maximum deviation from vacuum oscillation effect is realized at $\sin^2 2\theta \simeq 0.65$.

3.4 Conversion effects on diffuse neutrino fluxes

The results we have discussed in the sections 3.2 and 3.3 describe the conversion effect for a beam of neutrinos produced by a single source at a certain epoch z. Presently, the possibilities of detection of neutrinos from single sources are limited to objects with redshift $z \ll 1$. For these neutrinos no substantial effect is expected (see sec. 3.1.2). There is a hope, however, to detect the diffuse (integrated) neutrino flux which is produced by all the cosmological sources. For this flux matter effects can be observable.

In what follows we will calculate the ratio $F^\alpha(E_0)/F_0^\alpha(E_0)$, where $F^\alpha(E_0)$ and $F_0^\alpha(E_0)$ are the present diffuse fluxes of neutrinos of given flavour, ν_α, and a given energy, E_0, with and without conversion. The ratio can be written as:

$$\frac{F^\alpha(E_0)}{F_0^\alpha(E_0)} = 1 - \bar{P}_\alpha(E_0) \ , \tag{3.41}$$

where $\bar{P}_\alpha$ is the averaged transition probability:

$$\bar{P}_\alpha(E_0) \equiv \frac{1}{F_0^\alpha(E_0)} \int_0^{z_{max}} \frac{dF_0^\alpha(E_0, z)}{dz} P_\alpha(E_0, z) dz \ . \tag{3.42}$$

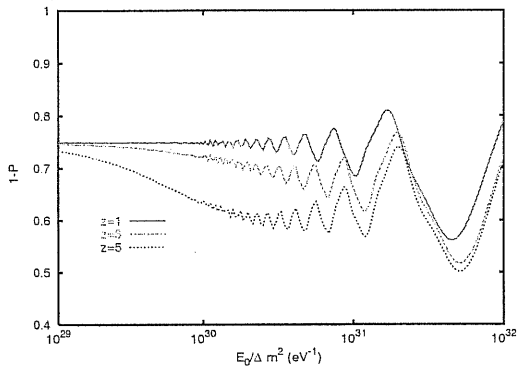

Figure 3.9: The survival probability $1 - P(\nu_\alpha - \nu_s)$ as a function of the ratio $E_0/\Delta m^2$ for various values of the production epoch z. We have taken $\sin^2 2\theta = 0.5$ and $F\eta = 6$.

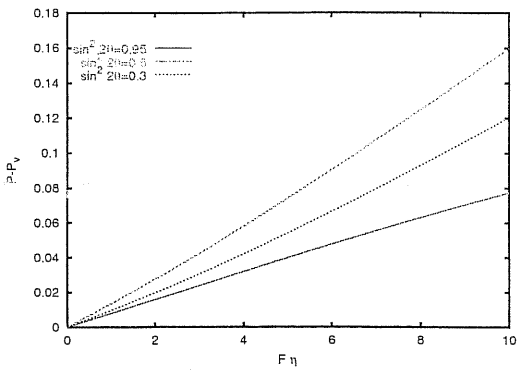

Figure 3.10: The deviation with respect to the vacuum oscillation probability, $P(\nu_\alpha - \nu_s) - P_v$ as a function of the product $F\eta$ for various values of $\sin^2 2\theta$. We have taken production epoch $z = 3$ and $E_0/\Delta m^2 = 10^{31}$ eV^{-1}.

Here $P_\alpha(E_0, z)$ is the transition probability for neutrinos produced in the epoch z, which has been discussed in sections 3.2.2 and 3.3.3. The quantity $dF_0^\alpha(E_0, z)$ is the contribution of the neutrinos ν_α produced in the interval $[z, z + dz]$ to the present flux in absence of oscillations.

We first derive the general expression for the differential flux $dF_0^\alpha(E_0, z)$. Let $f(E)$ be the flux of neutrinos generated by a single source. Then the total number of neutrinos produced in the unit volume in the time interval $[t, t + dt]$ with energy in the interval $[E, E + dE]$ can be written as:

$$f(E)n(t)dEdt \ , \tag{3.43}$$

where $n(t)$ is the concentration of sources in the epoch t. The contribution of these neutrinos to the present flux equals:

$$dF_0^\alpha(E_0, z) = \frac{c}{4\pi} f(E)n(t)(1+z)^{-3}\frac{dE}{dE_0}dt \ , \tag{3.44}$$

where c is the speed of light and the factor $(1+z)^{-3}$ accounts for the expanding volume of the universe. Transferring from t to z-variable we get:

$$dF_0^\alpha(E_0, z) = \frac{3ct_0}{8\pi} f(E)n(z)(1+z)^{-11/2}\frac{dE}{dE_0}dz \ . \tag{3.45}$$

The relation between the energy E and the present neutrino energy E_0 includes, in general, effects of energy losses and of redshift. Neglecting absorption we have

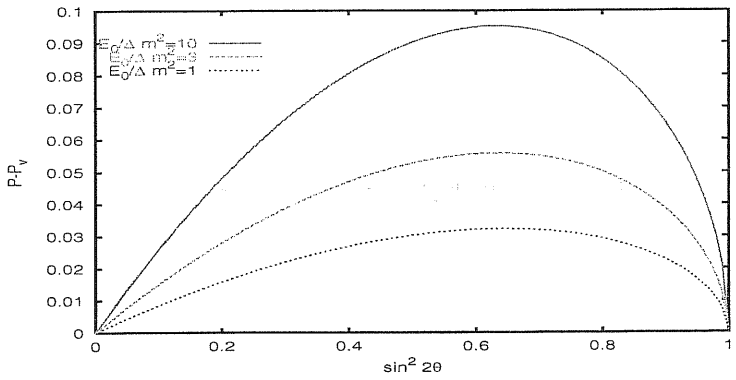

Figure 3.11: The deviation with respect to the vacuum oscillation probability, $P(\nu_\alpha - \nu_s) - P_v$ as a function of $\sin^2 2\theta$, for various values of $E_0/\Delta m^2$ (in units of 10^{30} eV^{-1}). We have taken production epoch $z = 3$ and $F\eta = 6$.

$dE/dE_0 = (1+z)$. The density of sources, $n(z)$, can be expressed in terms of the comoving density n_c as $n(z) = (1+z)^3 n_c(z)$. Notice that $n_c = const$, if the number of sources in the universe is constant in time. Thus, the evolution of sources is described by the dependence of n_c on the redshift z.

In terms of n_c and E_0 we get finally:

$$dF_0^\alpha(E_0, z) = \frac{3ct_0}{8\pi} f(E_0(1+z)) n_c(z) (1+z)^{-3/2} dz \ . \tag{3.46}$$

Inserting $dF_0^\alpha(E_0, z)$ in eq. (3.42) we find:

$$\bar{P}_\alpha(E_0) = \frac{1}{F_0^\alpha(E_0)} \frac{3ct_0}{8\pi} \int f(E_0(1+z)) n_c(z) (1+z)^{-3/2} P_\alpha(E_0, z) dz \ , \tag{3.47}$$

and $F_0^\alpha(E_0)$ is given by the same expression with $P_\alpha = 1$.

In what follows we will calculate the survival probability $1 - \bar{P}_\alpha$ for various possible sources of high-energy neutrinos, assuming certain forms for the produced flux $f(E)$ and the concentration of sources n_c.

3.4.1 Conversion of neutrinos from AGN and GRBs

There is an evidence that cosmological sources like Gamma Ray Bursters (GRBs) and Active galactic Nuclei (AGN) were more numerous in the past. In particular, the density of GRBs evolved as [96]:

$$n_c(z) \propto \begin{cases} (1+z)^3 & z \le z_p \\ (1+z_p)^3 & z_p < z \le z_{max} \\ \sim 0 & z > z_{max} \end{cases} \ . \tag{3.48}$$

where z_p is estimated to be $z_p \simeq 1-2$ [96]. The energy spectrum of neutrinos from GRBs scales as a power law [41] :

$$f(E) \propto \frac{1}{E^2} = \frac{1}{E_0^2(1+z)^2} \ . \tag{3.49}$$

Combining eqs. (3.48) and (3.49) with (3.47) we find the averaged probability:

$$\bar{P}_\alpha(E_0) = \frac{1}{N_p}\left[\int_0^{z_p}(1+z)^{-1/2}P_\alpha(E_0,z)dz + \int_{z_p}^{z_{max}}(1+z)^{-7/2}P_\alpha(E_0,z)dz\right] \ , \tag{3.50}$$

where the normalization factor N_p is given by the expression in square brackets with $P_\alpha = 1$. According to eq. (3.50) the contribution of the recent epochs to the present flux is enhanced in spite of the the larger number of sources in the past. This leads to suppression of the matter effects, which are more important at large z.

The figure 3.12 shows the averaged survival probability , $1-\bar{P}_\alpha$, for $\nu_\alpha - \nu_s$ conversion channel, as a function of $E_0/\Delta m^2$ for different values of $F\eta$. We have taken $z_p = 2$ and $z_{max} = 5$. The averaged probability is rather close to the non-averaged one (see fig. 4.10) for neutrinos produced at $z \simeq z_p = 2$. Indeed, the contribution to the flux from the earlier epochs, $z \gtrsim z_p$ is strongly suppressed, according to eq. (3.50). The integration over z leads to some smoothing of the oscillatory behaviour of the probability. The deviation of the ratio $F^\alpha(E_0)/F_0^\alpha(E_0)$ from its vacuum oscillation value can reach $\sim 25\%$. Maximal effect is realized for $F\eta \simeq 20$ in the resonance interval $E_0/\Delta m^2 \sim (1-5)\cdot 10^{31}$ eV^{-1}. For $F\eta \simeq 2$ the effect is about $(3-4)\%$.

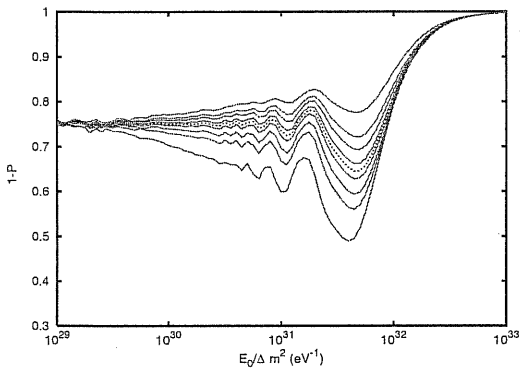

Figure 3.12: The averaged survival probability for $\nu_\alpha - \nu_s$ channel, $1-\bar{P}_\alpha$, as a function of the ratio $E_0/\Delta m^2$ for the diffuse flux of neutrinos from GRBs. The curves correspond to various values of $F\eta$. From the upper to the lower curve: $F\eta = -20, -10, -6, -2, 0, 2, 6, 10, 20$; the dotted line represents the effect of vacuum oscillations ($F\eta = 0$). We have taken $\sin^2 2\theta = 0.5$.

For conversion between active flavours the results are shown in fig. 3.13: the deviation of the survival probability from the value given by vacuum oscillations can be as large as $\sim 10\%$ for large asymmetry, $F\eta \gtrsim 10$, and high energies, $E_0/\Delta m^2 \gtrsim 10^{32}$ eV^{-1}, for which the matter-induced oscillation phase Φ_{matt} dominates over the vacuum oscillation phase Φ_{vac}.

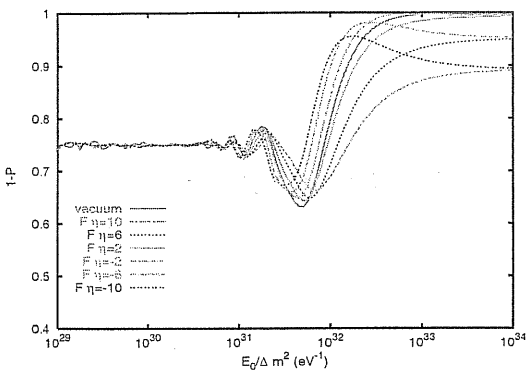

Figure 3.13: The averaged survival probability for $\nu_\alpha - \nu_\beta$ oscillations, $1 - \bar{P}_\alpha$, as a function of the ratio $E_0/\Delta m^2$ for the diffuse flux of neutrinos from GRBs. The curves correspond to various values of $F\eta$. We have taken $\sin^2 2\theta = 0.5$.

The astrophysical data about AGN indicate that the distribution of these objects has maximum at $z \sim 2$ [97], with a rapid decrease of the concentration with z. The power law $f(E) \propto E^{-2}$ is a good approximation for the most energetic part of the spectrum [98]. For these reasons, in the case of AGN the results are similar to those discussed here for neutrinos from GRBs.

3.4.2 Conversion of neutrinos from heavy particle decay

Very heavy particles, with mass of the order of the grand unification scale, are supposed to be produced in the universe by topological defects, e.g. in monopole-antimonopole annihilation, cosmic strings evaporation, etc. [99]. These particles would then decay very quickly, with lifetime $\tau \ll t_0$, into leptons and hadrons. Neutrinos may be produced either directly, as primary decay products, and/or as secondary products from decays of hadrons.

Let us calculate the contribution of the neutrinos produced in the epoch z to the present flux: $dF_0^\alpha(E_0, z)/dz$. In assumption of very fast decay of the heavy particle, X (so that the production epochs of X and of the neutrinos coincide), we can write the total number of neutrinos produced in the unit volume in the time interval $[t, t + dt]$ with energy in the interval $[E, E + dE]$ as:

$$\frac{dn_X(t)}{dt}\frac{dN_\nu}{dE}dtdE \ , \tag{3.51}$$

where $dn_X(t)$ is the number of X particles produced in the interval $[t, t + dt]$ in the unit volume, and dN_ν is the number of neutrinos in the energy interval $[E, E + dE]$ produced by a single particle X. The contribution of the neutrinos produced in the epoch t, eq. (3.51), to the present neutrino flux is:

$$dF_0^\alpha(E_0, z) = \frac{c}{4\pi}\frac{dn_X(t)}{dt}\frac{dN_\nu}{dE}(1+z)^{-3}\frac{dE}{dE_0}dt \ , \tag{3.52}$$

where we have taken into account the expansion of the universe. In terms of the redshift z we get:

$$dF_0^\alpha(E_0, z) = \frac{3ct_0}{8\pi}\frac{dn_X}{dt}(z)\frac{dN_\nu}{dE}(E_0(1+z))(1+z)^{-9/2}dz \ , \tag{3.53}$$

where we used also the relation $E = E_0(1+z)$.

The production rate of the X particles can be written as:

$$\frac{dn_X(t)}{dt} \propto t^{-4+p} \propto (1+z)^{6-\frac{3}{2}p} , \tag{3.54}$$

where $p = 1$ for monopole-antimonopole annihilation and cosmic strings [100] and $p = 2$ for constant comoving production rate.

For the fragmentation function of neutrinos we take a power law:

$$\frac{dN_\nu}{dE} \propto E^\alpha = E_0^\alpha (1+z)^\alpha . \tag{3.55}$$

If the neutrinos are produced mainly by hadronic decays the fragmentation function has a polynomial form [101]. The leading term of the polynome gives the expression (3.55) with $\alpha = -3/2$.

Inserting the expressions from (3.53), (3.54) and (3.55) in eq. (3.42) we get:

$$\bar{P}_\alpha(E_0) = \frac{1}{N_p} \int (1+z)^{6-\frac{3}{2}p+\alpha} P_\alpha(E_0, z) dz , \tag{3.56}$$

and, for $p = 1$ and $\alpha = -3/2$:

$$\bar{P}_\alpha(E_0) = \frac{1}{N_p} \int (1+z)^{-\frac{3}{2}} P_\alpha(E_0, z) dz . \tag{3.57}$$

Here N_p is a normalization factor.

We perform the integration (3.57) starting from the absorption epoch z_{abs}. The contribution of the neutrino flux produced at $z \gtrsim z_{abs}$ is very small due to absorption[4]. The dominant absorption processes are $\nu - \nu$ and $\nu - \bar{\nu}$ interaction with the neutrino background. The absorption epoch is given by:

$$1 + z_{abs} = \left[\frac{d_{abs}}{d_U} + 1 \right]^{\frac{2}{3}} , \tag{3.58}$$

where d_U is given in eq. (3.6) and d_{abs} is the the absorption width, which depends on the $\nu - \nu$ energy squared in the center of mass, s_Z, (see eq. (3.12)). Taking, for instance, $E \lesssim 10^{22}$ eV and $m_\nu \lesssim 0.05$ eV, we have $s_Z \lesssim 0.1$, and the corresponding absorption width is $d_{abs} \gtrsim 1.5 \cdot 10^{34}$ cm^{-2} [102]. With this value and $\eta \simeq 10$ eq. (3.58) gives $z_{abs} \simeq 50$.

[4]Clearly, the energy of the neutrinos at production can not exceed the mass of the parent particle, X. This gives a further constraint on the upper integration limit: $1 + z_{max} \lesssim m_X/E_0$. Stronger bounds can be found in some specific production mechanisms: taking, for instance, $X \to \pi^+\pi^-$ and subsequent production of neutrinos by pion decay, one gets $1 + z_{max} \lesssim 0.2134 m_X/E_0$ [39]. For $E_0 \lesssim 10^{22}$ eV and $m_X \sim 10^{16}$ GeV this gives the constraint $z_{max} \lesssim 200$, which is weaker than the one given by absorption.

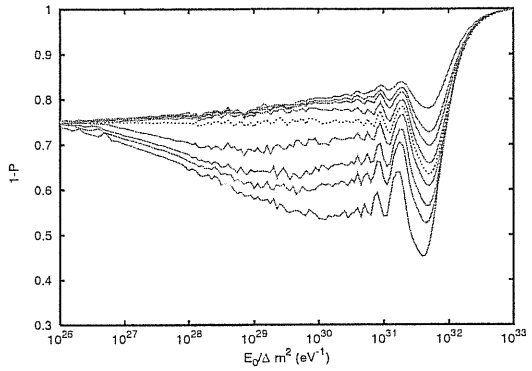

Figure 3.14: The averaged survival probability for $\nu_\alpha - \nu_s$ channel, $1 - \bar{P}_\alpha$, as a function of the ratio $E_0/\Delta m^2$ for neutrinos from the decay of heavy relics. The curves correspond to various values of $F\eta$. From the upper to the lower curve: $F\eta = -20, -10, -6, -2, 0, 2, 6, 10, 20$; the dotted line represents the effect of vacuum oscillations ($F\eta = 0$). We have taken $\sin^2 2\theta = 0.5$.

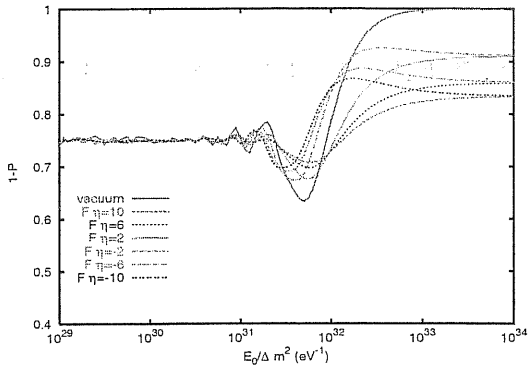

Figure 3.15: The averaged survival probability for $\nu_\alpha - \nu_\beta$ oscillations, $1 - \bar{P}_\alpha$, as a function of the ratio $E_0/\Delta m^2$ for the diffuse flux of neutrinos from the decay of heavy relics. The curves correspond to various values of $F\eta$. We have taken $\sin^2 2\theta = 0.5$.

In the figure 3.14 we show the averaged survival probability $1 - \bar{P}_\alpha$ for $\nu_\alpha - \nu_s$ conversion channel, as a function of $E_0/\Delta m^2$ for different values of $F\eta$. One can see that, in contrast with the case of neutrinos from GRBs, the deviation of the ratio $F^\alpha(E_0)/F_0^\alpha(E_0)$ from the value given by vacuum oscillation is significant (larger than $\sim 10\%$) in a wide range of energies: $E_0/\Delta m^2 \simeq 10^{26} - 10^{32}$ eV^{-1}.

For a given value of $E_0/\Delta m^2$ the matter effects are determined by the corresponding resonance epoch, z_R, and adiabaticity in resonance. For $E_0/\Delta m^2 \lesssim 10^{29}$ eV^{-1} the resonance was realized at $z_R \gtrsim 10$, when the adiabaticity condition was fulfilled (see fig. 3.2). Therefore, the matter effects are dominated by resonant adiabatic conversion which occurs for neutrinos produced at $z > z_R \sim 10$. As discussed in sect. 3.3.2, these neutrinos undergo almost total conversion (see fig. 3.3), however, their contribution to $\bar{P}_\alpha$ is suppressed according to eq. (3.57).

For $E_0/\Delta m^2 \gtrsim 10^{29}$ eV^{-1} the resonance is realized at $z_R \lesssim 10$, when the adiabaticity is broken (fig. 3.2), so that the matter effect is mostly due to non-adiabatic conversion and oscillations in the production epoch.

The maximal effect is realized in the interval $E_0/\Delta m^2 \simeq 10^{29} - 5 \cdot 10^{31}$ eV^{-1}; the relative deviation of $F^\alpha(E_0)/F_0^\alpha(E_0)$ with respect to the vacuum oscillations value equals $\sim 10\%$ for $F\eta = 2$ and can be as large as 50% for $F\eta = 20$.

The figure 3.15 shows the average survival probability, $1 - \bar{P}_\alpha$, for active-active

conversion. We see that, similarly to what discussed for neutrino from GRBs, a substantial ($\sim 15\%$) matter effect requires large asymmetry, $F\eta \gtrsim 10$, and very high energies, $E_0/\Delta m^2 \gtrsim 10^{32}$ eV^{-1}, for which the matter contribution to the oscillation phase is dominant.

3.5 Observable effects

Let us consider the experimental signatures of matter effects on neutrino propagation. The observable effects depend on the specific scheme of neutrino masses and mixings and on the initial flavour composition of the neutrino flux.

3.5.1 Conversion of cosmic neutrinos and neutrino mass schemes

As follows from the analysis of sections 3.4.1-3.4.2, a significant matter effect on active-active oscillations of high-energy neutrinos requires:

$$\frac{E_0}{\Delta m^2} \gtrsim 10^{32}\ \text{eV}^{-1}\ . \tag{3.59}$$

This is the condition for which the matter-induced oscillation phase, Φ_{matt}, dominates over the vacuum one, Φ_{vac} (see section 3.2.1). For conversion into a sterile neutrino the matter effect is substantial in the ranges:

$$\frac{E_0}{\Delta m^2} \gtrsim \begin{cases} 10^{30}\ \text{eV}^{-1} & \text{for AGN, GRBs} \\ 10^{28}\ \text{eV}^{-1} & \text{for heavy relics decay}\ . \end{cases} \tag{3.60}$$

For $E_0 \lesssim 10^{21}$ eV, the conditions (3.59)-(3.60) imply:

$$\Delta m^2 \lesssim \begin{cases} 10^{-11}\ \text{eV}^2 & \text{for } \nu_\alpha - \nu_\beta \\ 10^{-7}\ \text{eV}^2 & \text{for } \nu_\alpha - \nu_s\ . \end{cases} \tag{3.61}$$

For both the active-active and active-sterile channels the mixing angle should be large enough and, for $\nu_\alpha - \nu_s$, not too close to maximal (see fig. 3.11):

$$0.1 \lesssim \sin^2 2\theta \lesssim 0.95\ . \tag{3.62}$$

In the three neutrino schemes which explain the solar and atmospheric neutrino data the effect can be realized for ν_e-ν_τ/ν_μ mixing and the vacuum oscillation (VO) solution of the solar neutrino problem. If the LMA, the SMA or the LOW solution are confirmed, the effect of medium on vacuum oscillations of cosmic neutrinos can be neglected.

In presence of a sterile neutrino the conditions (3.60) - (3.62) can be realized in a number of situations. Oscillations of electron neutrino into a sterile state, $\nu_e - \nu_s$,

with $\Delta m^2 \lesssim 10^{-11}$ eV^2 and mixing close to maximal represent a possible solution of the solar neutrino problem [103]. Another possibility is to consider, e.g., the hierarchical mass spectrum with $m_3 \sim \sqrt{\Delta m^2_{atm}}$, $m_2 \sim \sqrt{\Delta m^2_{\odot}}$, $m_1 \lesssim 10^{-4}$ eV and $m_0 < m_1$ so that $\Delta m^2_{10} \simeq m_1^2 \lesssim 10^{-7}$ eV^2. In the simplest case the sterile state is mixed only in the lightest mass eigenstates ν_1 and ν_0. The mixing angle is only weakly restricted by the solar neutrino data[5].

3.5.2 Flavour composition of detected fluxes

Let us consider the numbers of events N_α and N^0_α induced in a detector by neutrinos of different flavours α with and without conversion respectively. These quantities are determined by the present fluxes F^α and F^α_0 (see section 3.4); if the detector provides total energy reconstruction and optimal event selection, the flavour composition of the numbers of detected events coincides with that of the fluxes.

In what follows we consider two possible types of flavour composition for the numbers of events in absence of conversion:
1). CP-symmetric: $N^0_\alpha = N^0_{\bar{\alpha}}$ $(\alpha = e, \mu, \tau)$. As far as flavour content is concerned we take the normalized numbers of events:

$$\begin{aligned} (N^0_e, N^0_\mu, N^0_\tau) &= (1, 2, 0) \\ (N^0_{\bar{e}}, N^0_{\bar{\mu}}, N^0_{\bar{\tau}}) &= (1, 2, 0) \ . \end{aligned} \tag{3.63}$$

Such a flavour composition is expected for neutrinos produced by the decays of π^+ and π^- mesons, which in turn appear in the process $X \to \pi^+\pi^-$ (see section 3.4.2).

2). CP-asymmetric: $N^0_\alpha \neq N^0_{\bar{\alpha}}$. We consider

$$\begin{aligned} (N^0_e, N^0_\mu, N^0_\tau) &= (1, 1, 0) \\ (N^0_{\bar{e}}, N^0_{\bar{\mu}}, N^0_{\bar{\tau}}) &= (0, 1, 0) \ . \end{aligned} \tag{3.64}$$

This flavour composition is realized for neutrinos produced by the scattering of highly energetic protons on a photon background, where the π^+ decay gives the dominant contribution. The p-γ interaction is supposed to be the main mechanism of neutrino production in GRBs [41].

Neutrinos of different flavours produced in the same decay reaction (X or π decay) share the energy of the parent particle equally with good approximation. Therefore the produced fluxes of neutrinos and antineutrinos of different flavours have the

[5]No restriction exists for $\Delta m^2_{10} \ll 10^{-11}$ eV^2; bounds follow from the solar neutrino data for $\Delta m^2_{10} \gtrsim 10^{-11}$ eV^2 (in this case the solar neutrino data should be treated in three neutrino context).

same energy dependence, and, in absence of conversion, the ratios N_e^0/N_μ^0, N_e^0/N_τ^0, N_μ^0/N_τ^0 are expected to be energy-independent.

In presence of vacuum oscillations the ratios of numbers of events are approximately independent of energy in two intervals:
(i) $E_0/\Delta m^2 \lesssim 5 \cdot 10^{30}$ eV^{-1} (see figs. 3.12-3.14), where oscillations are averaged out.
(ii) $E_0/\Delta m^2 \gtrsim 5 \cdot 10^{32}$ eV^{-1}, where the vacuum oscillation phase is very small or, equivalently, the vacuum oscillation length exceeds the size of the horizon. In this case the conversion probability is negligibly small and the ratios of numbers of events approach their values in absence of oscillations.

The effects of vacuum oscillations are modified by the interaction with the neutrino background. According to the results of sections 3.4.1-3.4.2 we find that:

1. The energy dependence of the ratios of numbers of events in the interval (i) would be a signal of active-sterile conversion with matter effects[6].

2. The deviation of the ratios of numbers of events in the interval (ii) from the values expected in absence of conversion would indicate matter-affected active-active oscillations. Two elements, however, will make the identification of the effect difficult: its appearance at very high energies, close to the end of the predicted spectra of ultra-high energy neutrinos, and the uncertainties on the flavour composition of the neutrino fluxes at production.

We notice an interesting aspect: the interaction with the neutrino background produces strongly different effects on active-active and active-sterile oscillations. Thus the observation of such effects would neatly distinguish between the two channels. In particular, the observation of the characteristics described in 1. would give indication of the existence of a sterile neutrino.

3.5.3 Ratios of numbers of events: active neutrino mixing

For three neutrino flavours, ν_e, ν_μ, ν_τ, the relation between the numbers of events N_α and N_α^0 can be expressed as:

$$\vec{N}_\nu = \mathcal{P}\vec{N}_\nu^0 \quad , \tag{3.65}$$

where:

$$\begin{aligned} \vec{N}_\nu^0 &= (N_e^0, N_\mu^0, N_\tau^0) \\ \vec{N}_\nu &= (N_e, N_\mu, N_\tau) \ , \end{aligned} \tag{3.66}$$

[6] If some difference exists in the energy dependences of the original fluxes of neutrinos of different flavours, this would appear in the total number of events $N_{tot}^0 = \sum_\alpha N_\alpha^0$, in contrast with the effect of neutrino conversion. Thus, the energy-dependence of ratios of numbers of events due to matter effects can be distinguished.

and $\mathcal{P}$ is the matrix of conversion probabilities: $\mathcal{P}_{\alpha\beta} \equiv P(\nu_\alpha \to \nu_\beta)$, $(\alpha, \beta = e, \mu, \tau)$.

As an example we consider the scenario in which the solar neutrino problem is solved by $\nu_e - \nu_\mu/\nu_\tau$ vacuum oscillations with $\Delta m^2_\odot = \Delta m^2_{21} \simeq 10^{-11}$ eV^2 and the atmospheric neutrino anomaly is explained by $\nu_\mu - \nu_\tau$ oscillations with $\Delta m^2_{atm} = \Delta m^2_{32} \simeq 10^{-3}$ eV^2. The mixing matrix can be written as:

$$U = \begin{pmatrix} c_\theta & -s_\theta & 0 \\ s_\theta c_\Theta & c_\theta c_\Theta & -s_\Theta \\ s_\theta s_\Theta & c_\theta s_\Theta & c_\Theta \end{pmatrix} , \tag{3.67}$$

where $c_\theta \equiv \cos\theta$ and $s_\theta \equiv \sin\theta$ and analogous definitions hold for s_Θ and c_Θ.

Since the values of Δm^2_{32} and Δm^2_{31} ($\Delta m^2_{31} \simeq \Delta m^2_{32}$) are out of the range of sensitivity to matter effects (see sect. 3.5.1) the the oscillations due to Δm^2_{31} and Δm^2_{32} are described by the average vacuum oscillation probability. The neutrino background influences the $\nu_1 - \nu_2$ system only. In these specific circumstances matter effects show up in the conversion of $\nu_e = \cos 2\theta \nu_1 + \sin 2\theta \nu_2$ into the orthogonal state $\nu' = -\sin 2\theta \nu_1 + \cos 2\theta \nu_2$. We denote by P the corresponding two-neutrino conversion probability. Taking the maximal mixing $\Theta = \pi/4$ in the matrix (3.67) we find the conversion matrix:

$$\mathcal{P} = \begin{pmatrix} 1-P & P/2 & P/2 \\ P/2 & 1/2 - P/4 & 1/2 - P/4 \\ P/2 & 1/2 - P/4 & 1/2 - P/4 \end{pmatrix} , \tag{3.68}$$

and an analogous expression for the matrix of probabilities for antineutrinos with the replacement $P \to \bar{P}$, where $\bar{P}$ represents the $\bar{\nu}_e \to \bar{\nu}'$ conversion probability.

Taking the CP-symmetric flavour composition (3.63), from eqs. (3.68) and (3.65) we find that the conversion probability P cancels in the expression of the numbers of events, N_α. Equal numbers of events for the three flavours are predicted independently of matter effects: $\vec{N}_\nu = \vec{N}_{\bar{\nu}} = (1, 1, 1)$.

For the CP-asymmetric composition (3.64) we obtain:

$$\begin{aligned} \vec{N}_\nu &= (1 - P/2, 1/2 + P/4, 1/2 + P/4) \\ \vec{N}_{\bar{\nu}} &= \left(\bar{P}/2, 1/2 - \bar{P}/4, 1/2 - \bar{P}/4\right) . \end{aligned} \tag{3.69}$$

Since the present detectors do not distinguish neutrinos from antineutrinos, we consider the sums of the events induced by ν and $\bar{\nu}$. From eqs. (3.69) we find:

$$\vec{N}_\nu + \vec{N}_{\bar{\nu}} = \left(1 - P/2 + \bar{P}/2, 1 + P/4 - \bar{P}/4, 1 + P/4 - \bar{P}/4\right) . \tag{3.70}$$

Two comments are in order. First, equal numbers of events induced by the muon and tau neutrinos are expected, with no dependence of ratios on matter effects: $(N_\mu + N_{\bar{\mu}})/(N_\tau + N_{\bar{\tau}}) = 1$. Conversely, matter effects are present in ratios involving

the electron neutrino. Second, if $P = \bar{P}$ the conversion probability cancels in (3.70) and one gets $\vec{N}_\nu + \vec{N}_{\bar{\nu}} = (1,1,1)$. This circumstance is realized in absence of matter effects ($F\eta = 0$) or in the extremely high energy limit, $E_0/\Delta m^2 \gtrsim 10^{33}$ eV^{-1}, in which the asymptotic value (3.24) for the conversion probability is realized (see also fig. 3.1). Therefore, the matter effect could be revealed by a deviation from the equality of number of events for the three flavours in the narrow interval $E_0/\Delta m^2 \simeq 10^{32} - 10^{33}$ eV^{-1} in which P and $\bar{P}$ are unequal and have significant deviation from the vacuum oscillation probability.

Considering, for instance, the ratio of e-like over non e-like events we find:

$$R \equiv \frac{N_e + N_{\bar{e}}}{N_\mu + N_{\bar{\mu}} + N_\tau + N_{\bar{\tau}}} = \frac{1 - P/2 + \bar{P}/2}{2 + P/2 - \bar{P}/2} , \tag{3.71}$$

The deviation of R from its value $R_p = 1/2$ without oscillations is entirely due to matter effects and equals:

$$\frac{R - R_p}{R_p} \simeq -\frac{3}{2}\Delta , \tag{3.72}$$

where $\Delta \equiv (P - \bar{P})/2$. The relative deviation (3.72) amounts to $\sim 15\%$ for $\Delta \simeq 0.1$. Similar conclusions are obtained for other ratios of numbers of events.

Results are different if the mixing angle Θ in the matrix (3.67) is not maximal. In the extreme case $\Theta = 0$ the problem reduces to two-neutrino conversion. In the limit $E_0/\Delta m^2 \gtrsim 10^{33}$ eV^{-1}, for both the compositions (3.63) and (3.64) we get:

$$\frac{R - R_p}{R_p} \simeq \frac{3}{2}P , \tag{3.73}$$

where we considered $P \simeq \bar{P}$. Taking $P \simeq 0.1$ the deviation (3.73) equals $\sim 15\%$.

3.5.4 Extension to four neutrinos

An example of four neutrino scheme with sterile neutrino, ν_s, was introduced in section 3.5.1: the sterile state is present in the two light mass eigenstates, ν_0 and ν_1, so that in the bases $\vec{\nu}_\alpha = (\nu_s, \nu_e, \nu_\mu, \nu_\tau)$, $\vec{\nu}_i = (\nu_0, \nu_1, \nu_2, \nu_3)$ the mixing matrix takes the form:

$$U^0 = \begin{pmatrix} c_\phi & s_\phi & 0 & 0 \\ -c_\theta s_\phi & c_\theta c_\phi & -s_\theta & 0 \\ -s_\theta s_\phi/\sqrt{2} & s_\theta c_\phi/\sqrt{2} & c_\theta/\sqrt{2} & -1/\sqrt{2} \\ -s_\theta s_\phi/\sqrt{2} & s_\theta c_\phi/\sqrt{2} & c_\theta/\sqrt{2} & 1/\sqrt{2} \end{pmatrix} , \tag{3.74}$$

where $c_\phi \equiv \cos\phi$, $s_\phi \equiv \sin\phi$, $c_\theta \equiv \cos\theta$, $s_\theta \equiv \sin\theta$. The angle ϕ describes the mixing between ν_s and the state $\tilde{\nu} \equiv c_\theta \nu_e + s_\theta \nu_\mu/\sqrt{2} + s_\theta \nu_\tau/\sqrt{2}$. Analogously to the

previous case, we consider $\Delta m^2_{10} \lesssim 10^{-7}$ eV^2 and all the other mass splittings to be much larger than this value, so that the interaction with the neutrino background affects the propagation of the $\nu_0 - \nu_1$ system only. As a consequence, the matter effect modifies the angle ϕ only; the changes of θ are negligibly small. Again, the dynamics of the four neutrino system is reduced to the evolution of the two states ν_s and $\tilde{\nu}$. Introducing the conversion probability $P \equiv P(\nu_s \to \tilde{\nu})$, we find the matrix of probabilities (see eq. (3.65)):

$$\mathcal{P} = \begin{pmatrix} 1-P & c_\theta^2 P & s_\theta^2 P/2 & s_\theta^2 P/2 \\ c_\theta^2 P & s_\theta^4 + c_\theta^4(1-P) & s_\theta^2 c_\theta^2(1-P/2) & s_\theta^2 c_\theta^2(1-P/2) \\ s_\theta^2 P/2 & s_\theta^2 c_\theta^2(1-P/2) & [1+c_\theta^4+s_\theta^4(1-P)]/4 & [1+c_\theta^4+s_\theta^4(1-P)]/4 \\ s_\theta^2 P/2 & s_\theta^2 c_\theta^2(1-P/2) & [1+c_\theta^4+s_\theta^4(1-P)]/4 & [1+c_\theta^4+s_\theta^4(1-P)]/4 \end{pmatrix} \quad (3.75)$$

Taking the CP-symmetric composition (3.63) and assuming that no sterile neutrinos are produced, $N_s^0 = 0$, from eq. (3.75) and (3.65) one gets the numbers of events:

$$\begin{aligned} \vec{N}_\nu &= \left(P, 1-c_\theta^2 P, 1-s_\theta^2 P/2, 1-s_\theta^2 P/2\right) \\ \vec{N}_{\bar{\nu}} &= \left(\bar{P}, 1-c_\theta^2 \bar{P}, 1-s_\theta^2 \bar{P}/2, 1-s_\theta^2 \bar{P}/2\right) . \end{aligned} \quad (3.76)$$

As in the three neutrino case, we have $(N_\mu + N_{\bar{\mu}})/(N_\tau + N_{\bar{\tau}}) = 1$ independently on matter effects. Notice that in the total numbers of events $\vec{N}_\nu + \vec{N}_{\bar{\nu}}$ the conversion probabilities appear in the combination $P+\bar{P}$: since the matter effects have opposite signs for neutrinos and antineutrinos, they partially cancel in this quantity.

Introducing the deviation from the averaged vacuum oscillation probability, $\delta_P \equiv P + \bar{P} - 2P_v$, we compute the ratio:

$$R \equiv \frac{N_e + N_{\bar{e}}}{N_\mu + N_{\bar{\mu}} + N_\tau + N_{\bar{\tau}}} = \frac{1 - c_\theta^2(P_v + \delta_P/2)}{2 - s_\theta^2(P_v + \delta_P/2)} . \quad (3.77)$$

The relative deviation of this ratio from the value given by vacuum oscillations equals:

$$\frac{R - R_v}{R_v} \simeq -\frac{\delta_P}{2} \frac{c_\theta^2 - s_\theta^2/2}{(1 - s_\theta^2 P_v/2)(1 - c_\theta^2 P_v)} . \quad (3.78)$$

Taking $\delta_P \simeq 0.1$, $s_\theta^2 \simeq c_\theta^2 \simeq 1/2$ and $P_v \simeq 0.4$, eq. (3.78) gives a deviation of $\sim 2\%$; the effect is larger, $\sim 10\%$, for small θ: $c_\theta^2 \simeq 1$, $s_\theta^2 \simeq 0$.

For the CP-asymmetric composition (3.64) we get:

$$\begin{aligned} \vec{N}_\nu^0 &= \Big(P(c_\theta^2 + s_\theta^2/2), 1 - s_\theta^2 c_\theta^2 - c_\theta^2 P(c_\theta^2 + s_\theta^2/2) , \\ &\quad (1 + s_\theta^2 c_\theta^2)/2 - s_\theta^2 P(c_\theta^2 + s_\theta^2/2)/2, (1 + s_\theta^2 c_\theta^2)/2 - s_\theta^2 P(c_\theta^2 + s_\theta^2/2)/2\Big) \\ \vec{N}_{\bar{\nu}}^0 &= \Big(s_\theta^2 \bar{P}/2, s_\theta^2 c_\theta^2(1 - \bar{P}/2), \\ &\quad [1 + c_\theta^4 + s_\theta^4(1 - \bar{P})]/4, [1 + c_\theta^4 + s_\theta^4(1 - \bar{P})]/4\Big) . \end{aligned} \quad (3.79)$$

For the ratio, R, of the e-like over non e-like events one gets:

$$\frac{R - R_v}{R_v} \simeq -\left[\delta(1 - s_\theta^2/2) + \bar{\delta} s_\theta^2/2\right] \left[\frac{c_\theta^2 - s_\theta^2/2}{(1 - s_\theta^2 P_v/2)(1 - c_\theta^2 P_v)}\right] , \qquad (3.80)$$

where $\delta \equiv P - P_v$ and $\bar{\delta} \equiv \bar{P} - P_v$.

with the values $\delta \simeq 0.1$, $\bar{\delta} \simeq -0.05$, $P_v \simeq 0.4$ and small mixing, $c_\theta^2 \simeq 1$, $s_\theta^2 \simeq 0$, the deviation (3.80) equals $\sim 15\%$ similarly to the case of CP-symmetric composition, eq. (3.78). The effect is smaller, $\sim 2\%$, for large mixing, $s_\theta^2 \simeq c_\theta^2 \simeq 1/2$.

Our estimation, $10-15\%$ effect, gives some hope that the discussed phenomenon will be observed in future large scale experiments with event rates ~ 1000 events/year.

Chapter 4

Supernova neutrinos: Earth matter effects and neutrino mass spectrum

In this chapter matter effects on oscillations of supernova neutrinos are considered. After an introductory section on the general features of the supernova neutrino fluxes, we focus on the regeneration of the neutrinos in the Earth due to matter effects. We discuss extensively the case of Earth matter effects with oscillation parameters from the LMA solution of the solar neutrino problem; the cases of LOW and SMA parameters are studied briefly in the last section.

4.1 Neutrinos from supernovae: fluxes and energy spectra

Core collapse and supernova explosion are the final stages of the life of massive stars ($M \gtrsim 8M_\odot$). As a consequence of the core collapse, the gravitational binding energy $E_B \simeq 3 \cdot 10^{53}$ ergs is radiated away almost totally in form of neutrinos.

Neutrinos and antineutrinos of all the three flavours, e, μ, τ, are predicted to be produced in the star. The detailed characteristics of these neutrino fluxes depend on the model of the star, however some features can be predicted on general – model-independent – grounds (see e.g. the discussion in [93]):

The equipartition of energy. The neutrinos and antineutrinos of the various flavours are predicted to share the total energy E_B equally with good approximation. Therefore, the energy L_α carried away by the neutrinos of flavour α is simply $L_\alpha \simeq E_B/6$.

The thermal spectrum. Due to their interactions with electrons and nucleons inside the star, the neutrinos of a given species, ν_α, have almost thermal Fermi-Dirac spectrum. Small deviations from the thermal form consist in a "pinching" of the spectrum, i.e. its depletion in the high and low energy tails due to the fact that the radius of the effective neutrinosphere is energy-dependent. However, the effect of pinching disappears in the time-integrated spectra once one considers the cooling of the neutrino gas with time. Therefore, in absence of mixing the ν_α flux at Earth, F^0_α, can be described by the Fermi-Dirac form:

$$F^0_\alpha(E, T_\alpha, L_\alpha, D) = \frac{L_\alpha}{4\pi D^2 T_\alpha^4 F_3} \frac{E^2}{e^{E/T_\alpha} + 1} \ , \tag{4.1}$$

where E is the energy of the neutrinos and T_α is the temperature of the ν_α gas in the neutrinosphere. Typical values of T_α lie in the $1 - 10$ MeV range; they will be discussed in the following of this section. Here D represents the distance of the supernova from the Earth; typically $D \sim 10$ Kpc for a galactic supernova. The quantity F_3 is given by $F_3 = 7\pi^4/120 \simeq 5.68$.

The hierarchy of temperatures. Since neutrinos of different species interact differently with the matter of the star, they have different temperatures. In particular non-electron neutrinos, $\nu_\mu, \nu_\tau, \bar{\nu}_\mu, \bar{\nu}_\tau$, interact by neutral current proccesses only and therefore their spectra are harder than the spectra of ν_e and $\bar{\nu}_e$. Since neutral currents are flavour-blind, muon and tau neutrinos and antineutrinos have approximatively the same temperature ($T_\mu \simeq T_\tau \simeq T_{\bar{\mu}} \simeq T_{\bar{\tau}}$) and therefore the same spectrum. They will be denoted as ν_x from now on. In summary, one gets the hierarchy:

$$T_e < T_{\bar{e}} < T_x \ . \tag{4.2}$$

The inequality of ν_e and $\bar{\nu}_e$ spectra is motivated (i) by the lower interaction cross section of $\bar{\nu}_e$ in matter and (ii) by the fact that ν_e and $\bar{\nu}_e$ are kept in thermal equilibrium mainly by the scattering on neutrons and on protons respectively, and the abundance of neutrons in the star is larger than the one of protons.

Typical values of the temperatures are:

$$T_e = 3 - 4 \text{ MeV} \ , \quad T_{\bar{e}} = 5 - 6 \text{ MeV} \ , \quad T_x = 7 - 9 \text{ MeV} \ . \tag{4.3}$$

Unless differently stated, in our calculations we will take $T_e = 3.5$ MeV, $T_{\bar{e}} = 5$ MeV and $T_x = 8$ MeV. Let us stress, however, that the values of the temperatures depend on the model of the star; lower values are obtained in recent calculations [104] and, moreover, lower temperatures are favoured by the SN1987A data (see chapter 5).

In presence of neutrino mixing and masses the neutrinos undergo flavour conversion on their way from the production point in the star to the detector at Earth.

Matter effects dominate the conversion inside the star, where a wide range of matter densities is met. The conversion effects depend on the distribution of matter in the star; the radial profile

$$\rho_s(r) = 10^{13}\ C \left(\frac{10\ \mathrm{Km}}{r}\right)^3\ \mathrm{g}\cdot\mathrm{cm}^{-3}\ , \tag{4.4}$$

with $C \simeq 1 - 15$ provides a good description of the matter distribution for $\rho_s \gtrsim 1\ \mathrm{g}\cdot\mathrm{cm}^{-3}$ [105, 21, 16, 106]. For $\rho_s \lesssim 1\ \mathrm{g}\cdot\mathrm{cm}^{-3}$ the exact shape of the profile depends on the details of the composition of the star. For the neutrino parameters we will consider the resonant transitions in the star occur at densities larger than $1\ \mathrm{g}\cdot\mathrm{cm}^{-3}$, where the profile (4.4) applies; the value $C = 4$ will be used unless differently stated.

4.2 Neutrino conversion in the star and in the Earth

In this section we summarize the general properties of the Earth matter effect on supernova neutrinos. We will focus on the 3ν-schemes which explain the atmospheric and the solar neutrino data.

4.2.1 Neutrino mass and mixing schemes

We assume that the atmospheric neutrinos have the dominant mode of oscillations $\nu_\mu \leftrightarrow \nu_\tau$ with parameters [107]:

$$|m_3^2 - m_2^2| \equiv \Delta m^2_{atm} = (1.5 - 4)\cdot 10^{-3}\mathrm{eV}^2, \qquad \sin^2 2\theta_{\mu\tau} > 0.88. \tag{4.5}$$

The solar neutrino data are explained either by vacuum oscillations (VO solution) or by one of the MSW solutions (LMA, SMA or LOW). The latter are based on the resonant conversion driven by the oscillation parameters

$$|m_2^2 - m_1^2| \equiv \Delta m^2_{\odot}, \qquad \sin^2 2\theta_{\odot}\ . \tag{4.6}$$

Moreover, we consider $\Delta m^2_{atm} \gg \Delta m^2_{\odot}$.

The electron flavor is distributed in the mass eigenstates ν_1 and ν_2 with admixtures $U_{e1} \approx \cos\theta_{\odot}$, $U_{e2} \approx \sin\theta_{\odot}$. We will call ν_1 and ν_2 the solar pair of states.

Three features of the neutrino schemes, which are important for the supernova neutrino conversion, are still unknown:

1. The admixture U_{e3} of the ν_e in the third eigenstate. Only an upper bound on this parameter is known from the CHOOZ and Palo Verde experiments [108, 109]:

$$|U_{e3}|^2 \lesssim 0.02\ . \tag{4.7}$$

2. The type of mass hierarchy. In the case of *normal* mass hierarchy the solar pair of states is lighter than ν_3: $m_3 > m_2, m_1$. In the case of inverted mass hierarchy the states of the solar pair are heavier than ν_3: $m_3 < m_2 \approx m_1$.

3. The values of the solar parameters $\Delta m^2_{\odot}$, $\sin^2 2\theta_{\odot}$. Different solutions correspond to substantially different values of the oscillation parameters (see e.g. [103]).

The masses and mixings determine the pattern of level crossings in the star [110]. There are two resonances (level crossings) in the schemes under consideration:

- The high density (H) resonance, determined by the parameters Δm^2_{atm} and U_{e3}. The conversion in the region of this resonance is described by the Landau-Zener type probability, P_H, of transition between the matter eigenstates ν_{2m} and ν_{3m}.

- The low density (L) resonance with parameters of the solar pair: $\Delta m^2_{\odot}$, $\sin^2 2\theta_{\odot}$. We denote as P_L the probability of $\nu_{2m} \to \nu_{1m}$ transition associated to this resonance.

Depending on the type of mass hierarchy and on the value of $\theta_{\odot}$, the resonances appear in different channels. There are four possibilities [110]:

1. normal mass hierarchy and $\theta_{\odot} < \pi/4$: both the resonances are in the neutrino channel.

2. normal mass hierarchy and $\theta_{\odot} > \pi/4$: the H resonance is in the neutrino channel, whereas the L resonance is in the antineutrino channel. This possibility is disfavored by the present data on solar neutrinos.

3. inverted mass hierarchy and $\theta_{\odot} < \pi/4$: the H resonance is in the antineutrino channel, the L resonance is in the neutrino channel.

4. inverted mass hierarchy and $\theta_{\odot} > \pi/4$: both the resonances are in the antineutrino channel.

These different schemes correspond to different conversion effects both inside the star and in the matter of the Earth. As it was shown in [110], the Earth effects in the 3ν context depend on (i) the type of mass hierarchy, (ii) the adiabaticity in the high density resonance, which is determined by $|U_{e3}|$ and by the density profile of the star, (iii) the oscillation parameters in the low resonance which are determined by the solution of the solar neutrino problem.

In what follows we will consider the various possibilities in order. We will take oscillation parameters from one of the regions of the solutions of the solar neutrino problem, and also assume that the mixing parameter $|U_{e3}|$ is small, so that oscillations inside the Earth are reduced to 2ν problem.

4.2.2 Antineutrino channels

Let us first consider the scheme with normal mass hierarchy.

As discussed in sect. 4.2.1, in this case there is no level crossing in the high resonance region in the antineutrino channel, so that the antineutrino flux at the detector does not depend on the jump probability P_H. We get:

$$F_{\bar{e}}^D = F_{\bar{e}} + (F_{\bar{e}}^0 - F_x^0)(1 - 2\bar{P}_L)(\bar{P}_{1e} - |U_{e1}|^2) \ , \tag{4.8}$$

where

$$F_{\bar{e}} \approx F_{\bar{e}}^0 - (F_{\bar{e}}^0 - F_x^0)[(1 - \bar{P}_L) - (1 - 2\bar{P}_L)|U_{e1}|^2] \tag{4.9}$$

is the $\bar{\nu}_e$ flux arriving at the surface of the Earth (without Earth matter effect) and the fluxes F_α^0 are defined in eq. (4.1). Here $\bar{P}_{1e}$ denotes the probability of $\bar{\nu}_1 \to \bar{\nu}_e$ conversion inside the Earth and $\bar{P}_L$ is the jump probability in the L resonance. The forms (4.8)-(4.9) are the consequence of the approximate factorization of the dynamics and reduction of the three neutrino problem to an effective two neutrino conversion (see [110] for details).

Let us consider the relative Earth effect expressed by the ratio:

$$\bar{R} \equiv \frac{F_{\bar{e}}^D - F_{\bar{e}}}{F_{\bar{e}}} \ . \tag{4.10}$$

From eqs. (4.8)-(4.9) we find

$$\bar{R} = \bar{r}(1 - 2\bar{P}_L)\bar{f}_{reg} \ , \tag{4.11}$$

where $\bar{r}$ is the ("reduced") flux factor:

$$\bar{r} \equiv \frac{F_{\bar{e}}^0 - F_x^0}{F_{\bar{e}}^0 \left[\bar{P}_L + (1 - 2\bar{P}_L)|U_{e1}|^2\right] + F_x^0 \left[(1 - \bar{P}_L) - (1 - 2\bar{P}_L)|U_{e1}|^2\right]} \ , \tag{4.12}$$

and $\bar{f}_{reg}$ the regeneration factor:

$$\bar{f}_{reg} \equiv (\bar{P}_{1e} - |U_{e1}|^2) \ . \tag{4.13}$$

The three factors present in eq. (4.11) describe the initial conditions (initial fluxes) and different stages of the evolution of the antineutrino state. Let us consider the

properties of these factors in order.

1. The **L-resonance factor**, $(1-2\bar{P}_L)$, is close to the adiabatic value 1 (i.e. $\bar{P}_L \simeq 0$) especially if the resonance is in the neutrino channel [111]. So, in this case from eqs. (4.11)-(4.12) we get the simplified expressions:

$$\bar{R} = \bar{r}\bar{f}_{reg} \ , \tag{4.14}$$

$$\bar{r} = \frac{F^0_{\bar{e}} - F^0_x}{F^0_{\bar{e}}|U_{e1}|^2 + F^0_x(1-|U_{e1}|^2)} \ . \tag{4.15}$$

2. The **flux factor**, eq. (4.15), determines the sign and the size of the effect. Due to the hierarchy of energies, eq. (4.2), a critical energy $\bar{E}_c$ exists at which $\bar{r} = 0$. Furthermore we have $\bar{r} > 0$ below the critical energy, $E < \bar{E}_c$, and $\bar{r} < 0$ for $E > \bar{E}_c$. For realistic temperatures of the neutrino fluxes (see sect. 4.1) one gets:

$$\bar{E}_c = (25-28) \text{ MeV} \ . \tag{4.16}$$

At $E \gg \bar{E}_c$ the flux factor (4.15) is dominated by the harder flux F^0_x, so that one finds the asymptotic behavior:

$$\bar{r}(E \gg \bar{E}_c) = -\frac{1}{(1-|U_{e1}|^2)} \simeq -\frac{1}{|U_{e2}|^2} \ . \tag{4.17}$$

Similarly, at $E \ll \bar{E}_c$ the flux $F^0_{\bar{e}}$ dominates, giving the limit:

$$\bar{r}(E \ll \bar{E}_c) = \frac{1}{|U_{e1}|^2} \ . \tag{4.18}$$

From eqs. (4.17)-(4.18) it follows that at very high, as well as at very low energies, the relative regeneration effect (4.14) becomes independent of the original fluxes.

3. The **regeneration factor**, eq. (4.13), describes the propagation effect inside the Earth and is analogous to the regeneration factor which appears for solar neutrinos. Notice that $\bar{f}_{reg}$ corresponds to genuine matter effect: it is zero in vacuum.

The dynamics of propagation and properties of the regeneration factor (4.13) are different for oscillation parameters from different solutions of the solar neutrino problem.

In what follows we perform numerical calculations of the Earth regeneration factor using a realistic density profile of the Earth [112]. We compare these results with results of the two layers approximation in the Appendix B.

4.2.3 Neutrino channels

If the hierarchy of the neutrino mass spectrum is normal, the H resonance is in the neutrino channel and the ν_e flux at the detector depends on P_H [110]:

$$F_e^D \simeq F_e + (F_e^0 - F_x^0) P_H (1 - 2P_L)(P_{2e} - |U_{e2}|^2) \ , \tag{4.19}$$

where the ν_e flux arriving at the surface of the Earth equals:

$$F_e \simeq F_e^0 - (F_e^0 - F_x^0)[1 - P_H P_L - P_H(1 - 2P_L)|U_{e2}|^2] \ . \tag{4.20}$$

Here P_{2e} is the probability of the transition $\nu_2 \to \nu_e$ inside the Earth.

From eqs. (4.19)-(4.20) one finds the relative Earth matter effect, $R \equiv (F_e^D - F_e)/F_e$, and the flux factor, r:

$$R = r P_H (1 - 2P_L) f_{reg} \ , \tag{4.21}$$

$$r = \frac{F_e^0 - F_x^0}{F_e^0 P_H \left[P_L + (1 - 2P_L)|U_{e2}|^2\right] + F_x^0 \left[1 - P_H P_L - P_H(1 - 2P_L)|U_{e2}|^2\right]} \ . \tag{4.22}$$

The regeneration factor, f_{reg}, is given by:

$$f_{reg} \equiv (P_{e2} - |U_{e2}|^2) = -(P_{1e} - |U_{e1}|^2) \ . \tag{4.23}$$

Let us comment on the features of the ratio R:

1. From eq. (4.21) it follows that if the adiabaticity in the high density (H) resonance inside the star is fulfilled, $P_H \to 0$, the Earth matter effect disappears. The reason is that in the adiabatic case the original electron neutrinos convert almost completely into ν_μ and ν_τ fluxes in the H resonance. Then the electron neutrinos detected at Earth result from the conversion of the original ν_μ and ν_τ fluxes. Since these fluxes are equal, (see sect. 4.1), no oscillation effect will be observed due to conversion in the low density resonance.

The Earth matter effect is maximal in the limit of strong violation of the adiabaticity in the H-resonance: $P_H \to 1$, when the dynamics is reduced to a two neutrino problem with oscillation parameters of the L resonance.

The jump probability P_H is determined by the density profile of the star and the oscillation parameters $|U_{e3}|^2 \approx \tan^2\theta_{13}$ and Δm^2_{atm}. In fig. 4.1 we show the lines of equal P_H in the $(\Delta m^2_{atm} - \tan^2\theta_{13})-$ plane, together with the exclusion region from the CHOOZ experiment. We use the density profile (4.4); the error in P_H due to the uncertainty in the density profile is estimated to be within a factor of 2 [110]. The figure shows that as $|U_{e3}|^2$ decreases in the range allowed by the bound (4.7) the transition in the H resonance varies from perfectly adiabatic ($P_H \simeq 0$), for

$|U_{e3}|^2 \gtrsim 5 \cdot 10^{-4}$, to strongly non-adiabatic ($P_H \simeq 1$), for $|U_{e3}|^2 \lesssim 10^{-6}$. The intervals of adiabaticity and strong adiabaticity violation change only mildly as Δm^2_{atm} varies in the presently allowed range. Notice that future atmospheric neutrino studies and the long base-line experiments will sharpen the allowed region of Δm^2_{atm}.

2. The low density resonance factor, $(1-2P_L)$, is zero if $P_L = 1/2$, which corresponds to a situation when the neutrino beam arriving at Earth consists in incoherent and equal fluxes of ν_1 and ν_2. In this case the effects of $\nu_1 \to \nu_e$ and $\nu_2 \to \nu_e$ oscillations cancel each other.

In fig. 4.2 we show the lines of $P_L = 1/2$, calculated with the density profile (4.4) in the $(\tan^2\theta_\odot - \Delta m^2_\odot)$ plane for different values of the neutrino energy. The lines cross the allowed region of the SMA solutions for the energy interval $E = 5-15$ MeV. In fig. 4.2 we show also the lines $P_L = 0.05$ for two different energies: $E = 5$ MeV and $E = 50$ MeV. These lines determine the lower edge of the adiabaticity region in the $(\tan^2\theta_\odot - \Delta m^2_\odot)$ plane. Notice that the LMA region is in the adiabaticity domain for all the relevant energies, whereas the SMA solution region is in the domain of significant adiabaticity violation. Depending on the details of the density profile of the star the LOW solution lies either in the adiabaticity region or in the region of partial adiabaticity breaking.

A qualitative treatment does not depend on whether the low density resonance is in the neutrino or antineutrino channel (dark side of the parameter space). Quantitatively the results are different.

3. The flux factor, r, eq. (4.22), changes sign at lower critical energy with respect to the case of antineutrinos, since the original ν_e spectrum is softer than the $\bar{\nu}_e$ spectrum. We get:

$$E_c = (16 - 24) \text{ MeV} . \tag{4.24}$$

Similarly to what was discussed for $\bar{\nu}_e$, the flux factor becomes independent of the original fluxes in the low and high energy limits:

$$r(E \gg E_c) = -\frac{1}{1 - P_H P_L - P_H(1-2P_L)|U_{e2}|^2} , \tag{4.25}$$

$$r(E \ll E_c) = \frac{1}{P_H\,[P_L + (1-2P_L)|U_{e2}|^2]} . \tag{4.26}$$

4. The Earth regeneration factor, eq. (4.23), depends on the mixing and mass squared difference of the solar pair and on the nadir angle θ_n. It will be described in detail in the following sections.

4.2.4 Schemes with inverted mass hierarchy

If the hierarchy of the mass spectrum is inverted the high density resonance is in the antineutrino channel (see sect. 4.2.1) and the Earth matter effect for $\bar{\nu}_e$ depends on the jump probability P_H. The expressions (4.8)-(4.9) for the $\bar{\nu}_e$ fluxes are immediately generalized to:

$$F_{\bar{e}}^D = F_{\bar{e}} + (F_{\bar{e}}^0 - F_x^0)P_H(1 - 2\bar{P}_L)(\bar{P}_{1e} - |U_{e1}|^2) \ , \tag{4.27}$$

$$F_{\bar{e}} \approx F_{\bar{e}}^0 - (F_{\bar{e}}^0 - F_x^0)[1 - P_H\bar{P}_L - P_H(1 - 2\bar{P}_L)|U_{e1}|^2] \ , \tag{4.28}$$

in analogy with eqs. (4.19)-(4.20).

Taking $\bar{P}_L = 0$ (see sect. 4.2.2), we find the relative deviation, $\bar{R}$, and the reduced flux factor:

$$\bar{R} = \bar{r}P_H\bar{f}_{reg} \ , \tag{4.29}$$

$$\bar{r} = \frac{F_{\bar{e}}^0 - F_x^0}{F_{\bar{e}}^0 P_H|U_{e1}|^2 + F_x^0(1 - P_H|U_{e1}|^2)} \ , \tag{4.30}$$

with the asymptotic limits:

$$\bar{r}(E \gg \bar{E}_c) = -\frac{1}{1 - P_H|U_{e1}|^2} \ , \tag{4.31}$$

$$\bar{r}(E \ll \bar{E}_c) = \frac{1}{P_H|U_{e1}|^2} \ . \tag{4.32}$$

Clearly, the conversion of ν_e is independent of P_H. The expressions of the neutrino fluxes F_e^D and F_e can be obtained from eqs. (4.19)-(4.20) by the replacement $P_H \to 1$; they become analogous to eqs. (4.8)-(4.9). With the same prescription, from eqs. (4.21)-(4.22) one gets the expressions of the ratios R and r.

Summarizing the results of sections 4.2.2-4.2.4 we can say that the mass hierarchy and the adiabaticity in the H density resonance (and thus U_{e3}) determine the channel (ν_e or $\bar{\nu}_e$) in which the Earth matter effects appear, which is:

- both the ν_e and $\bar{\nu}_e$ channels if the H resonance is strongly non-adiabatic, $P_H = 1$, regardless to the hierarchy.
- the $\bar{\nu}_e$ channel for adiabatic H resonance, $P_H = 0$, and normal hierarchy.
- the ν_e channel for adiabatic H resonance, $P_H = 0$, and inverted hierarchy.

The possibility of probing U_{e3} and the mass hierarchy by the study of Earth effects on supernova neutrinos will be discussed in chapter 6.

4.3 The Earth matter effects for LMA parameters

4.3.1 Antineutrino channels

Let us now study the features of the relative Earth matter effect, eq. (4.14), for $\bar{\nu}_e$ with mixing and mass squared difference in the LMA region.

The dynamics of the conversion inside the Earth is described by the regeneration factor $\bar{f}_{reg}$, eq. (4.13). For LMA parameters the Earth matter effect consists in an oscillatory modulation of the neutrino energy spectrum.

The fig. 4.3 shows the ratio $\bar{R}$ as a function of the neutrino energy for various trajectories of the neutrinos inside the Earth. The trajectory in the Earth is described by the nadir angle θ_n of the supernova with respect to the detector (see chapter 6 for a more detailed discussion). For $\theta_n > 33.2°$ the neutrinos cross the mantle of the Earth only; for $\theta_n < 33.2°$ the core is crossed too. For mantle crossing trajectories, the Earth effect is mainly due to the interplay of oscillations and adiabatic evolution. That is, oscillations in medium with slowly varying density. Small density jumps produce only rather weak effects. As a result, the features of the regeneration factor, $\bar{f}_{reg}$, are similar to what is predicted in the case of propagation in medium with constant density (see Appendix B). The factor is positive in the whole energy spectrum, so that the sign of the matter effect is determined by the flux factor (4.15): we have $\bar{R} > 0$ for $E < \bar{E}_c$ and $\bar{R} < 0$ for $E > \bar{E}_c$.

The energy spectrum shows regular oscillations in energy with period

$$\Delta E \approx \frac{2\pi}{\phi(\theta_n, E)} E \,, \tag{4.33}$$

where the oscillation phase ϕ is determined by the integral

$$\phi(\theta_n) = 2\pi \int_0^{r(\theta_n)} \frac{dx}{l_m(n(x), E)} \tag{4.34}$$

over the neutrino trajectory. Here l_m is the (instantaneous) oscillation length in matter, and $n(x)$ is the electron density along the trajectory. As follows from eqs. (4.33)-(4.34) the period of oscillations decreases with the nadir angle and increases with the energy. The dependence on the energy appears in ΔE, (see eq. (4.33)) explicitly, and implicitly via the oscillation length.

As a result of adiabatic evolution, the depth of oscillations of the regeneration factor is determined by the electron number density at the surface of the Earth (see Appendix B), n_e^0:

$$\bar{D}_f \approx 2\sqrt{2} G_F n_e^0 \frac{E}{\Delta m^2_\odot} \sin^2 2\theta_m^0 \,. \tag{4.35}$$

Here θ_m^0 is the mixing angle of the solar pair in matter at the surface.

The depth $\bar{D}_f$ has a resonant dependence on the quantity $x \equiv 2E|V|/\Delta m^2_{\odot}$, with V being the matter potential (see the Appendix B for details). Both $\bar{D}_f$ and l_m increase as the system approaches the resonance; correspondingly, the period $\Delta E/E$ increases. For neutrinos propagating in the mantle and $\Delta m^2_{\odot} = 5 \cdot 10^{-5}$ eV^2 (which is used in the figure 4.3) the resonance is realized at $E = \bar{E}_R \simeq 150$ MeV. Thus the Earth effect is larger in the highest energy part of the spectrum.

For core crossing trajectories the behavior of the Earth effect becomes irregular due to the interference of the oscillations in the core and in the mantle. The modulations in the energy spectra have smaller period both due to presence of large densities and larger length of the trajectory. Moreover, now the effect can change the sign both below and above the critical energy. That is, for some energies the Earth effect is negative at low energies and positive at high energies.

As $\Delta m^2_{\odot}$ decreases, as shown in fig. 4.4, the regeneration factor increases, since the resonance of the system is realized at lower energies. In particular, for $\Delta m^2_{\odot} = 2 \cdot 10^{-5}$ eV^2, the resonance energy equals $E_R \simeq 60$ MeV. The period (in the energy scale) of the oscillatory modulation of the spectrum increases with the decrease of $\Delta m^2_{\odot}$.

The change of the mixing parameter $|U_{e1}|^2 \approx \cos^2\theta_{\odot}$ (within the LMA region) influences the regeneration factor rather weakly. However variations of $|U_{e1}|^2$ change the spectrum arriving at the surface of the Earth. According to the eq. (4.9), with the increase of $|U_{e1}|^2$ (i.e. decrease of the mixing $\theta_{\odot}$), the contribution of the hard component in the spectrum decreases: the composite spectrum becomes softer.

Given the mixing U_{e1} the factor $\bar{r}$, eq. (4.15), depends only on the original fluxes, $F^0_{\bar{e}}$ and F^0_x. The fig. 4.5 shows the relative Earth effect, $\bar{R}$, as a function of the energy for different values of $\bar{r}$ determined by different temperatures of the original $\bar{\nu}_e$ spectrum. As it appears in the figure, the critical energy $\bar{E}_c$ decreases with $T_{\bar{e}}$, so that the region in which the flux factor suppresses the regeneration effect shifts to lower energies. For $E \ll \bar{E}_c$ and $E \gg \bar{E}_c$ the depth of oscillations depends only very weakly on variations of $T_{\bar{e}}$, according to the limits (4.18) and (4.17), which do not depend on temperatures. The values of $T_{\bar{e}}$ and T_x only affect the rapidity of the convergence to these limits: the convergence is faster for the larger difference $T_x - T_{\bar{e}}$. This appears in fig. 4.6 b), in which the flux factor $\bar{r}$ is plotted as a function of the antineutrino energy with the same parameters as in the fig. 4.5. For $\sin^2 2\theta_{\odot} = 0.75$, as used in the figs. 4.5-4.6, one finds $\bar{r}(E \ll \bar{E}_c) = 1.33$ and $\bar{r}(E \gg \bar{E}_c) = -4$. Thus the Earth effect has stronger enhancement at high energies.

If the hierarchy is inverted the Earth matter effect on $\bar{\nu}_e$ is affected by the adiabaticity in the high density resonance. Such dependence is illustrated in fig. 4.7, which shows the the relative effect $\bar{R}$ as a function of the energy for various values of P_H [1].

[1]Rigorously, P_H is energy dependent, however this dependence is weak (see e.g. [110]). There-

According to eq. (4.29) the effect is proportional to P_H and is maximal at $P_H = 1$. The dependence of $\bar{R}$ on P_H is transparent in the limits of high and low energies. Combining eqs. (4.29) and (4.31) we find that at high energies $\bar{R}$ depends on P_H as:

$$\bar{R}(E \gg \bar{E}_c) = -\frac{P_H}{1 - P_H|U_{e1}|^2} \bar{f}_{reg} \ , \tag{4.36}$$

that is, $\bar{R} \propto P_H$ for $P_H \ll 1$. The weak dependence of $\bar{R}$ on P_H in the softer part of the spectrum in fig. 4.7 is explained by the fact that the dependence on P_H cancels in the low energy limit, $E \ll \bar{E}_c$, as can be seen from eqs. (4.29) and (4.32).

4.3.2 Neutrino channels

Let us discuss the properties of the Earth regeneration effect in the ν_e channel.

As it was shown in fig. 4.2, for LMA oscillation parameters the adiabaticity in the L-resonance inside the star is satisfied, so that $P_L = 0$ and eqs. (4.21)-(4.22) reduce to:

$$R = r P_H f_{reg} \ , \tag{4.37}$$

$$r = \frac{F_e^0 - F_x^0}{F_e^0 P_H |U_{e2}|^2 + F_x^0 (1 - P_H |U_{e2}|^2)} \ . \tag{4.38}$$

The regeneration factor f_{reg}, eq. (4.23), and therefore R, have similar dependence on θ_n and $\Delta m^2_\odot$ as in the case of antineutrinos. These dependences are illustrated in the figs. 4.8 and 4.9, where $P_H = 1$ was taken. The oscillation length and the period of the modulations in the energy spectrum increase with the increase of the energy and the decrease of $\Delta m^2_\odot$ (fig. 4.9). The depth of the oscillations of the regeneration factor f_{reg} is larger than for antineutrinos since (if the L resonance is in the neutrino channel) matter enhances the ν_e mixing and suppresses the mixing of $\bar{\nu}_e$:

$$\sin^2 2\theta_m(\bar{\nu}) < \sin^2 2\theta_\odot < \sin^2 2\theta_m(\nu) \ . \tag{4.39}$$

The depth of oscillations has a resonant character (see Appendix B), increasing as the resonance energy is approached. According to eq. (4.35) the depth gets larger for smaller $\Delta m^2_\odot$ (fig. 4.9).

The dependence of the Earth matter effect on the flux factor, r, eq. (4.38), is illustrated in fig. 4.10, where the ratio R is plotted for different values of the temperature T_e, $T_x = 8$ MeV and $P_H = 1$. According to sects. 4.2.2 and 4.2.3 the flux factor suppresses the Earth matter effect at energies close to the critical energy, E_c, which is

fore, for illustrative purpose we considered P_H to be constant with energy.

slightly lower than for $\bar{\nu}_e$: $E_c \simeq 22$ MeV for $T_e = 3.5$ MeV. At high and low energies the asymptotic limits (4.25)-(4.26) are realized. This is shown in fig. 4.6 a), with the same values of the temperatures as in fig. 4.10 and $P_H = 1$. From eqs. (4.25)-(4.26) (with $P_L = 0$) and from the fig. 4.6 it follows that, in contrast to the case of $\bar{\nu}_e$, the Earth effect has stronger enhancement at low energy: for $\sin^2 2\theta_\odot = 0.75$ one gets $r(E \ll E_c) = 4$ and $r(E \gg E_c) = -1.33$. Notice that the convergence to these limits is faster than for $\bar{\nu}_e$ due to larger difference of the ν_e and ν_x temperatures.

According to eq. (4.37), the Earth matter effect is larger for larger P_H, i.e. for maximal adiabaticity breaking in the high density resonance inside the star. From eqs. (4.37) and (4.38) the following asymptotic limit follows:

$$R(E \gg E_c) = -\frac{P_H}{1 - P_H |U_{e2}|^2} f_{reg} \ , \tag{4.40}$$

similarly to eq. (4.36). The combination of eqs. (4.37) and (4.26) implies that R becomes independent of P_H at $E \ll E_c$. These features of the dependence of R on P_H are shown in fig. 4.11.

As discussed in sect. 4.2.4, the results for inverted hierarchy of the spectrum are obtained from the description given for normal hierarchy by the replacement $P_H \to 1$. Therefore the results shown in the figs. 4.8-4.10, in which $P_H = 1$ was used, apply to the case of inverted hierarchy.

4.4 The case of oscillation parameters in the LOW and SMA regions

4.4.1 LOW parameters

For oscillation parameters in the region of the LOW solution of the solar neutrino problem the mass squared difference is smaller by at least two orders of magnitude with respect to the LMA solution: $\Delta m^2_\odot \sim 10^{-8} - 10^{-7}$ eV^2. Therefore the resonance energy in the Earth is very small, $E_R < 1$ MeV, and in the whole energy spectrum of supernova neutrinos the neutrino system is far above the resonance. Both the ν_e and $\bar{\nu}_e$ mixings are suppressed in the matter of the Earth and the oscillation lengths approach the refraction length, $l_m \approx l_0 \sim 8000$ Km. As a consequence, the regeneration inside the Earth has only weak dependence on the neutrino energy and no oscillatory distortions appear in the energy spectra at the detectors. In contrast, the regeneration effect depends strongly on the nadir angle θ_n: for $E = 10$ MeV the regeneration factor has a maximum, $f_{reg} \simeq 0.04$, for $\theta_n \simeq 25^\circ$ (see e.g. [113]).

The fig. 4.12 shows the relative Earth effects for ν_e and $\bar{\nu}_e$ as functions of the energy for $\Delta m^2_\odot = 10^{-7}$ eV^2, $\sin^2 2\theta_\odot = 0.9$, $\theta_n = 25°$ and $P_H = 1$. We have also considered perfect adiabaticity in the L resonance inside the star, $P_L = 0$. The figure shows that for $E > 5$ MeV the effect is not larger than 20% for ν_e and 10% for $\bar{\nu}_e$; it decreases with the increase of energy with a $\sim 1/E$ behavior. In the neutrino channel the relative deviation R, eq. (4.21), is larger than in the antineutrino channel, especially in the very soft part of the spectrum, $E \lesssim 10$ MeV. This is explained (i) by the fact that the neutrino system approaches the resonance at low energies, and therefore the ν_e mixing is enhanced, and (ii) by the larger flux factor in the low energy limit, $E \ll E_c$ (see fig. 4.6). We get $\sim 50\%$ effect at $E = 2$ MeV and $\sim 100\%$ at $E = 1$ MeV.

4.4.2 SMA parameters

For oscillation parameters in the SMA region the fluxes at the detector, $F^D_{\bar{e}}$ and F^D_e, eqs. (4.8) and (4.19), are substantially different with respect to the case of LMA parameters, due to differences in the L resonance factor, $(1 - 2P_L)$, and in the regeneration factor.

In what follows we describe the Earth effect for ν_e; effects on $\bar{\nu}_e$ conversion are extremely small due to the suppression of the mixing in matter and will not be considered.

Let us first discuss the factor $(1 - 2P_L)$. For $\Delta m^2_\odot$ and $\sin^2 2\theta_\odot$ in the SMA region the conversion in the L resonance inside the star occurs in the adiabaticity breaking regime (fig. 4.2). The jump probability P_L differs from 0 significantly and, in particular, as shown in fig. 4.2, P_L is close to 1/2, thus suppressing the matter effect (eq. (4.21)).

In fig. 4.13 we show the factor $(1 - 2P_L)$ as a function of the neutrino energy for $\Delta m^2_\odot = 6 \cdot 10^{-6}$ eV^2 and two values of $\sin^2 2\theta_\odot$ in the SMA region. We used the profile (4.4) with $C = 4$. For the largest possible mixing, $\sin^2 2\theta_\odot \sim 5 \cdot 10^{-3}$, the factor is negative above 10 MeV; for the best fit point, $\sin^2 2\theta_\odot \sim 2.4 \cdot 10^{-3}$, it is negative in the whole detectable part of the spectrum ($E > 5$ MeV). These results, however, strongly depend on the model of the star. For massive stars ($M > 30 M_\odot$) the density profile may have smaller gradient, so that the adiabaticity breaking is weaker. In this case the energy at which $P_L = 1/2$ is larger, and in a significant part of the spectrum the low resonance factor can be positive. Notice that in the high energy part of the spectrum the factor can be as large as 0.7 - 0.8 in absolute value.

The regeneration factor, f_{reg}, eq. (4.23), has a peculiar resonant behaviour in dependence on the energy and on the nadir angle θ_n. For mantle crossing trajectories, $\theta_n > 33.2°$, the matter effect consists in resonantly enhanced oscillations, with os-

cillation length comparable or larger than the radius of the Earth. A peak appears in the ν_e spectrum at $E \sim 15$ MeV.

For core crossing trajectories, $\theta_n < 33.2°$, the regeneration factor exhibits a narrow peak at $E \simeq 7$ MeV due to parametric resonance, with two smaller peaks at higher and lower energy due to MSW resonances in the mantle and in the core respectively. These features are shown in the fig. 4.14, which represents the relative deviation R as a function of the energy for $P_H = 1$, $\theta_n = 0°$ and various values of the factor C in the density profile (4.4), corresponding to different values of P_L. With increase of C the jump probability P_L decreases, so that the region where $(1 - 2P_L) > 0$ expands to higher energies. With the decrease of P_L the Earth matter effect changes from negative to positive and the size of the effect increases; it can be as large as $\sim 30\%$.

As in the case of the LMA solution, the effect decreases with P_H and disappears for perfectly adiabatic transition in the H resonance, $P_H = 0$. If the mass hierarchy is inverted the matter effect exists, in the neutrino channel, independently of the character of the H resonance.

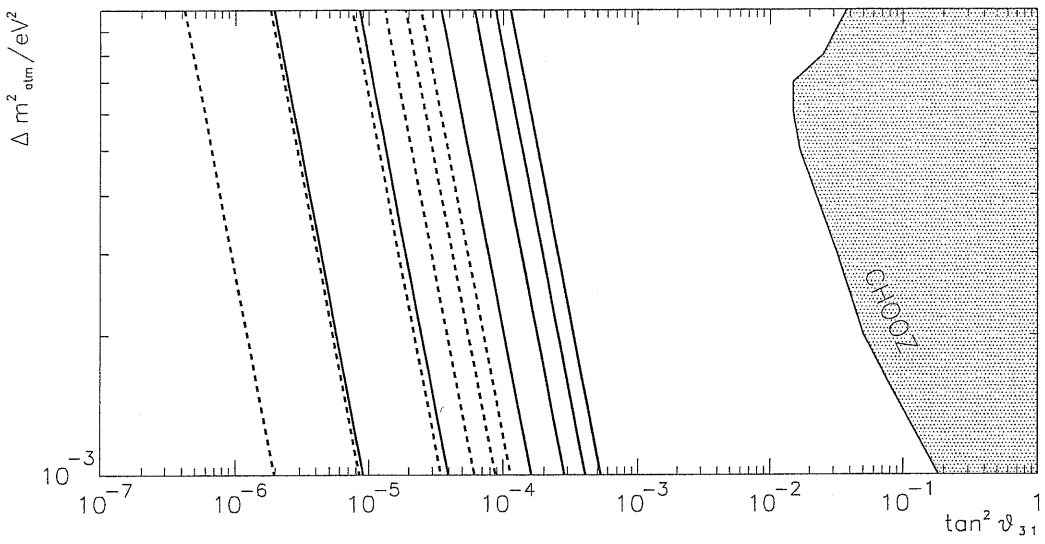

Figure 4.1: Lines of constant flip probability P_H in the Δm^2_{atm}-$\tan^2\theta_{31}$ plane. The solid lines refer to $E = 50$ MeV and correspond, from right to left, to $P_H = 0.05, 0.1, 0.2, 0.4, 0.8, 0.95$. The dashed lines correspond to the same values of P_H with $E = 5$ MeV. The exclusion region from the CHOOZ experiment is shown.

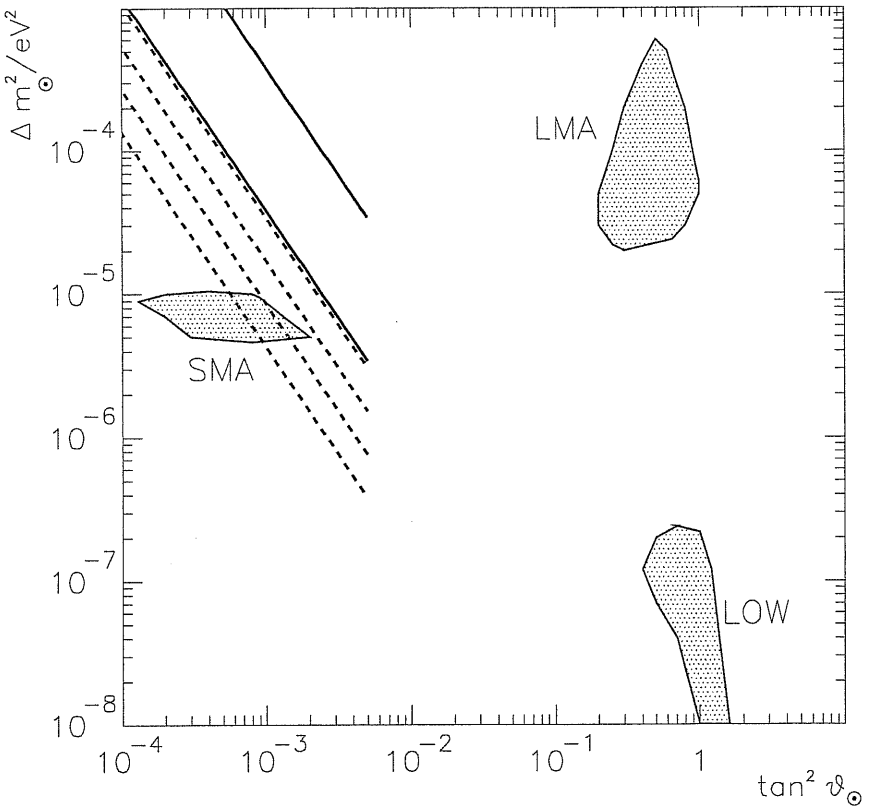

Figure 4.2: Lines of constant jump probability in the low density resonance, P_L, in the $\tan^2\theta_\odot$-$\Delta m^2_\odot$ plane. The solid lines correspond to $P_L = 0.05$, $E = 50$ MeV (upper line) and $E = 5$ MeV (lower line). The dashed lines correspond to $P_L = 0.5$ and, from the upper to the lower, $E = 40, 20, 10, 5$ MeV. The plot of the lines is restricted to the region of parameters for which the L-resonance inside the star occurs at densities larger than 1 $g \cdot cm^{-3}$ (see sect. 4.1 of the text). The allowed regions for the SMA, LMA and LOW solutions of the solar neutrino problem are represented.

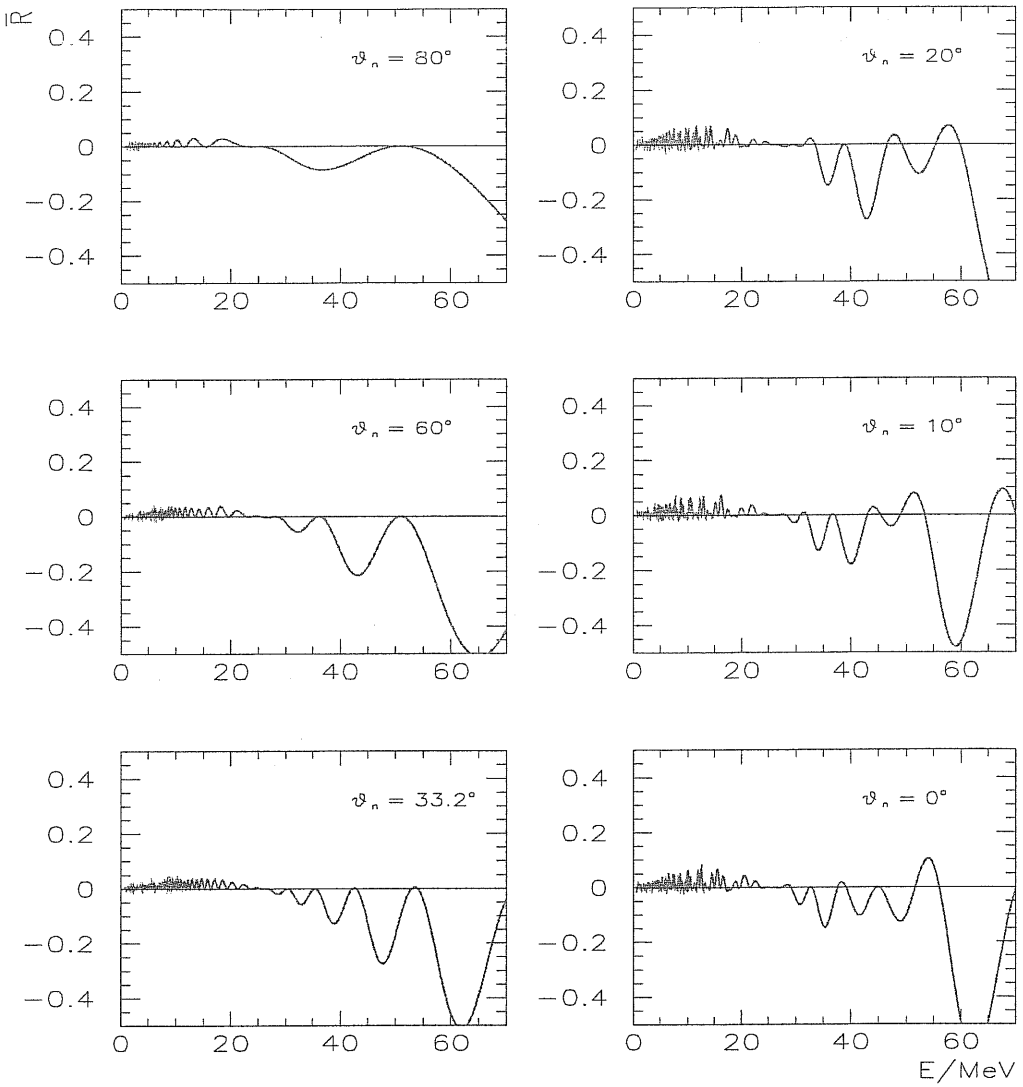

Figure 4.3: The relative Earth matter effect in $\bar{\nu}_e$ channel, $\bar{R}$, as function of the antineutrino energy for LMA oscillation parameters and various values of the nadir angle θ_n. We have taken $\Delta m^2_{\odot} = 5 \cdot 10^{-5}$ eV^2, $\sin^2 2\theta_{\odot} = 0.75$; $T_{\bar{e}} = 5$ MeV, $T_x = 8$ MeV. The figure refers to normal mass hierarchy (or inverted hierarchy with $P_H = 1$).

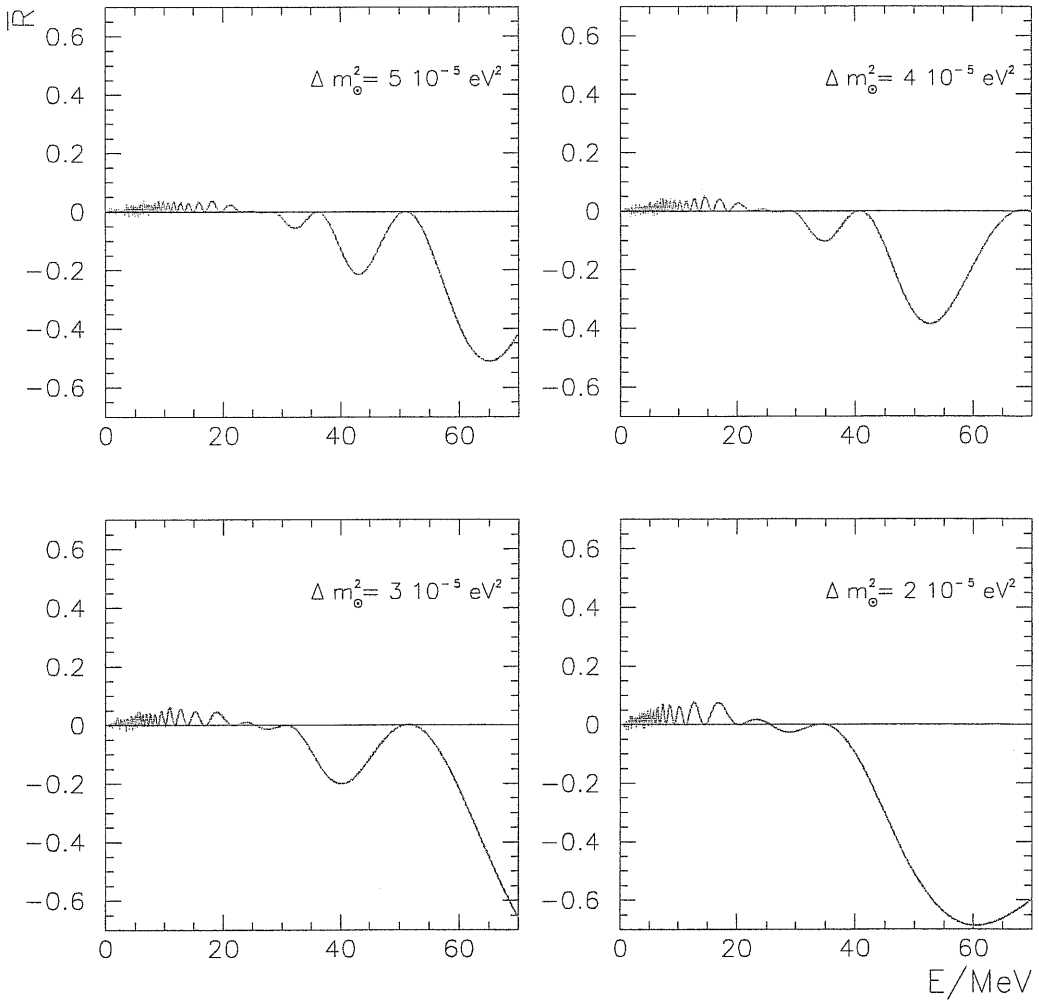

Figure 4.4: The same as fig. 4.3 for $\theta_n = 60°$ and various values of $\Delta m^2_{\odot}$.

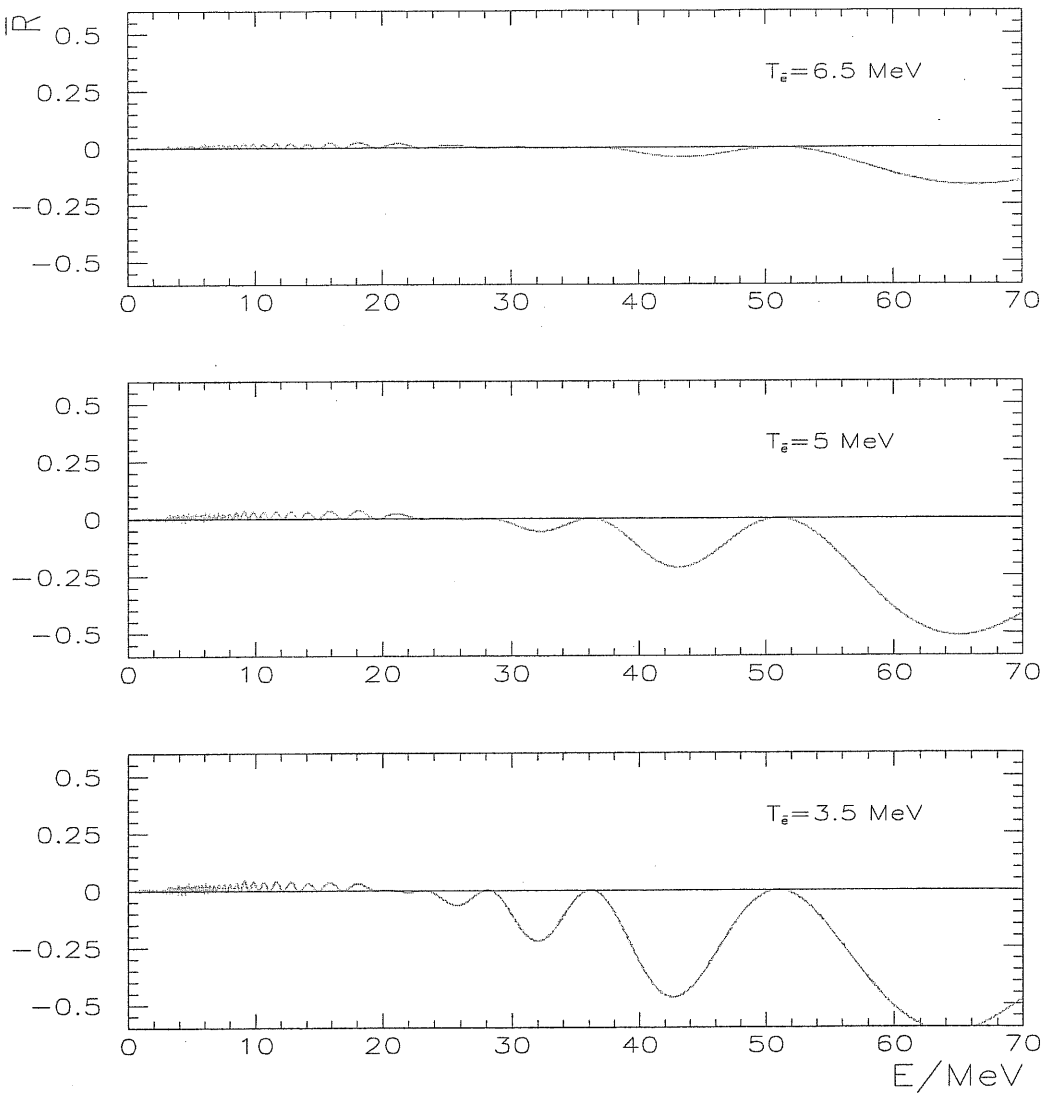

Figure 4.5: The same as fig. 4.3 for $\theta_n = 60°$ and various values of $T_{\bar{e}}$.

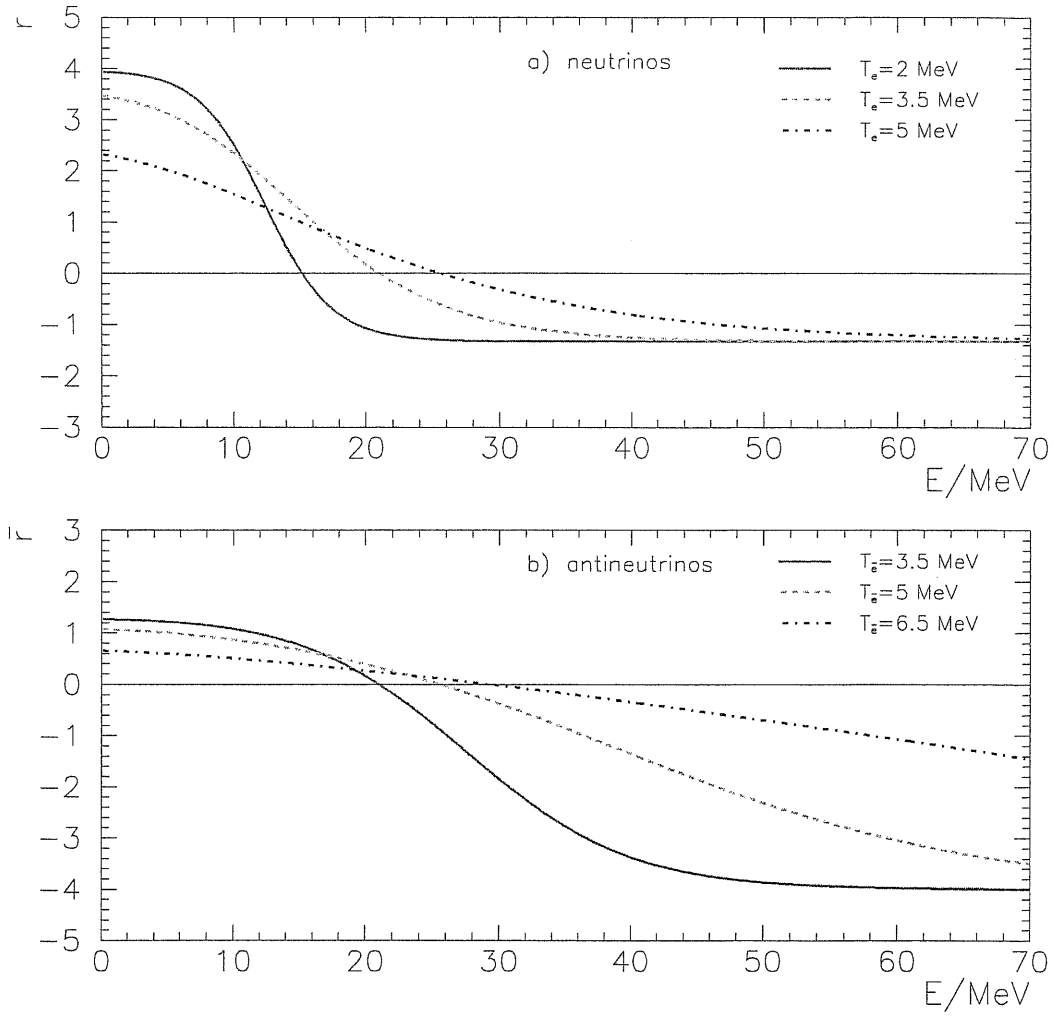

Figure 4.6: The flux factors r and $\bar{r}$ for various values of the temperatures T_e and $T_{\bar{e}}$. We have taken $T_x = 8$ MeV, $\Delta m^2_{\odot} = 5 \cdot 10^{-5}$ eV^2, $\sin^2 2\theta_{\odot} = 0.75$ and $P_H = 1$.

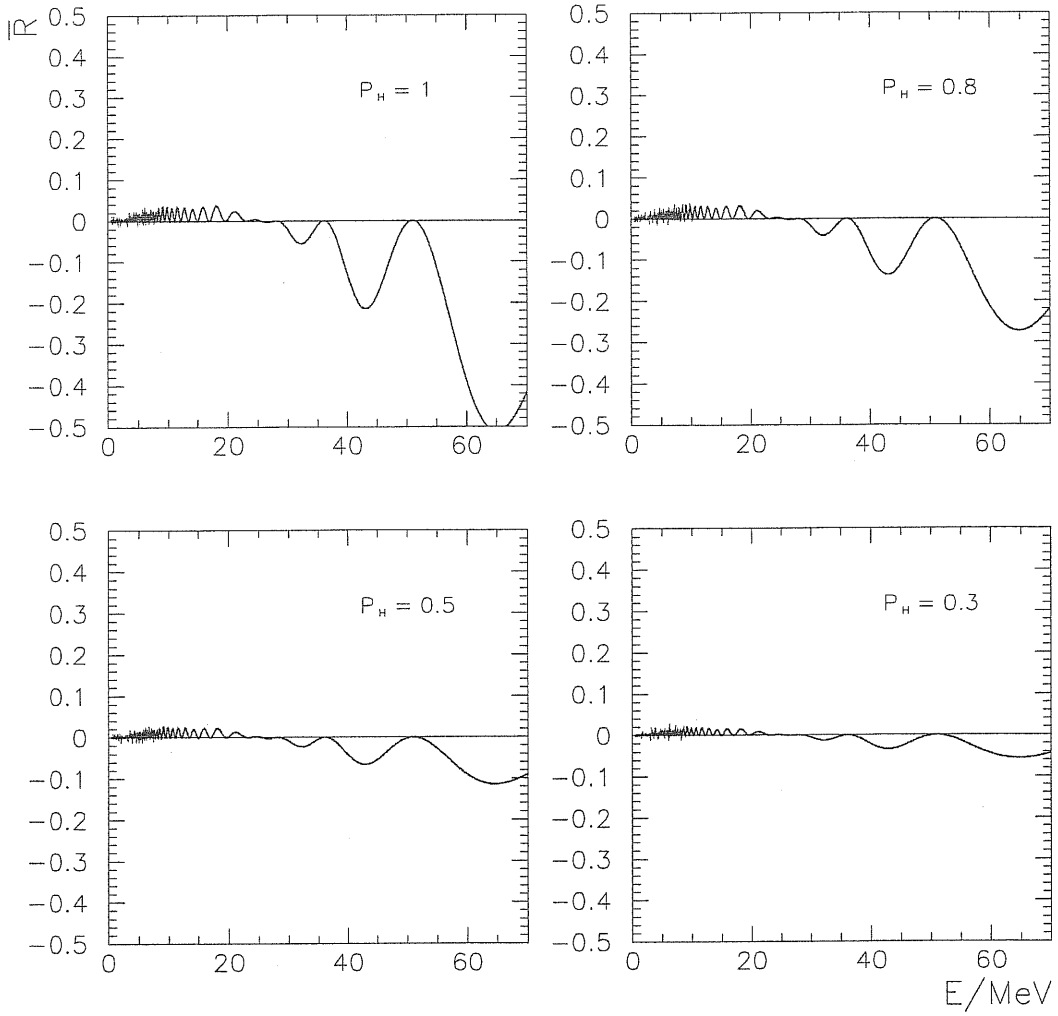

Figure 4.7: The same as fig. 4.3 for inverted mass hierarchy and various values of P_H. We have taken $\theta_n = 60°$.

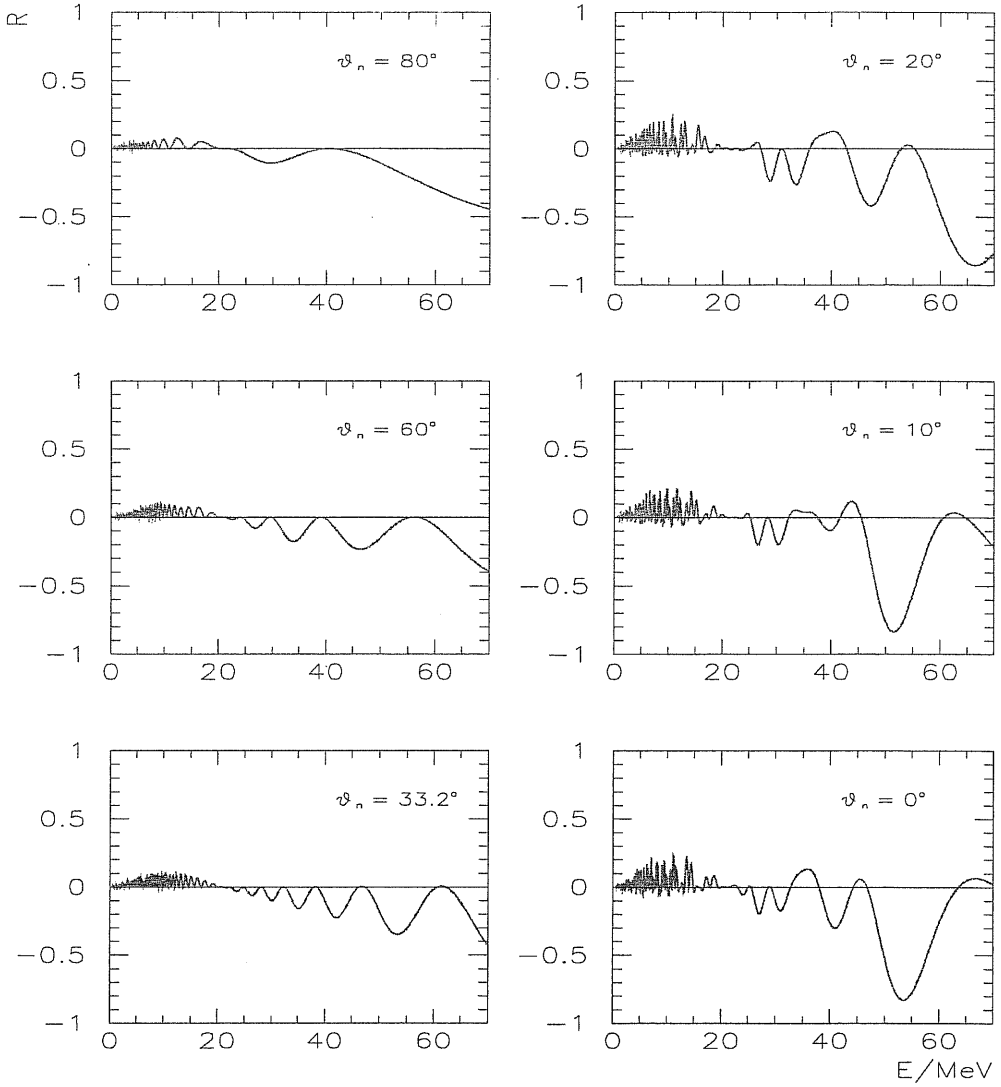

Figure 4.8: The relative Earth matter effect in ν_e channel, R, as function of the neutrino energy for LMA oscillation parameters and various values of the nadir angle θ_n. We have taken $\Delta m^2_\odot = 5 \cdot 10^{-5}$ eV^2, $\sin^2 2\theta_\odot = 0.75$; $T_e = 3.5$ MeV, $T_x = 8$ MeV; $P_H = 1$ (or inverted hierarchy).

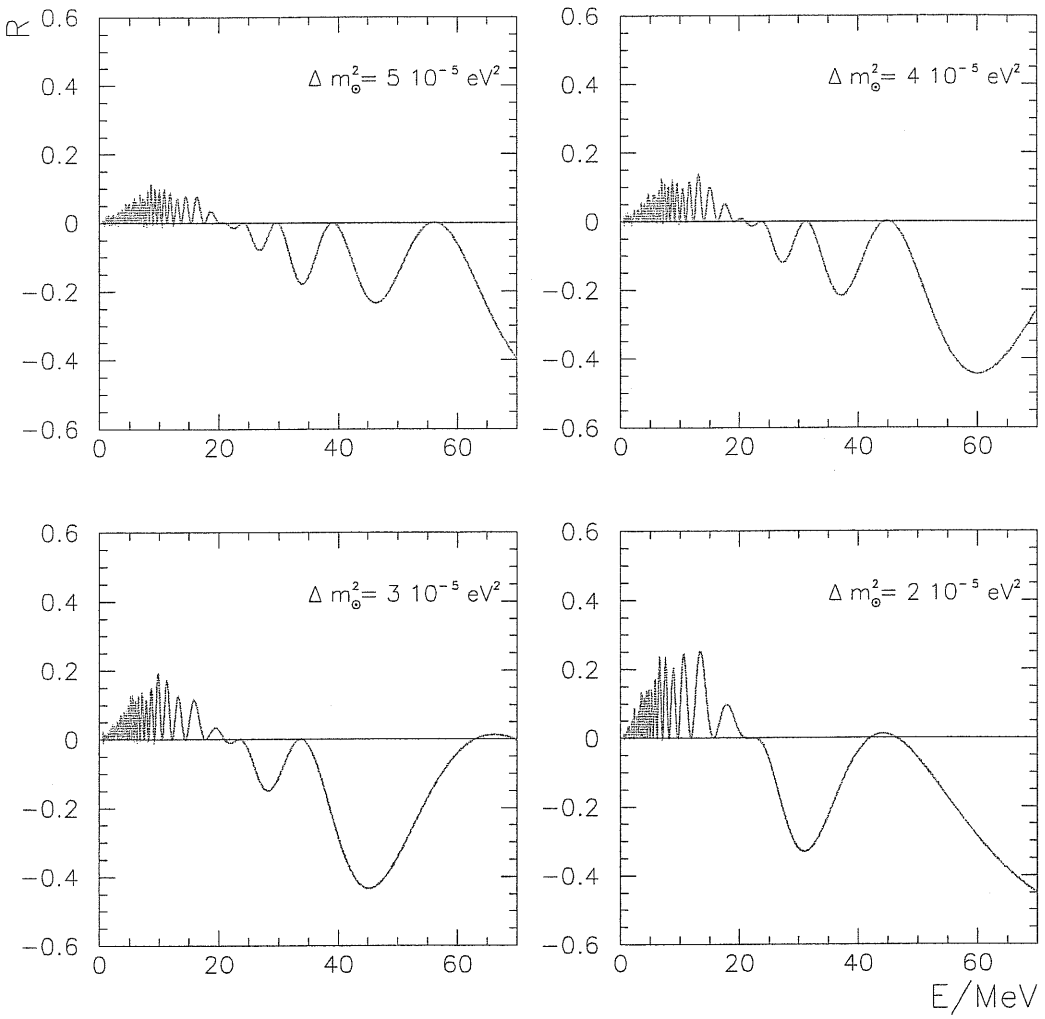

Figure 4.9: The same as fig. 4.8 for $\theta_n = 60°$ and various values of $\Delta m^2_\odot$.

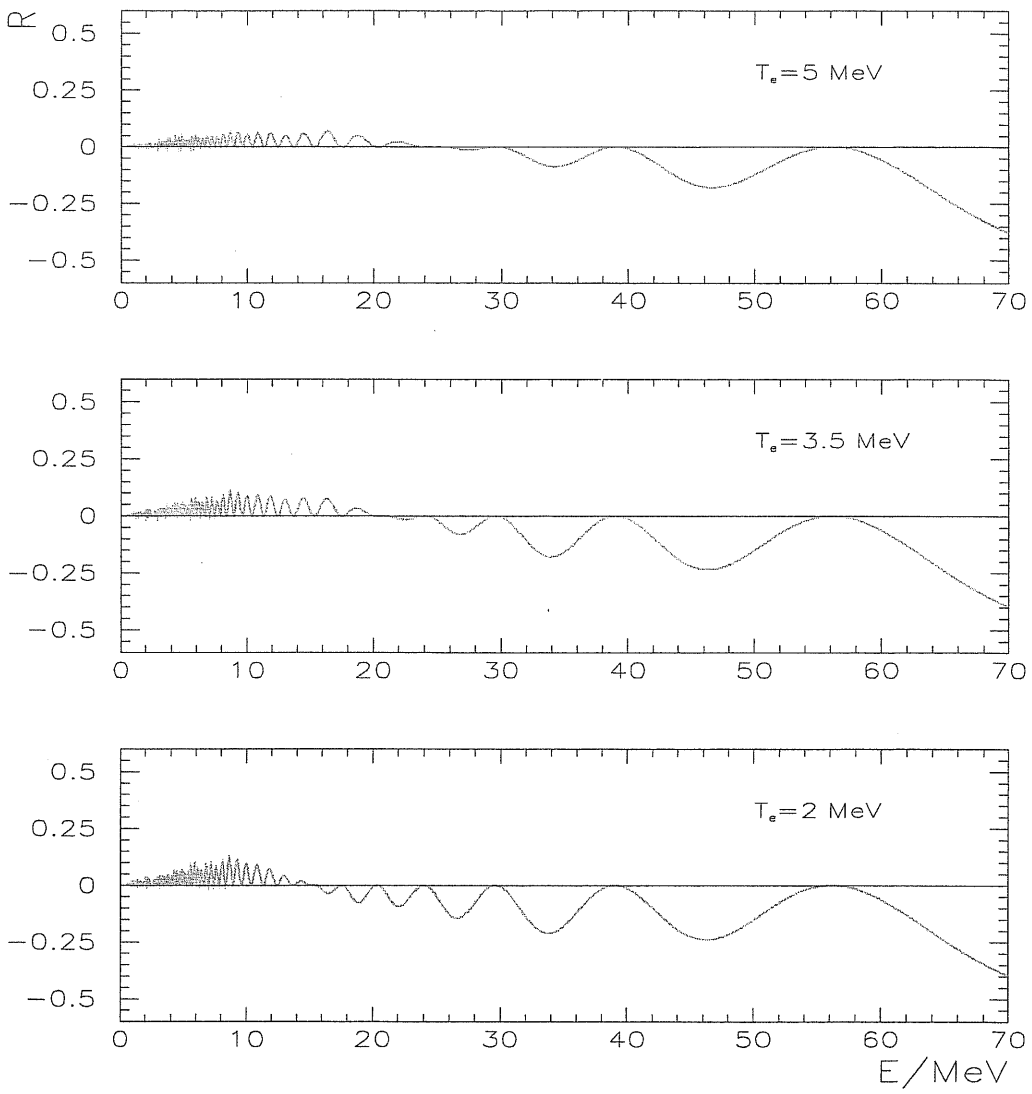

Figure 4.10: The same as fig. 4.8 for $\theta_n = 60°$ and various values of T_e.

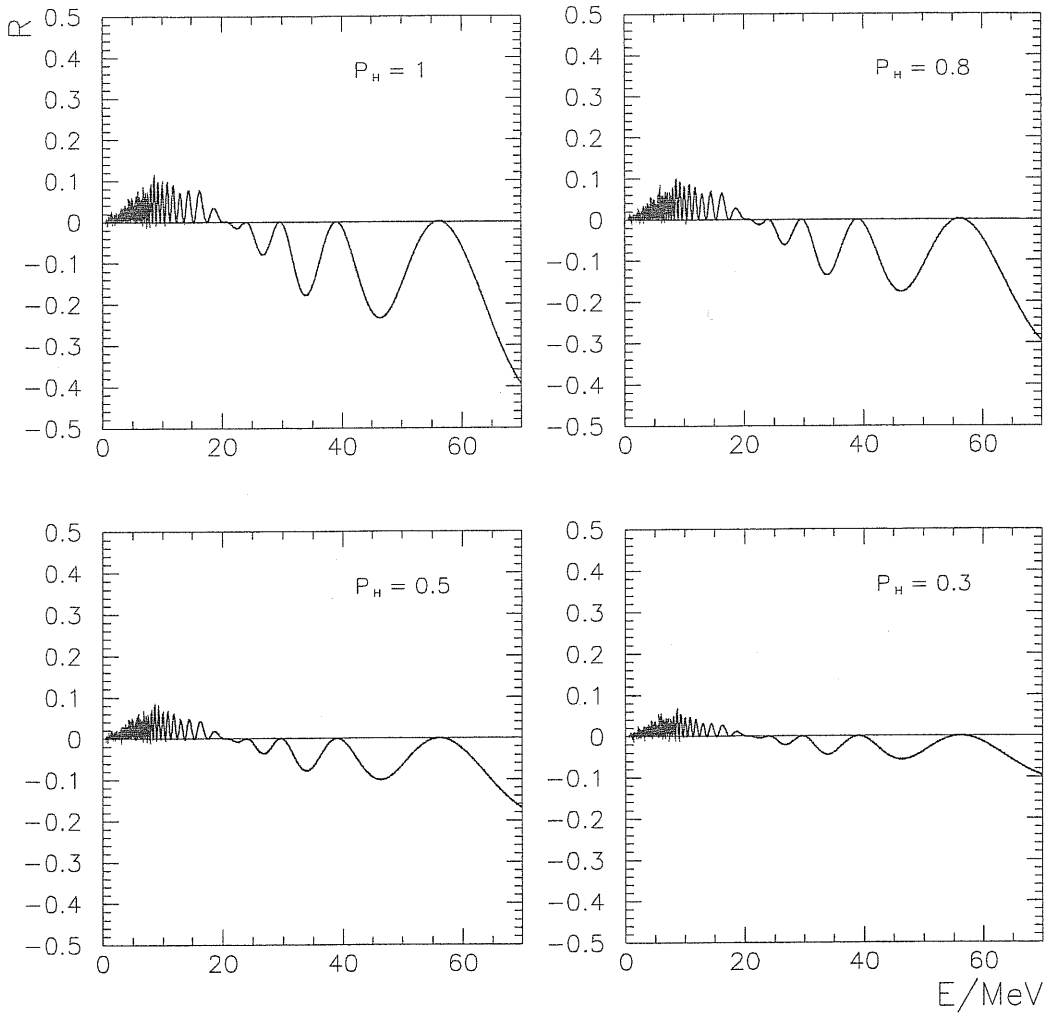

Figure 4.11: The same as fig. 4.8 for $\theta_n = 60°$ and various values of P_H.

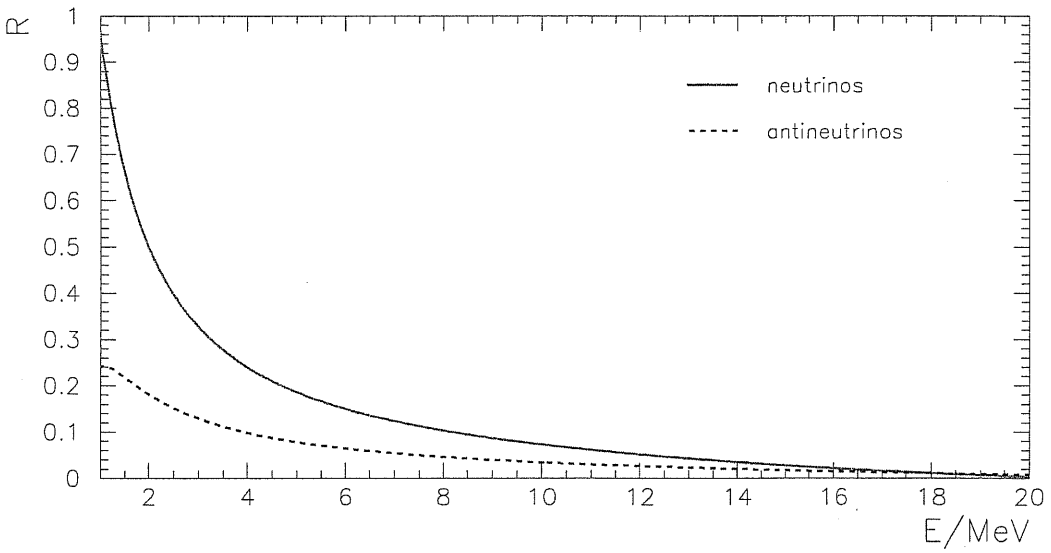

Figure 4.12: The relative deviations R (solid line) and $\bar{R}$ (dashed line) as functions of the neutrino (antineutrino) energy for LOW oscillation parameters. We have taken $\Delta m^2_{\odot} = 10^{-7}$ eV^2, $\sin^2 2\theta_{\odot} = 0.9$; $T_e = 3.5$ MeV, $T_{\bar{e}} = 5$ MeV, $T_x = 8$ MeV and $\theta_n = 25°$. We have also assumed $P_H = 1$ and $P_L = 0$.

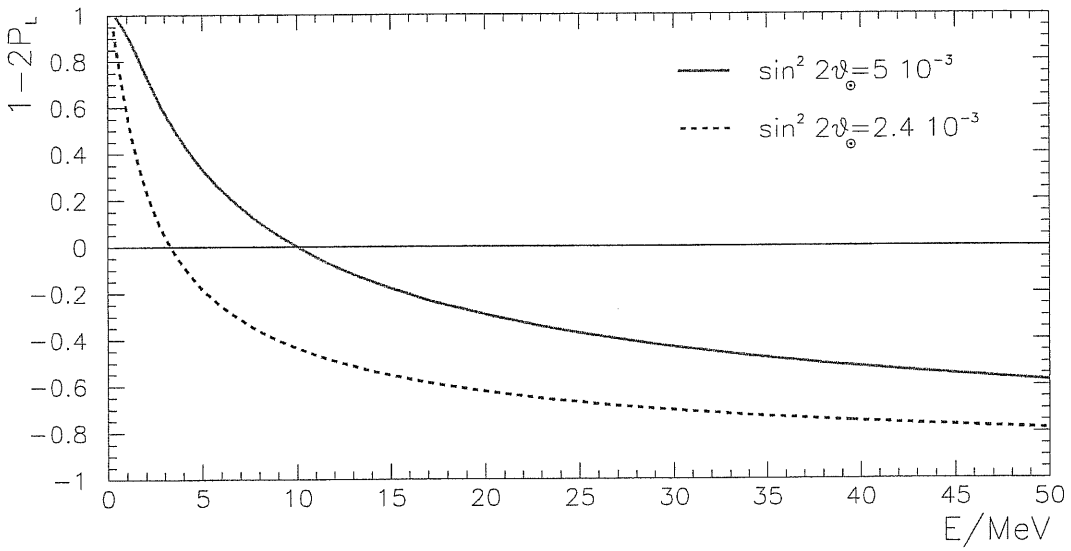

Figure 4.13: The quantity $1 - 2P_L$ as a function of the neutrino energy for $\Delta m^2_{\odot} = 6 \cdot 10^{-6}$ eV^2 and different values of $\sin^2 2\theta_{\odot}$ in the SMA region. We have taken $C = 4$ in the profile (4.4).

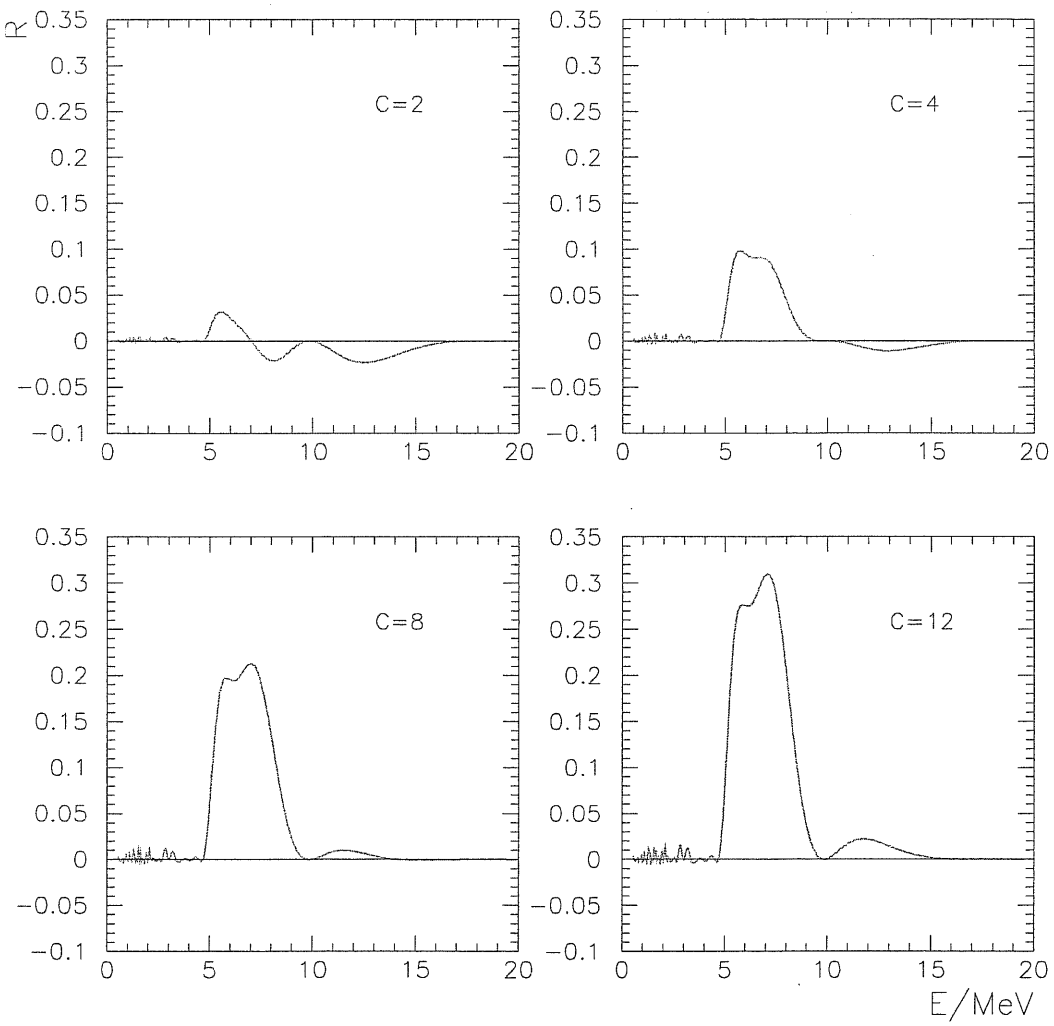

Figure 4.14: The relative Earth matter effect in ν_e channel, R, as function of the neutrino energy for SMA oscillation parameters and various values of the density profile factor C. We have taken $\Delta m^2_{\odot} = 6 \cdot 10^{-6}$ eV^2, $\sin^2 2\theta_{\odot} = 5 \cdot 10^{-3}$; $T_e = 3.5$ MeV, $T_x = 8$ MeV; $P_H = 1$ (or inverted hierarchy); $\theta_n = 0°$.

Chapter 5

Earth matter effects and SN1987A

We now turn to discuss the observation of Earth regeneration effects on supernova neutrinos. In this chapter we consider the data from SN1987A and their possible interpretation in terms of Earth effect. The possibility of observing the effect in the neutrino signal from future galactic supernovae will be discussed in chapter 6.

5.1 Detection of supernova neutrinos: numbers of events

As follows from the results of the previous chapter, the observation of the Earth matter effect requires: (i) separate detection of neutrinos of different flavours, (ii) separate detection of neutrinos and antineutrinos, (iii) the reconstruction of the neutrino energy spectrum.

In what follows we concentrate on events from charged current (CC) scattering on nucleons or nuclei at real-time detectors. These events better satisfy the requirements (i)-(iii); in particular CC processes have high sensitivity to the neutrino energy spectrum.

We consider:

1. The detection of $\bar{\nu}_e$ at water Cerenkov detectors (e.g. IMB and Kamiokande, which are relevant to SN1987A observation, SuperKamiokande and the outer volume of SNO) via the reaction:

$$\bar{\nu}_e + p \to e^+ + n \ . \tag{5.1}$$

Other CC reactions (e.g. the scattering of ν_e and $\bar{\nu}_e$ on oxygen nuclei) have substantially smaller cross section so that they contribute to the total number of events at few per cent level; they will not be considered further.

2. Heavy water detectors (the inner volume of SNO experiment) with the detection reactions:

$$\nu_e + d \rightarrow e + p + p \ , \tag{5.2}$$
$$\bar{\nu}_e + d \rightarrow e^+ + n + n \ , \tag{5.3}$$

which represent the dominant channel of CC detection. Events from the process (5.3) will be distinguished by those from (5.2) if neutrons are efficiently detected in correlation with the positron.

3. Liquid scintillator detectors (e.g. LVD), which are mostly sensitive to $\bar{\nu}_e$ via the reaction (5.1) with only little sensitivity to absorption processes on carbon nuclei.

Besides pure CC processes, the reactions

$$\nu_i + e \rightarrow \nu_i + e \ , \qquad i = e, \mu, \tau, \tag{5.4}$$
$$\bar{\nu}_i + e \rightarrow \bar{\nu}_i + e \ , \tag{5.5}$$

and the NC breakup of deuterium:

$$\nu_i + d \rightarrow \nu_i + n + p \ , \qquad i = e, \mu, \tau, \tag{5.6}$$
$$\bar{\nu}_i + d \rightarrow \bar{\nu}_i + n + p \ , \tag{5.7}$$

allow to reconstruct the total neutrino flux; moreover, due to its good directionality, the scattering of ν_e on electrons is relevant to the location of the supernova.

Radiochemical experiments could provide information on the total ν_e flux above a certain threshold.

The number of CC events with lepton having the observed kinetic energy E_e is given by

$$\frac{dN_\alpha}{dE_e} = N_T \int_{-\infty}^{+\infty} dE'_e R(E_e, E'_e) \mathcal{E}(E'_e) \int dE F_\alpha(E) \frac{\sigma(E'_e, E)}{dE'_e} \ , \tag{5.8}$$

where E'_e is the true energy of the electron (or positron), N_T is the number of target particles in the fiducial volume and $\mathcal{E}$ represents the detection efficiency. Here $\sigma(E'_e, E)/dE'_e$ is the differential cross section and $R(E_e, E'_e)$ is the energy resolution function, which can be described by a gaussian form:

$$R(E_e, E'_e) = \frac{1}{\Delta\sqrt{2\pi}} \exp\left[-\frac{(E_e - E'_e)^2}{2\Delta^2}\right] \ . \tag{5.9}$$

The energy resolution Δ and the other parameters (volume, efficiency, etc.) of some relevant detectors are summarized in the Appendix C.

The energy spectrum (5.8) of the charged leptons reflects the spectrum of the neutrinos, with the following differences:

- the energy dependence of the cross section[1], $\sigma \propto E^2$, substantially enhances the high energy part of the spectrum.

- the integration over the neutrino energy and the convolution with the energy resolution function, eq. (5.8), lead to averaging out the fast modulations in low energy part of the spectrum (appearing for LMA oscillation parameters, see chapter 4). Conversely, the large-period oscillations at high energies will appear in the lepton spectrum (5.8).

5.2 SN1987A observation: the data

The first and – by the time – only observation of a neutrino burst from a supernova occurred on February 23rd 1987, when the blue supergiant Sanduleak −69 202, located in the Magellanic Cloud (at distance $D \simeq 50$ kpc from the Earth), collapsed and exploded as a supernova (SN1987A).

Several signals were detected from SN1987A:

- detection of the neutrino burst from the core collapse was claimed to have occurred in the Cerenkov detectors Kamiokande (K2) [12] and IMB [13] and in the scintillator detectors at Baksan (BST) [118, 119] and Mont Blanc (LSD) [120, 121]. Kamiokande, IMB and Baksan agreed on the time of start of the signal – about 7:35 universal time (UT)– within the uncertainties related to the measurements of time and to statistics. The Mont Blanc experiment registered a signal about 5 hours earlier, when no data were observed in the other detectors. This suggests that these data may not be related to SN1987A; for this reason they will not be considered in this work. We will not discuss Baksan results because the number of recorded events (5) far exceeds the expectations from supernova theory, which are in general confirmed by K2 and IMB results.

- the gravitational wave antennas in Rome and Maryland reported signals which could have been related to SN1987A [122, 123, 124, 125]. This result is controversial and will not be discussed here [126].

- the optical observation of the supernova was successfully performed starting at 10:38 UT, i.e. few hours after the neutrino detection, as expected from the larger opacity of the matter of the star to photons with respect to neutrinos.

[1]The $\sigma \propto E^2$ dependence constitutes a good approximation at low energies; in the highest energy part of the supernova neutrino spectrum deviations due to weak magnetism and recoil effects are relevant, see e.g. [114, 115, 116]. In our calculations we used the cross sections in ref. [116] for the scattering (5.1) and in ref. [117] for the reactions (5.2)-(5.3).

Let us consider the K2 and IMB neutrino data in more detail. As discussed in sec. 5.1, the signal in Cerenkov detectors is expected to be dominated by $\bar{\nu}_e$ scattering on protons, eq. (5.1), therefore we will interpret all the K2 and IMB data as $\bar{\nu}_e$ events[2]. The figure 5.1 shows the distribution of K2 and IMB events in arrival time, energy and angle with respect to the direction of the supernova. As it appears from the figure, the K2 detector recorded 11 [3] events within a time interval of about 13 seconds. The signal in IMB was shorter: 8 events were detected in a time interval of less than 6 seconds. The angular distribution of the events suggests some accumulation of the data in the forward direction, in contrast to the isotropy which is expected for $\bar{\nu}_e - p$ scattering. We refer to [93] (see also references therein) for a discussion of this possible anomaly.

The energy spectra observed by K2 and IMB look remarkably different. Besides the absence of low energy events in IMB, which is due to the higher threshold with respect to K2 (see Appendix C), some differences in the energy distribution of the data are difficult to be explained:

(i) Concentration of the IMB events in the energy interval $E \simeq 35 \div 40$ MeV.

(ii) Absence of events at IMB above $E \simeq 40$ MeV (which looks like a sharp cut of the spectrum).

(iii) Absence of events with $E \gtrsim 35$ MeV at K2.

Due to the limited number of events these and other anomalous characteristics of the data distributions may not be statistically significant. Indeed, the combined analysis of the K2 and IMB data – performed for standard massless and unmixed neutrinos – gave satisfactory confirmation of the general picture of neutrino emission from a supernova [128].

On the other hand, in the light of the increasing evidence of neutrino masses and mixing, the inclusion of oscillation effects in the interpretation of SN1987A data is now mandatory. In what follows we will discuss these effects and show that the tension between the K2 and IMB observed spectra is reduced once one considers oscillation parameters from the LMA solution of the solar neutrino problem, which is currently favoured by the solar neutrino experiments [71, 72].

[2]The interpretation of the first two events as due to ν_e was suggested [127] to explain their pointing to the direction of the supernova, see fig. 5.1.

[3]A twelfth event (the sixth in arrival time) is sometimes included in the sample of events; following other authors (see e.g. [23]) we consider this event as due to background.

5.3 Regeneration in the Earth

5.3.1 Expected signals in Kamiokande and IMB

Let us consider the difference of signals at K2 and IMB which can be produced by oscillations in the Earth. This difference is related to the different directions of the supernova with respect to the two detectors: $\theta_n^{IMB} = 48°$ for IMB and $\theta_n^{K2} = 70°$ for K2, corresponding to the distances $d_{IMB} \simeq 8535$ Km and $d_{K2} \simeq 4363$ Km travelled by the neutrinos in the Earth. Since the neutrinos crossed the mantle only, the regeneration effects can be described approximatively by propagation of neutrinos in uniform medium with the densities equal to the average values along the trajectories (see Appendix B): $\rho_{IMB} \simeq 4.5$ g $\cdot$ cm^{-3}, $\rho_{K2} \simeq 3.5$ g $\cdot$ cm^{-3}.

Let us show that the features (i)-(iii) indicated in sec. 5.2 can be explained by oscillations in the matter of the Earth. Moreover, the explanation implies certain values of Δm^2 and $\sin^2 2\theta$. We consider three active neutrinos with normal mass hierarchy; the case of inverted hierarchy will be discussed in the sec. 5.3.2.

To reproduce the characteristics described in (i)-(iii) we require that:

(1) The phase of oscillations at IMB detector at $E \simeq 38 \div 42$ MeV equals

$$\phi_{IMB}(40) \equiv \frac{\pi d_{IMB}}{l_m} = k\pi \ , \qquad k = 1, 2, 3, \ldots \ . \tag{5.10}$$

Under this condition the oscillations in the matter of the Earth do not suppress the signal.

(2) The phase of oscillations at IMB at $E \simeq 50 \div 60$ MeV is a semi-integer of π:

$$\phi_{IMB}(60) = \pi \left(\frac{1}{2} + k\right) \ , \qquad k = 0, 1, 2, .. \ , \tag{5.11}$$

so that in this range of energy one expects maximal suppression effect. It is easy to check that, in the range of parameters of interest, the conditions (5.10) and (5.11) are satisfied simultaneously with good precision.

(3) The phase of oscillations at K2 at $E \simeq 38 \div 42$ MeV is

$$\phi_{K2}(40) \equiv \frac{\pi d_{K2}}{l_m} = \pi \left(\frac{1}{2} + k\right) \ , \qquad k = 0, 1, 2, \ldots \ , \tag{5.12}$$

so that the Earth matter effect produces maximal suppression of the K2 signal in the range $E \simeq 38 \div 42$ MeV.

(4) The depth of oscillations is maximal, $\bar{D} \simeq \bar{D}_{max}$, at IMB at the energies $E \simeq 50 \div 60$ MeV, which requires the resonance energy:

$$E_R^{IMB} \simeq 50 \div 60 \text{ MeV} . \tag{5.13}$$

In fig. 5.2 we show the conditions (5.10), (5.12) and (5.13) in the $\Delta m^2_\odot - \cos 2\theta_\odot$ plane. As follows from the figure, there are bands in which the requirements (5.10) and (5.12) are satisfied simultaneously. They correspond to $\phi_{IMB} \simeq 2\phi_{K2} = 3\pi, 5\pi, 7\pi, \ldots$. The phase increases with $\Delta m^2_\odot$. Notice that the requirements (5.10)-(5.12) are satisfied in the whole relevant range of $\cos 2\theta_\odot$ if ϕ_{IMB} equals odd multiples of π.

The condition of maximal effect, eq. (5.13), gives $\Delta m^2_\odot = (1.7 \div 2.1) \cdot 10^{-5}$ eV^2. Large Earth matter effect, e.g. $\bar{D} \gtrsim 0.7\bar{D}_{max}$, is realized in much wider interval, whose borders depend on $\cos 2\theta_\odot$ (the upper border is represented by the dashed line in fig. 5.2).

As follows from fig. 5.2 the explanation of the properties (i)-(iii) implies the oscillation parameters to be in the regions $\phi_{IMB} = 3\pi$ for all the relevant values of θ, and $\phi_{IMB} = 5\pi$ for $\cos 2\theta_\odot \gtrsim 0.2$. The central values of these bands are described, approximatively, by the following lines:

$$\begin{aligned} \Delta m^2_\odot &\simeq 3.3 \cdot 10^{-5} \text{ eV}^2 \, [1 - 0.35 \cos 2\theta_\odot] \ , \\ \Delta m^2_\odot &\simeq 5.6 \cdot 10^{-5} \text{ eV}^2 \, [1 - 0.18 \cos 2\theta_\odot] \ . \end{aligned} \tag{5.14}$$

For $\cos 2\theta_\odot \gtrsim 0.1$ the values (5.14) are well inside the 99% C.L. allowed region of the LMA solution (dotted-dashed contour in fig. 5.2, from ref. [129]). Moreover, the best-fit point, $\cos 2\theta_\odot \simeq 0.5$, $\Delta m^2_\odot \simeq 5.2 \cdot 10^{-5}$ eV^2 [4], lies in the band $\phi_{IMB} \simeq 5\pi$ (see eq. (5.14)).

The fig. 5.2 shows also the 99% C.L. exclusion curve obtained in ref. [22] (dotted line), corresponding to the upper bound on the permutation parameter $p = 0.35$. One can see that the region $\cos 2\theta_\odot \lesssim 0.25$ is excluded; this region was obtained taking $T_{\tilde{e}} \simeq 4.5$ MeV and $T_x \simeq 7.4$ MeV; it becomes narrower for lower values of the temperatures.

The expected distributions of events are rather sensitive to variations of $\Delta m^2_\odot$ (see fig. 4.4). For instance, a change of $\Delta m^2_\odot$ by $\sim 20\%$ in the $\phi_{IMB} = 3\pi$ band will lead to the prediction of strong suppression of the number of events in the interval $E \simeq 35 \div 40$ MeV of the IMB spectrum and enhancement of the signal at $E \simeq 50$ MeV, in contradiction with observations.

[4] This result is given by the global two-neutrinos fit of the solar neutrino data including the total rates and the day and night spectra at Super-Kamiokande [129].

Let us consider the expected spectra of events at K2 and IMB. As discussed in sec. 4.1 the original $\bar{\nu}_e$ and ν_x spectra are well approximated by a Fermi-Dirac form once they are integrated over arrival time intervals Δt of several seconds, as an effect of the decay with time of the neutrino luminosities and temperatures. This description is good if Δt is not larger than the typical decay time τ of the temperatures and luminosities. For $\Delta t \gtrsim \tau$ the integrated spectra can not be approximated by a Fermi-Dirac form. This is the case of the SN1987A data, which show a rapid cooling of the neutrino spectra with decay time comparable or smaller than the duration of the burst, $\tau \lesssim \Delta t_b \simeq 13$ s. Therefore, we have divided the whole time interval of observations in two bins, $t_1 = 0 \div 6.5$ s and $t_2 = 6.5 \div 13$ s, and described the integrated fluxes over each bin by Fermi-Dirac spectra with different temperatures ($T(t_1) > T(t_2)$) and luminosities ($L(t_1) > L(t_2)$). We mark that the values of T and L we give should be considered as effective (time averaged) quantities.

In figures 5.3-5.4 we show the expected spectra of events at K2 and IMB in the first time bin ($t < 6.5$ s) for two sets of parameters from the preferable regions (5.14). They have been obtained taking $T_{\bar{e}} = 3.5$ MeV, $T_x = 7$ MeV and $L_{\bar{e}} = L_x = 3 \cdot 10^{52}$ ergs. The energy thresholds and detection efficiencies have been taken into account (see the Appendix C).

According to the figures, the predicted spectra with oscillations (solid lines) fit better the observed distributions of events at K2 and IMB. As expected, the spectra without oscillations (dashed lines) can not describe the concentration of IMB events at $E \simeq 30 \div 40$ MeV and the absence of an excess of K2 events in this range. The conversion in the star only leads to an appearance of high energy tails (short dashed lines) which contradict the observations of both K2 and IMB. The oscillations in the matter of the Earth (solid lines) suppress the tails above 45 MeV in IMB and above 35 MeV in K2 [5]. Notice that the figures have illustrative character and do not correspond to the optimal (best fitted) choice of parameters of the original spectra.

To quantify the improvement of the fit due to conversion inside the star and the Earth matter effect we have performed the likelihood analysis following, in general, the prescriptions of ref. [23]. There are, however, some differences:

1). We have divided the whole energy range of the detected events into several bins. The size ΔE of each bin has been chosen according to the experimental errors ϵ in the measurements of energy: $\Delta E \sim 2\epsilon$. We used three bins with $\Delta E = 10$ MeV for K2 and two bins with $\Delta E = 15$ MeV for IMB (see histograms in the figs. 5.3-5.4).

2). We computed the realization probability P of a given theoretical prediction

[5]Notice that in our analysis the maximal suppression, due to oscillations in the Earth, of the antineutrino signal in IMB occurs at energies above 50 MeV. For such energies the efficiency of the IMB detector was high ($\mathcal{E}_{IMB} \gtrsim 0.7$, see Appendix C).

using the Poissonian distribution:

$$P = \prod_i \frac{(n_i)^{N_i}}{N_i!} e^{-n_i} \ , \tag{5.15}$$

where N_i is the number of observed events in the i-th bin and $n_i = n_i(T_{\bar{e}}, T_x, L_{\bar{e}}, L_x, \Delta m^2, \theta)$ is the corresponding number of expected events which depends on the parameters of the original neutrino spectra and oscillation parameters. We find the maximum of P and the contours of given confidence levels according to ref. [23].

Notice that, in contrast with [23] we use a discrete (binned) expression of the probability P and we calculate n_i by integrating the corresponding predicted function $n(E)$ over the i-th energy bin.

3). We performed separate analyses of the K2 and IMB data collected in the two time bins t_1 and t_2; no events are discarded in this procedure.

In fig. 5.5 we show the results of the likelihood analysis of the IMB and K2 data of the first time bin in the $T_{\bar{e}} - L_{\bar{e}}$ plane in absence of mixing, $\theta = 0$ (upper panel). As follows from the figure, K2 and IMB imply substantially different temperatures of the original $\bar{\nu}_e$ spectrum: $T_{K2} \simeq 2.8$ MeV and $T_{IMB} \simeq 4.2$ MeV. There is no overlap of the 68% C.L. regions.

The lower panel of fig. 5.5 shows the analogous plot in presence of oscillations in the star and in the matter of the Earth. We have taken $T_x/T_{\bar{e}} = 1.8$ and $L_x/L_{\bar{e}} = 1$ with oscillation parameters from the preferable bands (see fig. 5.2). With oscillations the best fit parameters inferred from IMB and K2 become closer: $T_{K2} \simeq 1.96$ MeV and $T_{IMB} \simeq 2.75$ MeV. We get $\Delta T/T \equiv 2(T_{IMB} - T_{K2})/(T_{IMB} + T_{K2}) \simeq 0.33$ and 0.41 with and without oscillations respectively. Overlap of the 68% C.L. regions appears. The combined fit gives $T_{\bar{e}} \simeq 2.77$ MeV and $L_{\bar{e}} \simeq 4.4 \cdot 10^{52}$ ergs, which are in good agreement with recent calculations [104]. Thus, the likelihood analysis with oscillations shows some improvement of the fit and does not imply too low temperatures and high luminosities.

In the second time bin K2 has detected 3 events with low energies, close to the threshold (fig. 5.1), whereas IMB has no signals. This can be easily interpreted in the assumption of lower temperatures of the $\bar{\nu}_e$ and ν_x original spectra and smaller difference of T_x and $T_{\bar{e}}$. Taking for instance $T_{\bar{e}} \simeq T_x \simeq 1.8$ MeV and $L_{\bar{e}} \simeq L_x \simeq 3 \cdot 10^{52}$ ergs we predict ~ 2 events in K2 with energy $E \simeq 5 \div 15$ MeV and less than 0.5 events at $E \geq 15$ MeV. With the same values of the parameters we get less than 0.2 events in IMB, that is, with high probability all the events are below the IMB threshold.

As discussed in sec. 4.4, for neutrino parameters from the LOW and SMA solutions the Earth matter effect is small, threfore no improvement of the fit can be

obtained in this case.

5.3.2 Implications for the neutrino mass spectrum

According to the results of sec. 4.2 the same results we obtained in sec. 5.3.1 for normal mass hierarachy are realized for inverted hierarchy provided that $P_H \simeq 1$, corresponding to $|U_{e3}|^2 \lesssim 10^{-5}$ (fig. 4.1). If the hierarchy is inverted and $|U_{e3}|^2 \gtrsim 10^{-3}$ we get $P_H \simeq 0$ and the Earth matter effect vanishes (eq. 4.27). Moreover, the $\bar{\nu}_e$ flux will have the spectrum of the original ν_x flux, which is disfavoured by observations [22]. If $|U_{e3}|^2 \simeq 10^{-5} \div 10^{-3}$, one can observe an intermediate situation: harder $\bar{\nu}_e$ spectrum and partially suppressed Earth matter effect. Therefore, we conclude that reconciling the differences in the K2 and IMB energy spectra by Earth regeneration effects requires normal mass hierarchy or very small values of $|U_{e3}|^2$ if the hierarchy is inverted [25, 26].

Let us consider the Earth matter effect for supernova neutrinos in the case of $\nu_e - \nu_s$ mixing. As for active neutrinos, for $\nu_e - \nu_s$ a significant effect is possible for large mixing angles (notice, however, that large mixing $\nu_e \to \nu_s$ conversion gives poor fit of the solar neutrino data).

We assume that no sterile antineutrino fluxes are generated in the central part of the star[6]. In this case we get the result for the $\bar{\nu}_e$ flux at the detector from eq. (4.8) putting $F_x^0 = 0$:

$$F_{\bar{e}}^D = P_{1\bar{e}}^s F_{\bar{e}}^0 \ . \tag{5.16}$$

Here $P_{1\bar{e}}^s$ is the probability of $\bar{\nu}_1 \to \bar{\nu}_e$ oscillations in the matter of the Earth for mixing with sterile neutrino and we considered $\bar{P}_L \simeq 0$.

The difference of potentials for the $\nu_e - \nu_s$ system, $V_{es} = \sqrt{2} G_F \left(n_e - n_n/2\right) \simeq V_{e\mu}/2$, is about two times smaller than the one of the ν_e and ν_μ species, $V_{e\mu}$. In the last equality we considered that the medium is almost isotopically neutral in the mantle of the Earth. Correspondingly, the refraction length is two times larger than in the active-active case, so that the range of large matter effects is shifted to smaller Δm^2 by a factor 2.

From eq. (5.16) we see that, in contrast with $\nu_e - \nu_\mu/\nu_\tau$ mixing, the observed events in the detector are due to the original $\bar{\nu}_e$ flux only, and no hard tail appears in the spectrum. As a consequence, no improvement in the fit of K2 and IMB data is obtained with respect to the $\theta = 0$ case. Moreover, it is possible to check that a larger $\bar{\nu}_e$ luminosity is required.

The discussion of the section 5.3.1 can be immediately generalized to the case in which the electron neutrino is mixed with both an active neutrino ν_μ and a sterile

[6] A sterile state ν_s can be produced, however, by conversion of active neutrinos at high densities in the star. This happens in some schemes with four neutrinos which explain the LSND result.

one, ν_s. The problem can be reduced to $\nu_e - \nu_x$ mixing, with $\nu_x = \sqrt{1-\delta}\nu_\mu + \sqrt{\delta}\nu_s$; the pure active and pure sterile mixings correspond to $\delta = 0$ and $\delta = 1$ respectively. Now the $\bar{\nu}_e$ flux in the detector is given by eq. (4.8) with $F_x^0 = (1-\delta)F_x^0$. Thus, with respect to the pure active case, one gets a reduction by a factor $\sim (1-\delta)$ of the hard part of the detected spectrum. For $\delta \lesssim 0.5$ still one gets a good fit of the K2 and IMB signals.

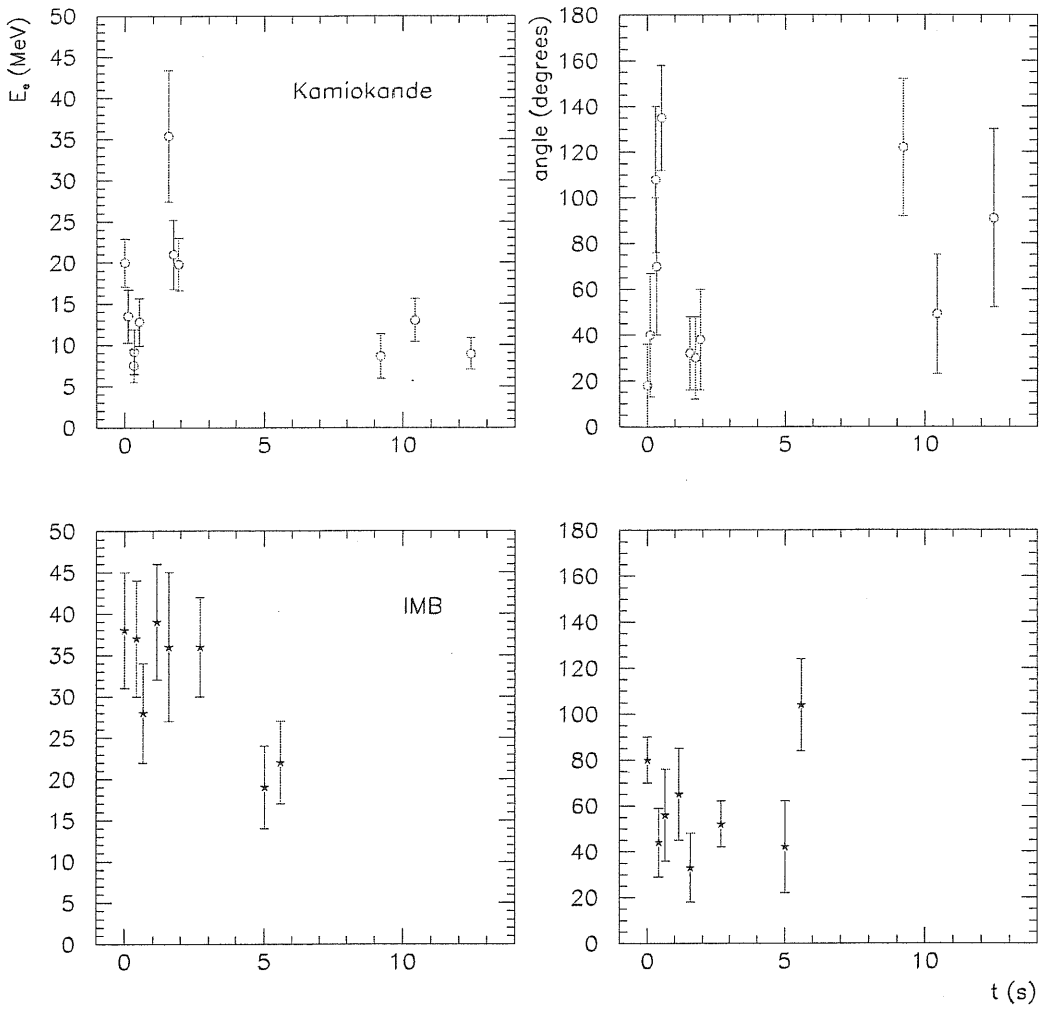

Figure 5.1: The time, energy and angular distributions of SN1987A data recorded by the Kamiokande and IMB detectors. We denote by t the time after the first event and by E_e the observed positron energy.

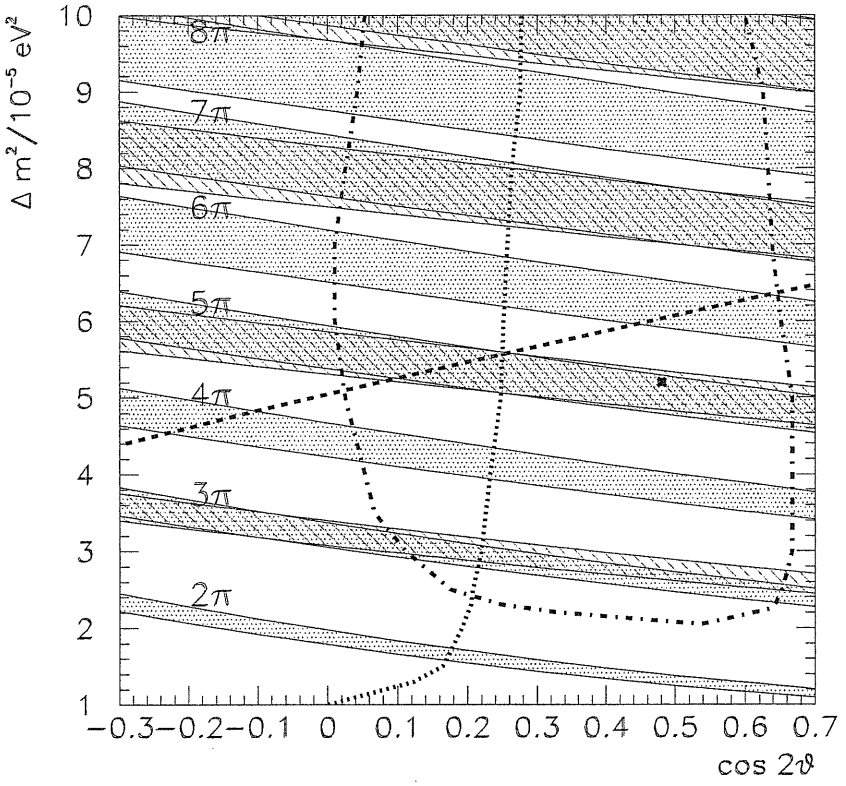

Figure 5.2: Bands of equal phases $\phi_{IMB}(40) = k\pi$ (dotted regions) and $\phi_{K2}(40) = \pi\,(1/2 + k)$ (dashed regions) in the $\Delta m^2_{\odot}$-$\cos 2\theta_{\odot}$ plane. The widths of the bands are determined by the requirement that the conditions (5.12) and (5.10) are satisfied in the energy interval $E = 38 \div 42$ MeV. The region below the dashed line represents the band of strong Earth matter effect, where $\bar{D} \gtrsim 0.7\bar{D}_{max}$ (see eq. (5.13)). For comparison we show the 99% C.L. allowed region of the LMA solution of the solar neutrino deficit (dotted-dashed contour, from [129]) where the best fit point is marked by an asterisk. The dotted line represents the 99% C.L. exclusion curve from fig. 3a of ref. [22].

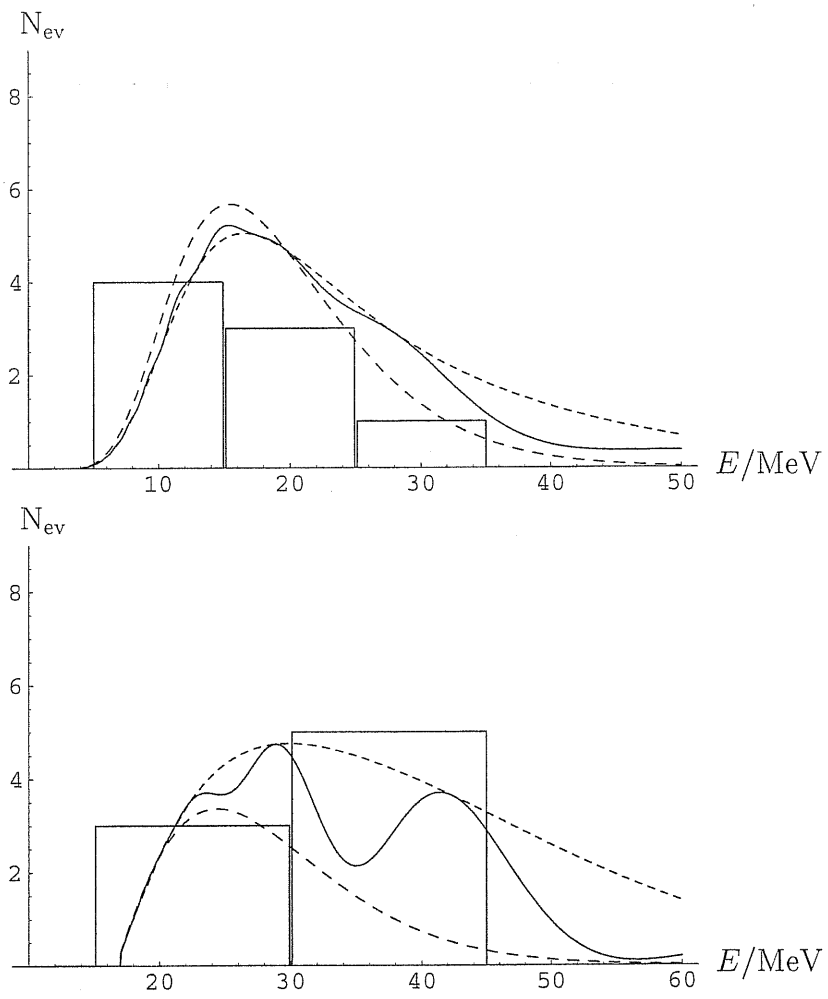

Figure 5.3: The predicted spectra of $\bar{\nu}_e$ events at Kamiokande-2 (upper panel) and IMB (lower panel). We show: the original spectra without oscillation effects (long dashed lines), spectra with conversion in the star only (dashed lines), spectra with oscillation effects both in the star and in the Earth (solid lines). We used the following set of oscillation parameters and characteristics of the original $\bar{\nu}_e$ and ν_x spectra: $T_{\bar{e}} = 3.5$ MeV, $L_{\bar{e}} = 3 \cdot 10^{52}$ ergs, $T_x = 7$ MeV, $L_x = 3 \cdot 10^{52}$ ergs, $\cos 2\theta_\odot = 0.5$, $\Delta m^2_\odot = 2.75 \cdot 10^{-5}$ eV^2. The histograms show the observed distributions of events during the first 6.5 seconds.

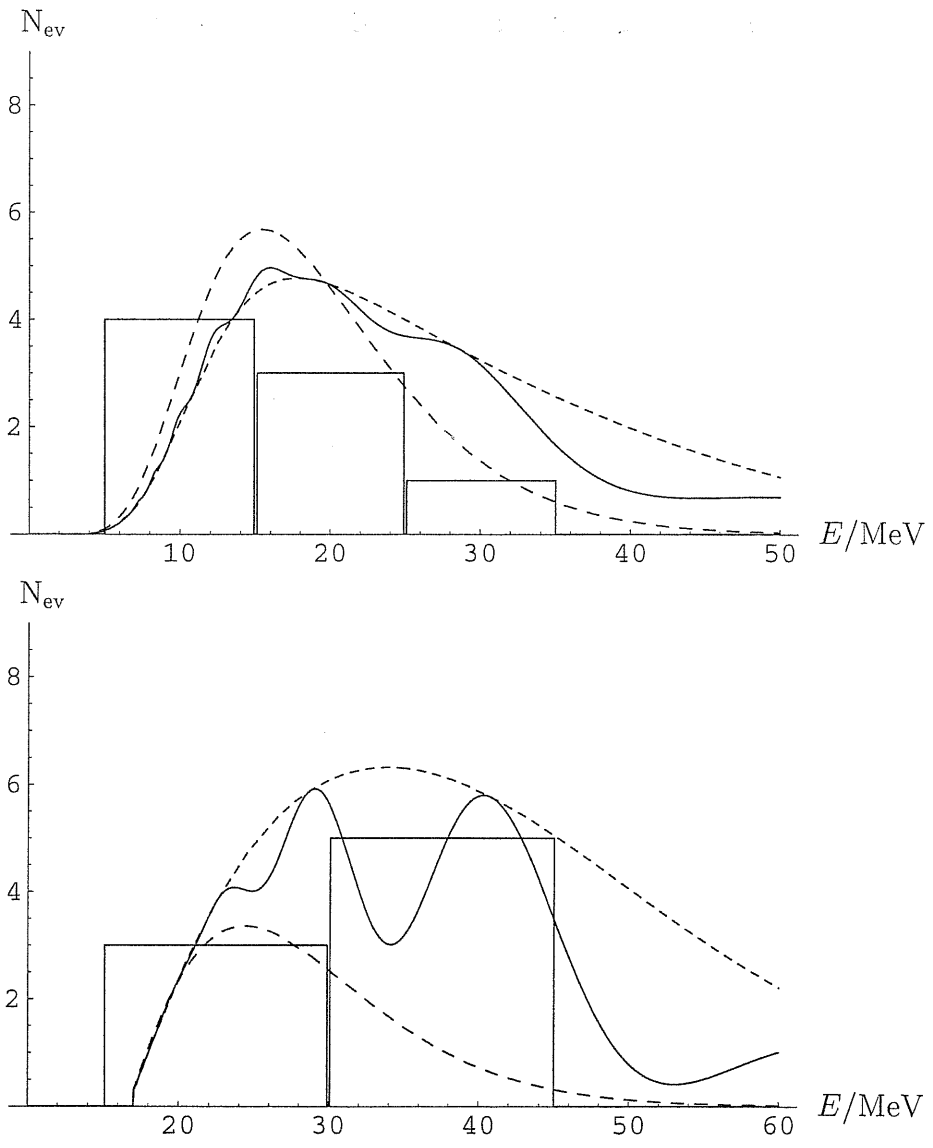

Figure 5.4: The same as fig. 5.3 with $\cos 2\theta_{\odot} = 0.2$, $\Delta m^2_{\odot} = 3 \cdot 10^{-5}$ eV^2.

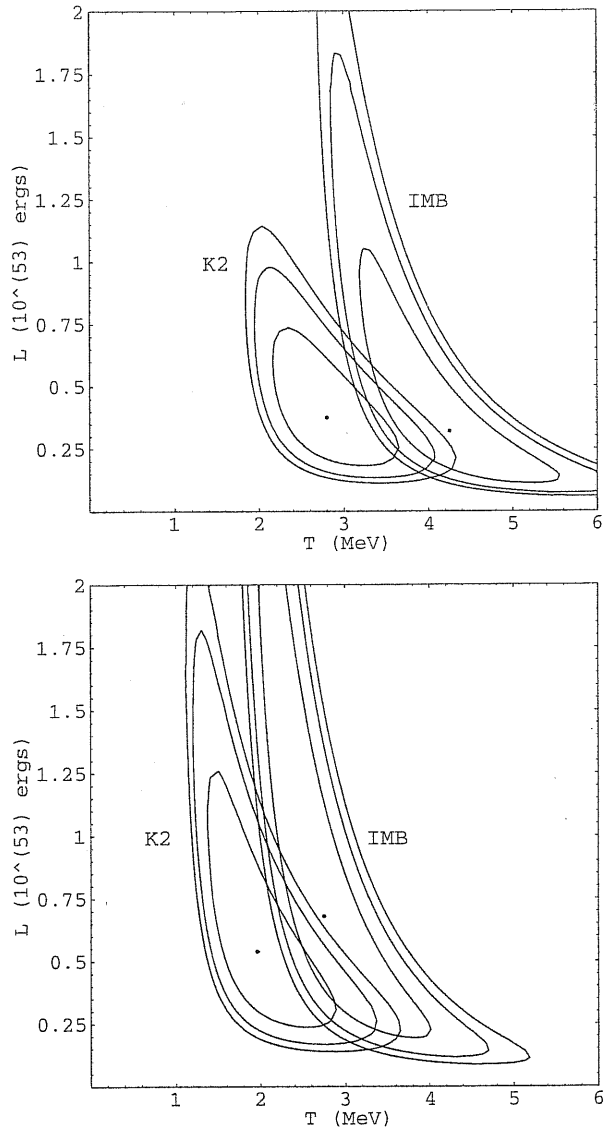

Figure 5.5: Best fit points and contours of equal $68, 90, 95.4\%$ likelihood for K2 and IMB in the $T_{\bar{e}} - L_{\bar{e}}$ plane. The upper panel shows the result of the separate fits of K2 and IMB data without oscillation effects. The lower panel represents a similar fit in presence of oscillations. The following values for the oscillation parameters and characteristics of original spectra have been used: $T_x/T_{\bar{e}} = 1.8$, $L_x/L_{\bar{e}} = 1$ and $\cos 2\theta_\odot = 0.2$, $\Delta m^2_\odot = 3 \cdot 10^{-5}$ eV^2.

Chapter 6

Observation of Earth effects on neutrinos from a future galactic supernova

In this chapter we consider the possibility of detecting the Earth matter effects in observations of future galactic supernovae. We study the possible trajectories of the neutrinos in the Earth and give examples of results of observations of these neutrinos by present detectors. Finally, we discuss methods to establish the Earth effect and comment on the physics potential of the study of this effect for the reconstruction of the neutrino mixing matrix and mass spectrum.

6.1 Neutrinos from a galactic supernova: trajectories

Let us consider the possibility that a supernova explosion will occur in our galaxy. What is the chance that one, two or even three detectors situated in different places of the Earth will detect the Earth matter effect on the observed neutrino burst?

Due to the short duration of the burst, and the spherical symmetry of the Earth, for a given detector the trajectories of neutrinos (and therefore the regeneration effect) can be completely described by the nadir angle θ_n of the supernova with respect to the detector: if $\cos\theta_n > 0$ the detector is shielded by the Earth. The angle θ_n depends (i) on the location of the supernova in Galaxy, (ii) on the time t of the day at which the burst arrives at Earth and (iii) on the position of the detector itself.

We first consider a supernova located in the galactic center (declination[1] $\delta_s = -28.9°$) and three detectors [130]: LVD [44], SNO [131] and SK [132]. The positions

[1] We define δ_s as the the angle of the star with respect to the equatorial plane of the Earth.

of these detectors on the Earth are given in the Appendix C.

The fig. 6.1 a) shows the dependence of $\cos\theta_n$ on the time t for the three detectors. We fixed $t = 0$ to be the time at which the star lies on the Greenwich meridian. The horizontal line at $\cos\theta_n = 0.83$ corresponds to the trajectory tangential to the core of the Earth ($\theta_n = 33.2°$), so that trajectories with $\cos\theta_n < 0.83$ are in the mantle of the Earth. For $\cos\theta_n > 0.83$ the trajectories cross both the mantle and the core.

From the figures it appears that:

1. For most of the arrival times the supernova is seen with substantially different nadir angles at the different detectors, so that one expects different Earth matter effects observed.

2. At any time t the neutrino signal arrives at Earth, at least one detector is shielded by the Earth ($\cos\theta_n > 0$) and therefore will see the regeneration effect. Earth shielding is verified even for two detectors simultaneously for a large fraction of the times.

3. At any possible arrival time t one of the detectors is not shielded by the Earth. So that, once the direction to the supernova is known, one can identify such a detector and use its data to reconstruct the neutrino energy spectrum without regeneration effect.

4. For a substantial fraction of the times for one of the detectors the trajectory crosses the core of the Earth.

In fig. 6.1 b), c), we show similar dependences of $\cos\theta_n$ on the time t for other locations of the star in the galactic plane. Notice that in the case b) two detectors are not shielded by the Earth for most of the times and no one trajectory crosses the core. In contrast, for the position c) all the three detectors are always shielded by the Earth. In general for the detectors we are considering, which are placed in the northern hemisphere, the Earth shielding is substantial for a supernova located in the southern hemisphere, as it is the case for stars in the region of the galactic center. If a supernova event occurs in the northern hemisphere ($\delta_s > 0$), corresponding to some peripherical regions of the galactic disk, the Earth coverage of northern detectors will be scarce, or even null in the limit $\delta_s = 90°$. In this case southern detectors would be more promising for the observation of Earth matter effects.

Clearly the determination of the position of the supernova is important for predictions and the experimental identification of the regeneration effect. The localization of the star can be done either by direct optical observations or by the experimental study of the neutrino scattering on electrons [133], which has substantial directionality. Triangulation techniques and neutron recoil methods have also been discussed [133, 134]; moreover, the study of Earth matter effects by high-statistics experiments can allow to reconstruct the direction to the star.

6.2 Observation and identification of Earth matter effects

Using the results of chapter 4 we caculated the energy spectra expected at SK, SNO and LVD for oscillation parameters from the LMA solution, $P_H = 1$ and various arrival times of the neutrino burst. We considered a supernova located in the direction of the galactic center (fig. 6.1 a)) at a distance $D = 10$ Kpc and releasing a total energy $E_B = 3 \cdot 10^{53}$ ergs. The detection efficiencies, thresholds and energy resolutions of the detectors have been taken into account and are summarized in the Appendix C.

The predicted spectra are shown in the figs. 6.2-6.5. The histograms represent the numbers of events from the reaction (5.1) for SK (panels a)) and LVD (panels b)); the panels c) show the sum of the numbers of events from the reactions (5.3) and (5.1) at SNO. In d) we plot the numbers of events in the inner volume of SNO from the scattering (5.2).

As can be seen in fig. 6.1 a), for $t = 1$ hour the neutrinos arriving at SK have core crossing trajectory ($\cos\theta_n = 0.93$). For SNO the trajectory crosses the mantle only and is rather superficial ($\cos\theta_n = 0.10$); the LVD detector is not shielded by the Earth. The corresponding spectra are shown in fig. 6.2 for $\Delta m^2_\odot = 5 \cdot 10^{-5}$ eV^2 and $\sin^2 2\theta_\odot = 0.75$ and the same temperatures as in the figs. 4.3 and 4.8. The spectrum of SK events exhibits deviations from the undistorted spectrum in some isolated bins, which correspond to the minima in the antineutrino spectrum. At SNO the Earth effect produces a narrowing of the spectrum. The difference with respect to the SK spectrum is attributed to the smaller oscillation phase (shorter trajectory in the Earth) of the neutrinos arriving at SNO. In both SK and SNO the Earth effect is not larger than $20 - 30\%$.

The size of the effect increases for smaller $\Delta m^2_\odot$ and larger difference between the ν_e, $\bar{\nu}_e$ and ν_x temperatures (see figs. 4.4 and 4.5): the figure 6.3 shows the same spectra as fig. 6.2 for $\Delta m^2_\odot = 3 \cdot 10^{-5}$ eV^2, $\sin^2 2\theta_\odot = 0.9$, $T_e = 3$ MeV and $T_{\bar{e}} = 4$ MeV. In this case the regeneration effect is as large as $50 - 60\%$.

As a further illustration, in figs. 6.4 and 6.5 we show the expected spectra for the same parameters as in fig. 6.2 but different arrival times of the signal (see fig. 6.1 a)). For $t = 8$ hours SNO is unshielded while SK and LVD have deep trajectories in the mantle. For $t = 17$ hours SNO has core crossing trajectory ($\cos\theta_n \simeq 1$) and LVD observes effects of regeneration in the mantle only; SK is unshielded.

The Earth matter effects can be identified:

1. at a single detector, by the observation of deviations of the energy spectrum with respect to what expected from conversion in the star only.

2. by the comparison of energy spectra from different detectors.

The comparison of the results of SK, SNO and LVD – given in the figs. 6.2-6.5 – can be performed in various ways. Let us consider, for instance, the cases shown in figs. 6.2 and 6.3. If the direction to the supernova is determined, the LVD spectrum is known to be free from regeneration effects. Therefore it can be used to predict the energy distributions at SK and SNO without Earth matter effects. Such predictions can be compared to the observations of SNO and SK. Due to the relatively small statistics of the LVD events, however, the accuracy of the reconstruction will not be high and the deviation from the undistorted spectrum (e.g. in the range 40 - 65 MeV) will not be larger than $2 - 3\ \sigma$.

Higher statistical significance is obtained if data from a second large volume detector are available. Kilometer-scale neutrino telescopes, though primarily devoted to the study of high-energy neutrinos, are expected to be sensitive to supernova neutrinos. In particular, for a supernova at distance $D = 10$ Kpc the ice Cerenkov detector of AMANDA [135] would observe more than $2 \cdot 10^4$ events from $\bar{\nu}_e$ scattering on protons, eq. (5.1) [136, 137]. Unfortunately, the presence of a relatively large background and the absence of sensitivity to the neutrino energy spectrum [136, 137, 138] strongly restrict the potential of the study of this signal. We mark, however, that substantial upgrades of the experimental apparatus are possible [138] and the optimization of the detector for supernova neutrino observation would be of great interest. Besides the present neutrino telescopes, the detection of supernova neutrinos is among the goals of future large volume detectors, like UNO [50] and NUSL [51]. We find that the comparison of the energy spectra observed by SK and by another detector with comparable or larger statistics could establish the Earth matter effects at more than $\sim 5\ \sigma$ level.

Notice also that the statistics of each experiment, and therefore the power of the comparison between different detectors, is higher for smaller distance D to the supernova and/or larger binding energy E_B. For instance for $D = 3$ Kpc and $E_B \simeq 4.5 \cdot 10^{53}$ ergs the statistics is ~ 17 times higher and the differences between the spectra of SK and LVD (unshielded) can be as large as $(6 - 10)\ \sigma$.

Besides the comparison of the spectra, more specific criteria of identification of the Earth effect can be elaborated if the location of the supernova and the solar neutrino oscillations parameters are known. For instance, for LMA parameters and rather superficial trajectory in the mantle the effect consists in a narrowing of the spectrum (see e.g. figs. 6.2-6.3 panels c)-d)). Thus the comparison of the widths of the spectra at different detectors may establish the Earth effect.

Already the very fact of establishing the Earth matter effect in the neutrino and/or in antineutrino channel will have important implications for the neutrino mass and flavor spectrum. For this it will be enough to study some integral effect of regeneration. Let us consider the following possibility. As we have discussed in chapter 4, for LMA parameters the regeneration effect is negative above the

critical energy and moreover the relative size of the effect increases with E. The Earth matter effect at low energy is small mainly due to the dependence of the regeneration factor $f_{reg} \propto E$ (eq. (4.35)). Therefore to identify the regeneration effect one can compare the signals from the process (5.1) in the various detectors at low, $E < E_s$, and high, $E > E_s$, energies [139], where E_s is some separation energy. Let us introduce the numbers of events

$$N_L \equiv \int_{E_{th}}^{E_s} dE_e \frac{dN(\bar{\nu}_e p)}{dE_e} , \qquad N_H \equiv \int_{E_s}^{\infty} dE_e \frac{dN(\bar{\nu}_e p)}{dE_e} , \tag{6.1}$$

where dN/dE_e is given in eq. 5.8, and take the ratio

$$\mathcal{R} \equiv \frac{N_L}{N_H} . \tag{6.2}$$

In absence of Earth effects $\mathcal{R}$ has the same value for every experiment provided that the detection efficiencies are independent of energy at $E > E_{th}$, or in the particular case of equal efficiencies. Therefore, differences in the quantity (6.2) are entirely due to regeneration effects: stronger effect corresponds to larger $\mathcal{R}$. In fig. 6.6 we show the dependence of $\mathcal{R}$ on the separation energy E_s for different detectors; we have taken $E_{th} = 20$ MeV. The panels a) and b) of the figures refer to the situations illustrated in figs. 6.2 and 6.3 respectively. In agreement with the analyses of the spectra, in the latter case (panel b)) the effect is stronger: the deviation of the ratio $\mathcal{R}$ for SK from the value $\mathcal{R}_0$ in absence of regeneration, given by LVD, can be as large as $(2-3)\ \sigma$. Larger deviation ($(4-5)\ \sigma$) is realized if $\mathcal{R}_0$ is provided by an experiment with volume comparable or larger than the one of SK.

6.3 Discussion: what will be learnt

Within 2 - 3 years the solution of the solar neutrino problem can be identified by the results of the SNO, KamLAND and BOREXINO experiments. In particular, KamLAND will be able to establish the LMA solution and to measure $\Delta m^2_{\odot}$ and $\sin^2 2\theta_{\odot}$ with 10 - 20% accuracy [140, 141, 142, 143]. This will enormously sharpen the predictions for the Earth matter effects.

The possibility exists that U_{e3} will be determined by MINOS [144] provided that its value is not too far from the present upper bound, eq. (4.7). In this case, U_{e3} is certainly in the adiabatic range. In a long perspective, a neutrino factory [145] will be able to cover the whole the range of U_{e3} relevant for supernova neutrinos. Thus, either U_{e3} will be measured or the upper bound on U_{e3} will be so strong that the transition in the supernova will be certainly non-adiabatic.

Let us consider possible implications of the supernova neutrino results depending on the solution of the solar neutrino problem.

1). Suppose that the LMA solution will be identified with parameters close to the present best fit point ($\Delta m^2_{\odot} = (3-6)\cdot 10^{-5}$ eV^2). As we have seen, in this case the regeneration effect can be observed.

The features of the Earth matter effects depend on the value of U_{e3} and on the type of mass hierarchy. For normal mass hierarchy and U_{e3} in the adiabatic range (which appears as the most plausible scenario) we expect regeneration effects in the antineutrino channel and no effect in the neutrino channel (see sect. 4.2.4). In the supernova data further confirmations of such a possibility are (i) the absence of the neutronization peak in ν_e and appearance of the ν_μ/ν_τ neutronization peak, (ii) hard spectrum of ν_e during the cooling stage: $\langle E_e \rangle > \langle E_{\bar{e}} \rangle$.

The relative size of the effect in $\bar{\nu}_e$ channel, $\bar{R}$, is determined by the regeneration factor and the flux factor, according to eq. (4.14). At high energies, when the flux factor reaches the asymptotic value (4.17), eq. (4.14) gives:

$$\bar{R}(E \gg \bar{E}_c) \sim -\frac{\bar{f}_{reg}}{\sin^2\theta_{\odot}} \,. \tag{6.3}$$

That is, the effect is completely predicted in terms of solar oscillation parameters.

In the case of inverted mass hierarchy the Earth matter effect should be observed in the neutrino channel and no effect is expected in the antineutrino channel if $|U_{e3}|^2 > 10^{-5}$ (see fig. 4.1). This possibility will be confirmed by the observation of the ν_e-neutronization peak and of an hard spectrum of the $\bar{\nu}_e$ during the cooling stage. The relative size of the Earth matter effect, R, is given by eq. (4.37) (with the replacement $P_H \to 1$) with the high energy asymptotic (see eq. (4.40))

$$R(E \gg E_c) \sim -\frac{f_{reg}}{\cos^2\theta_{\odot}} \,. \tag{6.4}$$

In the limit $|U_{e3}|^2 \ll 10^{-5}$ the high density resonance is inoperative, so that the result is insensitive to the mass hierarchy. Oscillations appear in both the neutrino and antineutrino channels, and, at high energies, they are determined by the solar oscillation parameters (eqs. (6.3) and (6.4)). The ratio of the relative effects at high energies equals:

$$\frac{R}{\bar{R}} \simeq \tan^2\theta_{\odot}\frac{f_{reg}}{\bar{f}_{reg}} \,. \tag{6.5}$$

So, possible checks of this equality would be the confirmation of the neutrino scheme with very small U_{e3}.

If U_{e3} is in the intermediate region: $|U_{e3}|^2 \sim 10^{-6} - 10^{-5}$ the situation is more complicated. One expects to observe oscillations both in the neutrino and antineutrino channels; the regeneration effect depends on the mass hierarchy and on the specific value of U_{e3}. In the case of normal mass hierarchy, the relative effect in the neutrino channel is proportional to $P_H = P_H(U_{e3})$ (eq. (4.37)) and at high energies, when the flux factor reaches the asymptotic value we get, (eq. (4.40)):

$$R(E \gg E_c) \sim -\frac{P_H}{1 - P_H \sin^2\theta_\odot} f_{reg} \ . \tag{6.6}$$

Since f_{reg} is determined by the solar parameters, by measuring the relative deviation R we can determine the value of P_H via the eq. (6.6) and therefore get information about U_{e3}.

For antineutrinos with inverted hierarchy we find the high energy asymptotic (see eq. (4.36)):

$$\bar{R}(E \gg \bar{E}_c) \sim -\frac{P_H}{1 - P_H \cos^2\theta_\odot} \bar{f}_{reg} \ . \tag{6.7}$$

In practice, the observation of the Earth matter effect in the $\bar{\nu}_e$ channel and absence of the effect in ν_e channel will testify for normal mass hierarchy and $|U_{e3}|^2 > 10^{-5}$. In the opposite situation, effect in the ν_e channel and absence of the effect in $\bar{\nu}_e$ channel, the inverted hierarchy will be identified with $|U_{e3}|^2 > 10^{-5}$. However the present experiments have lower sensitivity to ν_e fluxes with respect to the fluxes of $\bar{\nu}_e$, so that it may be difficult to establish "zero" regeneration effect with high enough accuracy.

If the Earth matter effect is observed in both channels, one should compare the size of the effect with that predicted in the absence of the high resonance in a given channel. Thus, if the observed signal in the neutrino channel is smaller than what is predicted in the assumption of $P_H = 1$, whereas in the antineutrino channel prediction and observation coincide, we will conclude that the hierarchy is normal and the ratio of the observed to predicted signals in the neutrino channel can give the value of P_H. The opposite case of coincidence of the predicted and observed signals in the neutrino channel and suppressed observed signal in the antineutrino channel will testify for the inverted mass hierarchy.

Besides the probing of the neutrino mass spectrum and mixing, a study of the properties of the original neutrino fluxes can be done with Earth matter effects. In principle, a detailed study of the observed energy spectra will allow to reconstruct the flux factor as well as to determine the critical energy E_c.

2). Suppose that the future solar neutrino experiments will identify the SMA solution. In this case, the Earth matter effect is expected in the neutrino channel only,

and only if the high density resonance is inoperative. This requires the inverted mass hierarchy or very small U_{e3} in the case of normal mass hierarchy. As discussed in sect. 4.4.2, the effect is small and difficult to be observed even in the most favorable situations.

For the rather plausible case of the normal mass hierarchy and $|U_{e3}|^2 > 10^{-5}$ no Earth matter effect should be seen.

The observation of the Earth matter effect in the SMA case will allow to conclude that the mass hierarchy is inverted or the hierarchy is normal but U_{e3} is very small: $|U_{e3}|^2 \ll 10^{-5}$. In principle, the intermediate case $|U_{e3}|^2 \sim 10^{-5}$ can be identified if the observed signal will be smaller that the expected one for $P_H = 1$. Notice that from eqs. (4.21) and (4.22) one gets the low energy asymptotic for the flux factor:

$$R(E \ll E_c) = P_H(1 - 2P_L) f_{reg} \frac{1}{P_H P_L} = f_{reg}(1 - 2P_L)\frac{1}{P_L} , \qquad (6.8)$$

which does not depend on P_H. So it will be difficult to disentangle the effect of P_H from uncertainties in the original neutrino fluxes.

The situation can be much more complicated if a sterile neutrino exists. This can be clarified in 2 - 3 years: the MiniBooNE experiment and further searches for sterile neutrinos in the solar and atmospheric neutrino experiments will allow to establish the existence of sterile neutrinos.

Negative results of the searches will strongly favor the 3ν schemes discussed in this paper. Still some uncertainty will remain: sterile neutrinos, unrelated to the LSND result, may exist and weakly mix with active neutrinos. Even a very small mixing (unobservable by other means) of sterile states with masses in the wide range from sub eV up to 10 keV can strongly modify the properties of the neutrino burst.

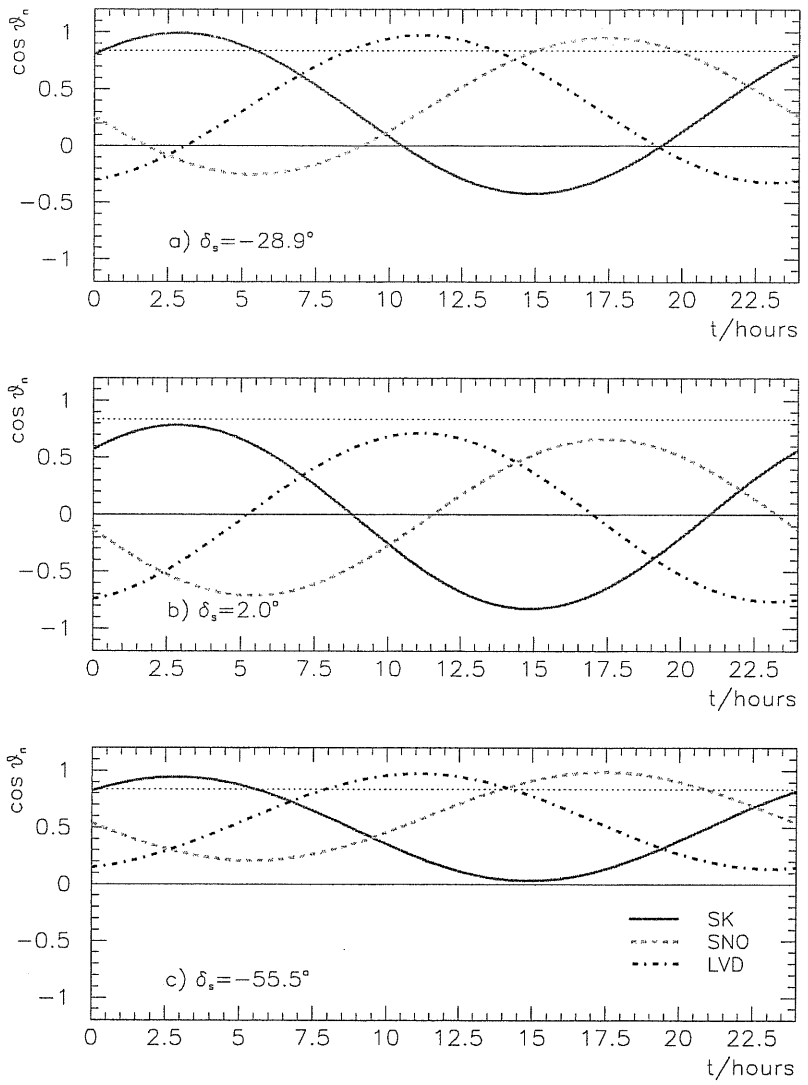

Figure 6.1: The cosines of the nadir angles θ_n of SuperKamiokande, SNO and LVD detectors with respect to the supernova as functions of the arrival time of neutrino burst. The three panels refer to three different locations of the star in the galactic plane (given by the declination angle δ_s). We fixed $t = 0$ as the time at which the star is aligned with the Greenwich meridian.

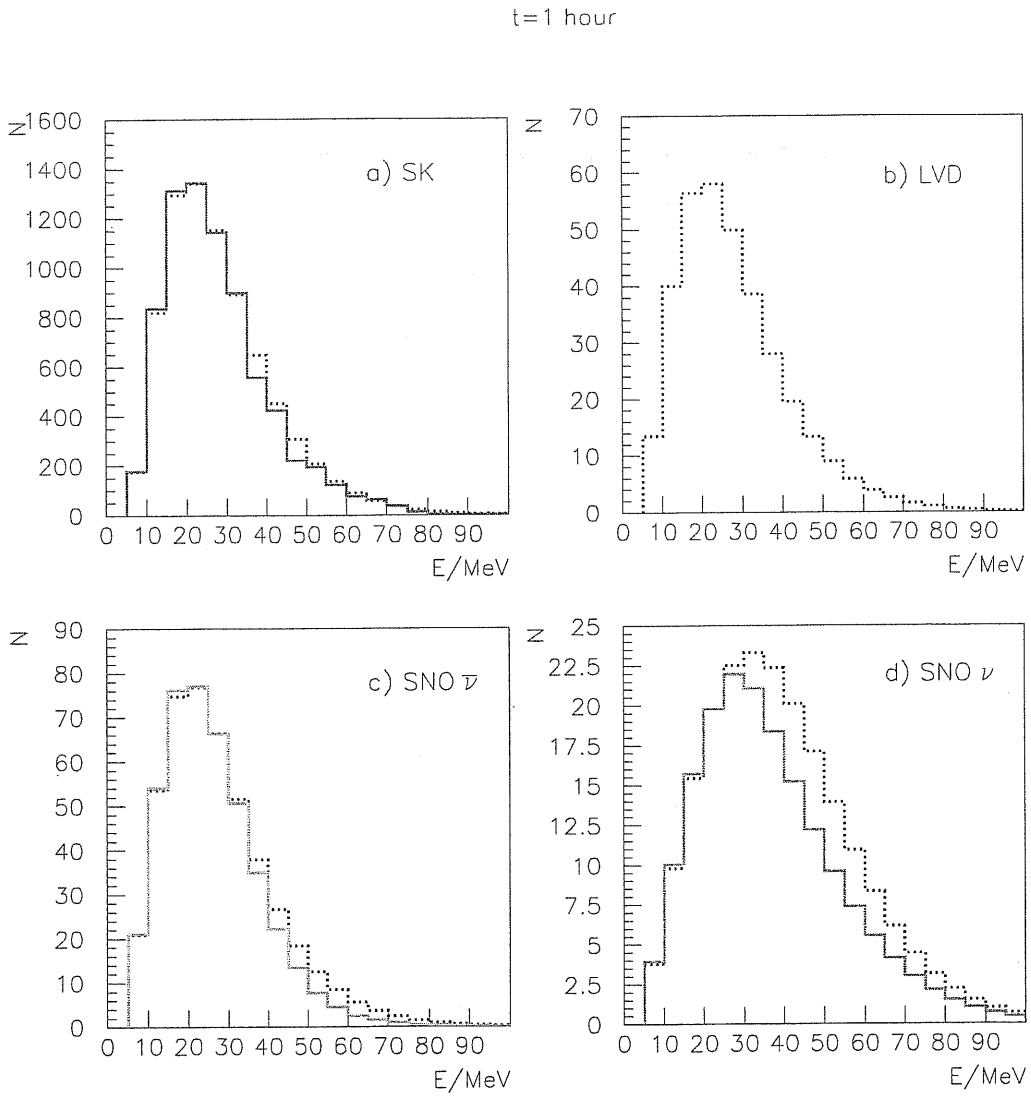

Figure 6.2: The energy spectra expected at SK, SNO and LVD with (solid lines) and without (dotted lines) Earth matter effect, for the same parameters as in figs. 4.3 and 4.8 and $t = 1$ hour of fig. 6.1 a). A distance $D = 10$ Kpc from the supernova and binding energy $E_B = 3{\cdot}10^{53}$ ergs have been taken. In this specific configuration LVD is not shielded by the Earth, thus observing undistorted spectrum. The histogram c) refers to the sum of events from $\bar{\nu}_e + p \rightarrow e^+ + n$ and $\bar{\nu}_e + d \rightarrow e^+ + n + n$ scatterings, while the panel d) shows the events from $\nu_e + d \rightarrow e + p + p$. In a) and b) only the events from $\bar{\nu}_e + p \rightarrow e^+ + n$ are shown.

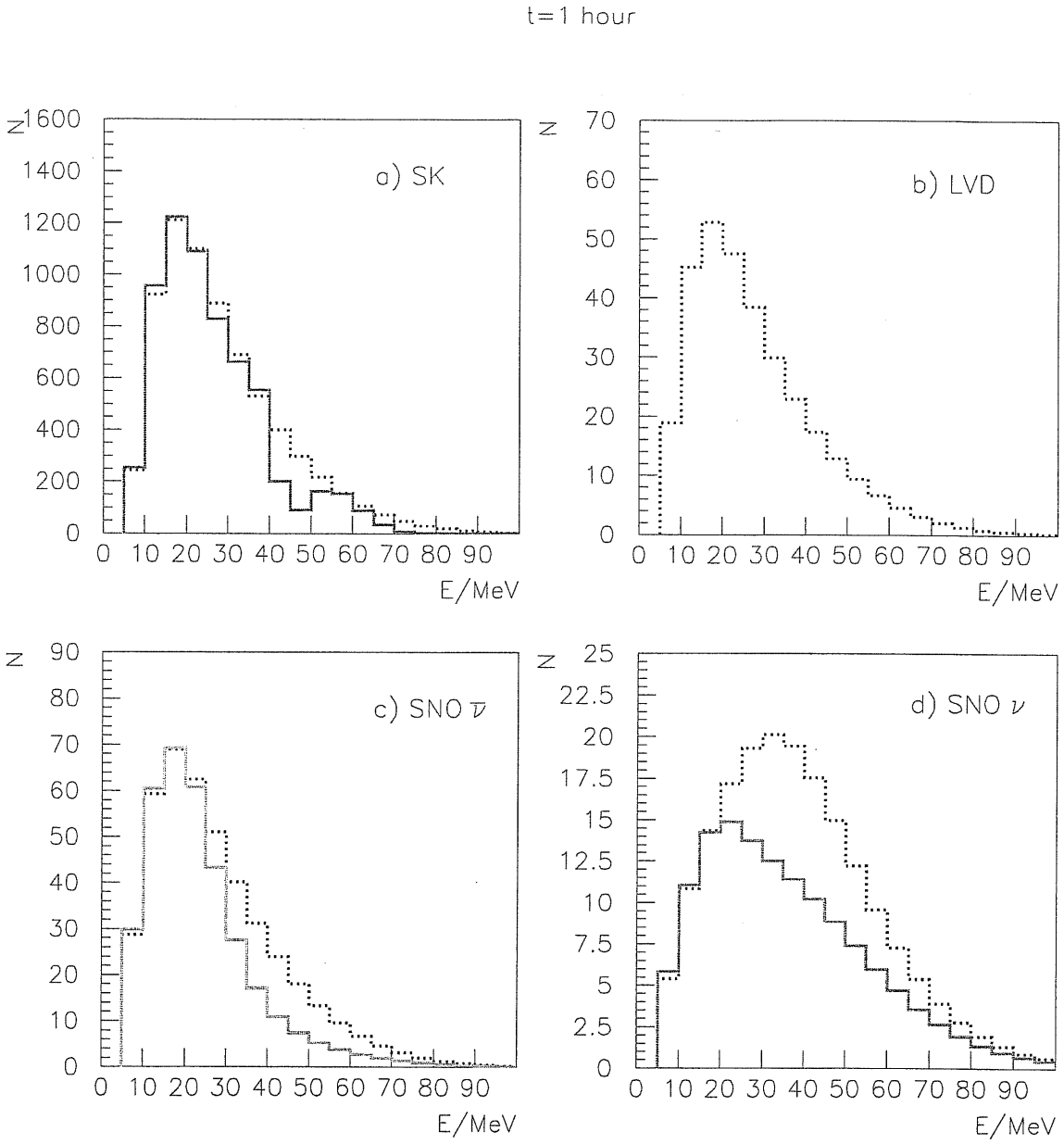

Figure 6.3: The same as fig. 6.2 for different values of some parameters: $\Delta m^2_{\odot} = 3 \cdot 10^{-5}$ eV^2, $\sin^2 2\theta_{\odot} = 0.9$; $T_e = 3$ MeV, $T_{\bar{e}} = 4$ MeV.

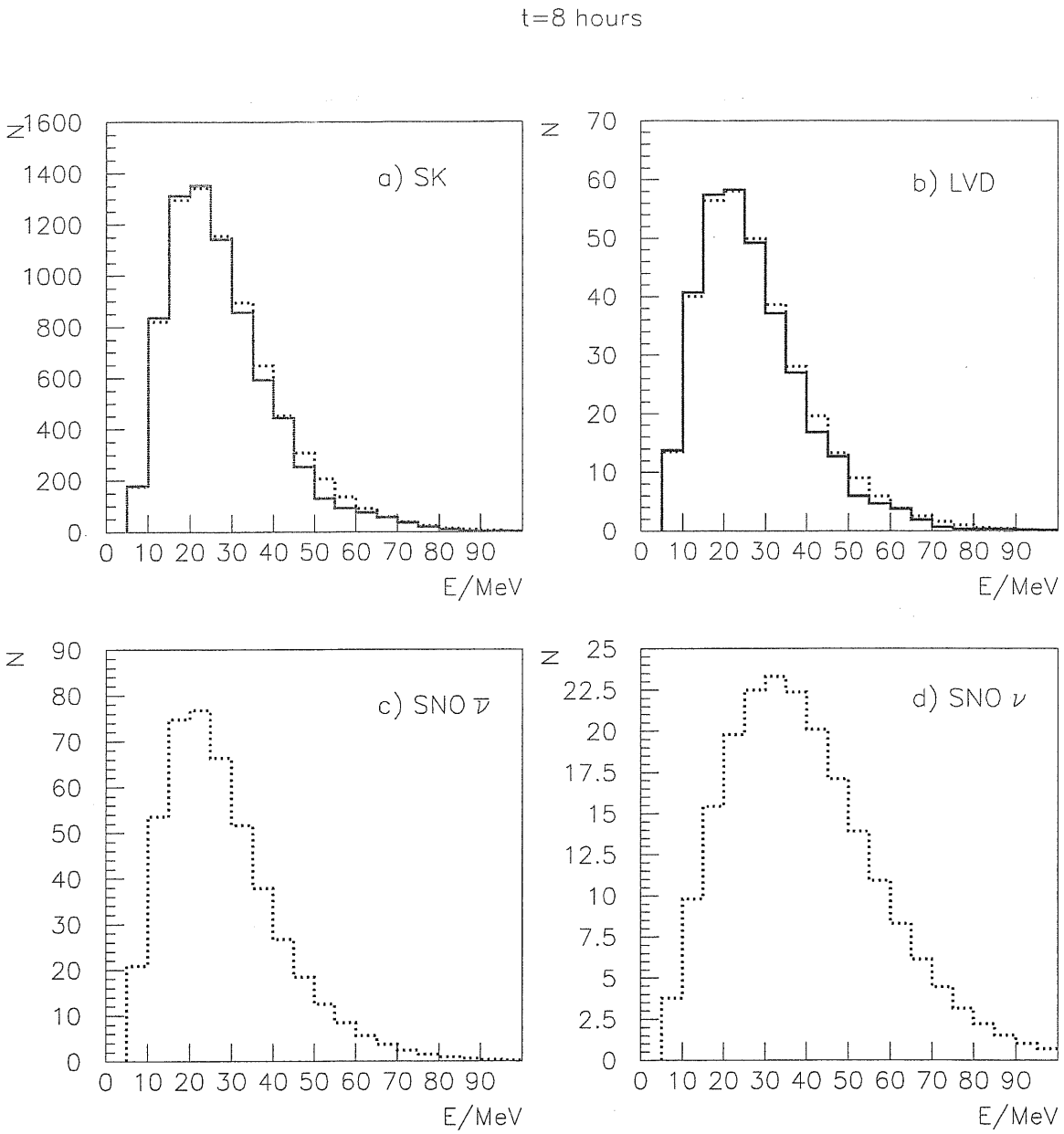

Figure 6.4: The same as fig. 6.2 for $t = 8$ hours of fig. 6.1 a). For this configuration SNO is unshielded by the Earth.

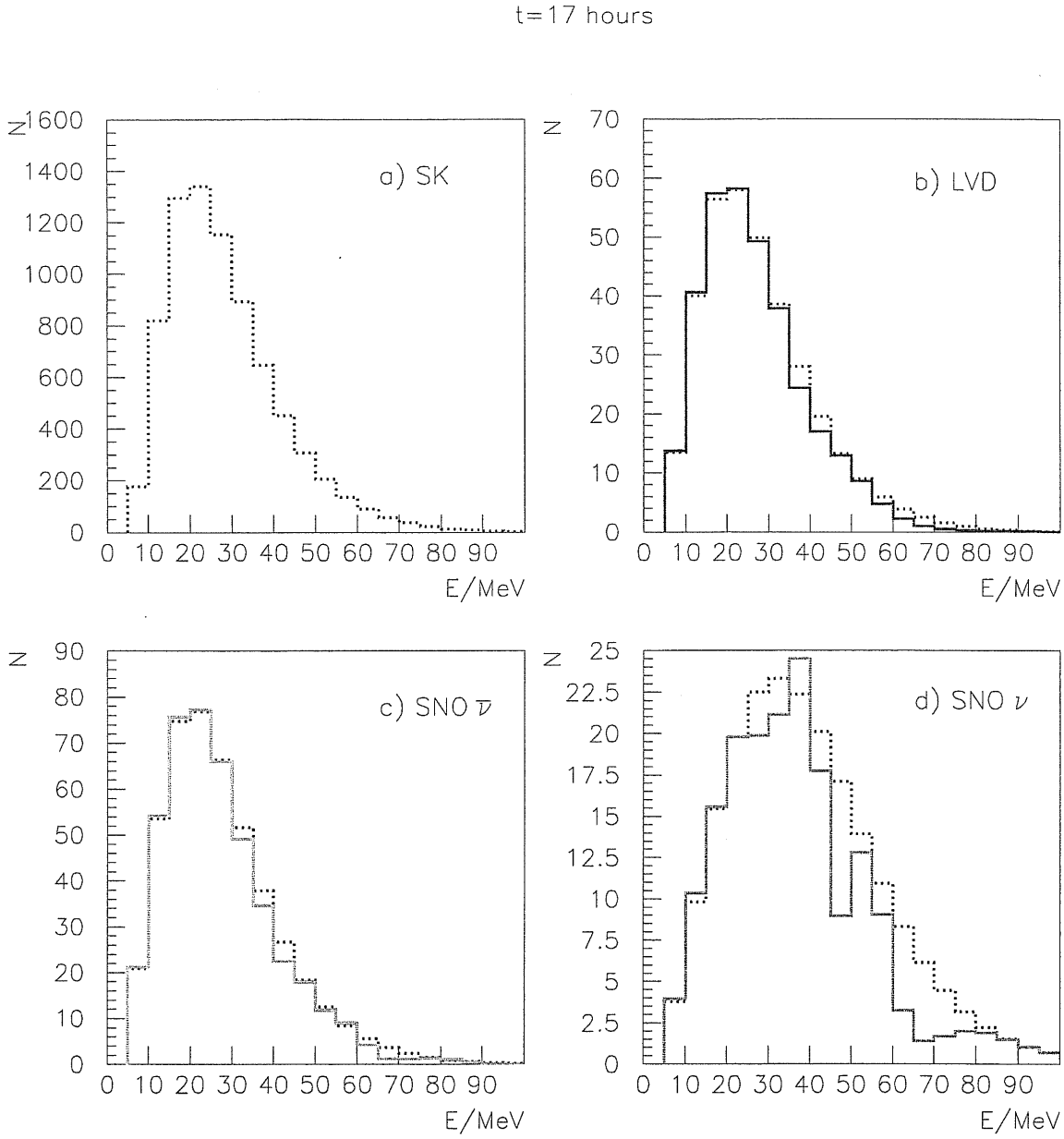

Figure 6.5: The same as fig. 6.2 for $t = 17$ hours of fig. 6.1 a). For this configuration SK is unshielded by the Earth.

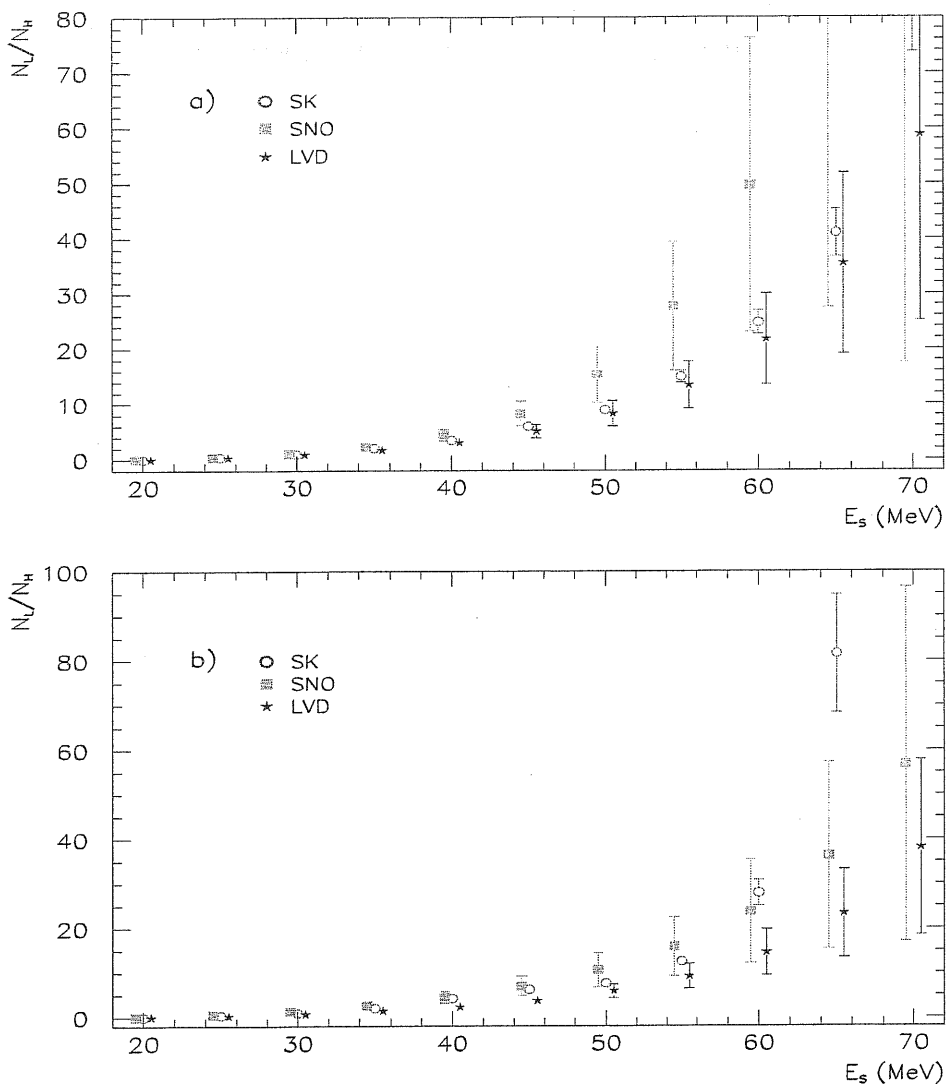

Figure 6.6: The ratio of the numbers of low and high-energy events from $\bar{\nu}_e + p \rightarrow e^+ + n$ reaction at SK, SNO and LVD, as a function of the separation energy E_s. The bars represent 1 σ statistical errors. The panels a) and b) refer to the spectra shown in figs. 6.2 and 6.3 respectively. We have taken a minimum energy $E_{th} = 20$ MeV for the calculation of the numbers of low-energy events.

Conclusions

Let us summarize the results presented in this thesis.

Matter effects can lead to strong neutrino flavour transition even for small vacuum mixing angle: $\theta \ll 1$. Besides the resonance and the adiabaticity conditions, a significant conversion requires that a sufficiently large amount (width) of matter is crossed by the neutrinos. This is expressed by the minimum width condition, $d \geq d_{min}$, where $d_{min} = \pi/(2\sqrt{2}G_F \tan 2\theta) = d_0/\tan 2\theta$, for low neutrino energies, $s \ll M_Z^2$, and conversion probability $P \geq 1/2$. The absolute minimum d_{min} is realized for uniform medium with resonance density; for all the other realistic situations the required width, $d_{1/2}$, is larger than d_{min}.

The minimum width condition allows one to conclude on the relevance of the matter effect without knowledge of the density profile, once the width d is known, as it is the case in some astrophysical situations. Significant matter effect is excluded if $d < d_0$ (or $d < d_{min}$ if the mixing angle is known), while the condition $d \geq d_{min}$ is necessary but not sufficient for strong conversion effect.

As an application we considered neutrinos produced by AGN and GRBs and propagating in the matter of the source. Using the estimates of the width d from X-ray or optical observations one finds $d/d_0 \lesssim 10^{-5}$, thus excluding significant matter effect.

In contrast, strong transition can be produced by the interaction with the intergalactic medium. Indeed, the width of this medium exceeds the minimum width d_0 if the relic neutrino background of the universe has large CP (lepton) asymmetry, $\eta \gtrsim 1$, and the source of neutrinos is at cosmological distances. The contributions of the other components (baryon, photons) of the intergalactic medium to the width d is very small and can be neglected.

The dynamics of high-energy neutrino conversion in the CP-asymmetric neutrino background was studied.

For conversion between active neutrinos the matter effects consist in a modification of the vacuum oscillation length. The effect is significant for large mixing angle, $\sin^2 2\theta \gtrsim 0.3$, and high energies, $E_0/\Delta m^2 \gtrsim 5 \cdot 10^{32}$ eV^{-1}, for which the matter contribution to the oscillation phase dominates over the vacuum oscillation

one. In these circumstances the conversion probability can differ by $\sim 30\%$ from the vacuum oscillations value.

For active-sterile conversion the matter effects can be important in the interval $E_0/\Delta m^2 \gtrsim 10^{28} - 10^{32}$ eV^{-1}, for which the resonance condition is satisfied. In the majority of realistic situations (with $z \lesssim 10$, $\eta \lesssim 10$), the adiabaticity is broken. This implies that the matter effect is reduced to non-adiabatic level crossing or enhancement (suppression) of mixing and therefore of the depth of oscillations in the production epoch. The relative change of the conversion probability can be as large as $20 - 50\%$. For extreme values of the asymmetry and large redshift of production the adiabatic conversion can take place with almost maximal conversion probability.

For the diffuse flux of neutrinos from GRBs and AGN the relative deviation of the flux due to matter effects with respect to vacuum oscillations can reach 20%, while for neutrinos from the decay of super-heavy relics the effect can be larger, up to $\sim 40\%$.

Possible signatures of matter effects consist in the deviation of ratios of numbers of observed events, $N_e/N_\mu, N_e/N_\tau, N_\mu/N_\tau$, from the values predicted by pure vacuum oscillations. Presumably, neutrino mixings and masses will be measured in laboratory experiments and vacuum oscillations effects will be reliably predicted.

For conversion into a sterile state one expects also a characteristic energy dependence of the ratios which in principle will allow to distinguish matter effects from the uncertainties in the flavour content of original neutrino fluxes.

For illustration purpose we estimated the observable effects for two possible schemes of neutrino masses and two different flavour compositions of the detected fluxes in absence of conversion. In a scheme with three flavour states only and parameters in the region of VO solution of the solar neutrino problem the deviation of ratios of numbers of events from their vacuum oscillation values can be of $\sim 10\%$. Similar conclusion is obtained for schemes with an additional sterile neutrino.

The identification of matter effects on fluxes of high-energy neutrinos requires new large scale detectors with relatively high statistics, ~ 1000 events/year. It would provide an evidence of large CP (lepton)-asymmetry in the universe, which will have far going consequences for our understanding of the evolution of the universe.

In the second part of the thesis the propagation of supernova neutrinos was considered. In particular, we studied the effect of regeneration in the matter of the Earth in the framework of three flavours with either normal or inverted hierarchy.

The strongest regeneration effect is expected for oscillation parameters in the region of the LMA solution of the solar neutrino problem, especially for the lowest values of $\Delta m^2_\odot$ in this region: $\Delta m^2_\odot = (2 - 5) \cdot 10^{-5}$ eV^2.

In the $\bar{\nu}_e-$ channel the effect exists in the scheme with normal mass hierarchy

(ordering of the states) or in the scheme with inverted mass hierarchy for $|U_{e3}|^2 < 10^{-5}$, when the conversion in the high density resonance is non-adiabatic. The effect consists in an oscillatory modulation of the energy spectra and is negative (except in small energy intervals for core crossing trajectories) above the critical energy $E_c \sim 25$ MeV, thus suppressing the signal. The relative size of the effect increases with energy and at $E \sim 60 - 70$ MeV it can reach $50 - 70\%$. The period of modulation increases with energy and above $E \sim 40$ MeV no averaging occurs in the energy spectrum of events. At low energies the effect is small and the modulations are averaged out. Thus, in the LMA case the most sensitive region to the Earth matter effect is above $E \sim 40$ MeV .

The oscillatory picture (position of minima and maxima) is very sensitive to $\Delta m^2_{\odot}$. For trajectories in the mantle only the modulation of the spectrum is rather regular. For the core-crossing trajectories the structures become narrower and irregular.

The Earth matter effect decreases with the increase of $\Delta m^2_{\odot}$ and for $\Delta m^2_{\odot} > 10^{-4}$ eV^2 its observation will be difficult.

For the ν_e- channel substantial Earth matter effect is expected in the case of normal mass hierarchy, provided that $|U_{e3}|^2 < 10^{-5}$, or in the case of inverted mass hierarchy. The effect has oscillatory character, similarly to the $\bar{\nu}_e$ – case, and can be as large as 100 % at $E > 50 - 60$ MeV.

Thus, as in the case of antineutrinos, one should search for an oscillatory modulation of the signal in the energy range $E > 40$ MeV.

The size of the effect depends on the properties of the original neutrino fluxes via the flux factor. This dependence, however, disappears in the high-energy limit, $E \gtrsim 50$ MeV.

For oscillation parameters from the SMA solution the effect appears in the ν_e- channel only, and only if the H-resonance is inoperative (very small U_{e3} or inverted mass hierarchy). The relative effect can be as large as 30% for core crossing trajectories due to the parametric enhancement of oscillations. The effect is localized in the low energy part of the spectrum: $E = 5 - 10$ MeV, and will be strongly smoothed in the spectrum of observed events by integrations over the neutrino energy and the true energy of electron. Therefore, practically no distortion can be seen.

In the case of LOW solution the Earth matter effect is significant at very low energies, $E \sim 1$ MeV, with a smooth $1/E$ behaviour. At $E = 5$ MeV, the relative effect in the flux is below $(10 - 20)\%$.

The application of the Earth regeneration effect to the neutrino burst from SN1987A showed that certain features of the neutrino signals observed by K2 and IMB detectors (difference of spectra, absence of events above $E \sim 40$ MeV) can be explained by oscillations in the Earth and different positions of the detectors. This requires (i) the oscillation parameters $\Delta m^2_{\odot}$ and $\sin^2 2\theta_{\odot}$ to lie in rather narrow

bands within the region of the LMA solution of the solar neutrino problem and (ii) nomal mass hierarchy if $|U_{e3}|^2 \gtrsim 10^{-3}$. The hierarchy can be inverted provided that $|U_{e3}|^2 \lesssim 10^{-5}$.

The consistency of the $\bar{\nu}_e$ spectra implied by K2 and IMB data improves when oscillations are taken into account.

Clearly, in view of the low statistics of SN1987A neutrino signals, our conclusions have an indicative character, as far as the interpretation of the K2 and IMB data is concerned. Conversely, statistically solid results will be obtained in future galactic supernova observations.

With high probability, at least one of the existing detectors (SK, SNO, LVD) will be shielded by the Earth at the moment of arrival of a supernova neutrino burst, so that the Earth matter effect on the neutrino flux will be observed. For supernova in a region close to the galactic center the most plausible configuration is that for two detectors the trajectories of the neutrino burst cross the Earth, whereas the third detector is unshielded.

The detectors considered can register Earth matter effects ($\cos\theta_n > 0$) for a significant fraction ($\gtrsim 60\%$) of the possible arrival times of the signal and core effect for $\sim 20\%$ of the times. These fractions may be even larger depending on the specific location of the star in the galaxy.

The identification of the Earth matter effect is possible in a single detector (in the LMA case) by the observation of the oscillatory modulation of the energy spectrum in the high energy part: $E > 40$ MeV. Another method consists in the comparison of signals from two (or several) different detectors. If one of the detectors is unshielded by the Earth its result can be used to reconstruct the spectrum of the neutrinos arriving at Earth and make predictions of the signal expected in the other detectors in absence of matter effect. This approach allows to reduce substantially the uncertainties related to the model of the star and to the original neutrino fluxes. For a supernova at distance $D = 10$ Kpc and with energy release $E_B = 3 \cdot 10^{53}$ ergs we estimated that the Earth matter effects can be established at $(2-3)\sigma$ level by comparison between SK, SNO and LVD results, and at $(4-5)\sigma$ by comparison between the spectra from two large volume detectors (of SK size or larger).

Another method to identify the Earth matter effect is to study the ratio of numbers of events in the high- and in the low-energy parts of the spectrum in different detectors.

Studies of the Earth matter effect will allow to establish or most probably to confirm the solution of the solar neutrino problem, to get information about U_{e3} and to identify the type of hierarchy of the neutrino mass spectrum.

Acknowledgements

I want to say сердечное спасибо to my supervisor, Alexei Yu. Smirnov, for the way he worked with me in the last two years. He did that with enthusiasm, continuously, spending for me an amount of time and energy which goes far beyond my expectations. Moreover, he taught me not only physics, but how to be a good physicist, always encouraging me to seek this goal.

I am grateful to SISSA and in particular to the faculty of the High Energy Physics sector for providing me with a friendly environment and constant support, which were precious to my work.

I wish to warmly thank the colleagues and friends of SISSA and ICTP for the great scientific and personal enrichment I got from them. In particular I am thankful to Enrico Lunghi, Marco Peloso, Orlando Peres, Lorenzo Sorbo and Alessandro Tomasiello for their friendship, support and patience when sharing the same office.

Finally, I wish to thank my family, relatives and all those friends to whom this PhD subtracted part of my time, for their understanding and participating to this part of my life.

Appendix A

Conversion effects in the relic neutrino background

In this appendix we consider the time evolution of the flavour composition of the relic neutrino background due to mixing and oscillation effects. We assume that large CP-asymmetries[1] are produced at some epoch before the Nucleosynthesis (BBN) epoch, i.e., at temperature $T \gtrsim T_{BBN} \simeq 1$ MeV, and study how they change with time. The evolution of the flavour densities n_e, n_μ and n_τ of the neutrino gas is a non-linear many-body problem, which, in general, requires a numerical treatment[146, 147]. In some specific cases, however, an analytical description is possible[148] and conclusions can be obtained on general grounds.

A.0.1 Three-neutrino system evolution

Let us first consider the case of mixing between three active neutrinos, ν_e, ν_μ, ν_τ. In refs.[146, 148] it has been shown that the evolution of the flavour densities has peculiar aspects for the ideal case of a monoenergetic gas of neutrinos (with no antineutrinos, $n_{\bar{\nu}} = 0$) initially produced in flavour states. For this specific ensemble of neutrinos the potential due to neutrino-neutrino interaction cancels in the evolution equation, so that the collective behaviour of the system is described by vacuum oscillations. This result holds with a good approximation [146] also for realistic neutrino energy spectra and in presence of a small component of antineutrinos. For this reason it can be applied to our case of interest, in which the background is strongly CP-asymmetric, $n_\nu \gg n_{\bar{\nu}}$, and neutrinos have a thermal spectrum. In what follows we approximate the neutrino energies with the average thermal energy of the gas: $E \simeq \langle E_\nu \rangle = \alpha T_\nu$, where T_ν denotes the temperature of the neutrino gas.

[1] We recall that the CP-asymmetry of the relic neutrino gas is defined as the difference of the concentrations of neutrinos and antineutrinos normalized to the density of photons: $\eta_\nu \equiv (n_\nu - n_{\bar{\nu}})/n_\gamma$ (see chapter 3, eq. 3.1). The asymmetry is bounded by several cosmological constraints which are given in sec. 3.1.

The numerical factor α depends on the CP-asymmetry η (defined in sec. 3.1.1) of the background: we have $\alpha \simeq 3.15$ in absence of asymmetry, $\eta \simeq 0$, and $\alpha \simeq 3.78$ for $\eta \simeq 1$.

The length scale of flavour conversion is given by the vacuum oscillation length:

$$\begin{aligned} l_v &= \frac{4\pi E}{\Delta m^2} \simeq \frac{4\pi\alpha\beta T}{\Delta m^2} \\ &= 2.48 \cdot 10^5 \text{ cm } \alpha\beta \left(\frac{T}{1\text{MeV}}\right) \left(\frac{10^{-3}\text{eV}^2}{\Delta m^2}\right) , \end{aligned} \tag{A.1}$$

where β is the ratio between the temperature of the neutrino background and the temperature T of the electromagnetic radiation: $\beta \equiv T_\nu/T$. We have $\beta = 1$ before the electron-positron recombination epoch, $T \gtrsim 0.5$ MeV, and $\beta = (4/11)^{1/3}$ after this epoch.

Besides oscillations, for temperatures $T \gtrsim 1$ MeV other phenomena, and therefore other length scales, are relevant:

- Inelastic collisions. Let us consider a system of two mixed neutrinos, ν_a, ν_b $(a, b = e, \nu, \tau)$. After its production as a flavour state, e.g. $\nu = \nu_a$, a neutrino oscillates in vacuum until a collision occurs with a particle X of the background. At the time of the collision the quantum state of the neutrino is a coherent mixture of the two flavours: $\nu = A\nu_a + B\nu_b$. The effects of the collision depend on the specific reactions that take place [149, 150, 151] (see also the discussion in [93]). If the reaction is a scattering, $\nu X \to \nu X$, and the interaction is flavour blind, i.e. it is the same for the two flavours a and b, after the collision the neutrino continues to propagate as a coherent superposition of ν_a and ν_b and the collision does not affect oscillations. For scattering with flavour-sensitive interaction or for absorption processes[2], $\nu X \to any$, the effect of the collision is to break the coherence between ν_a and ν_b, so that after the collision the two flavours evolve independently, developing vacuum oscillations until the next collision happens.

  As a result, one easily obtains that for a beam of neutrinos propagating in a medium oscillations are damped according to the expression:

$$n_a(L) = \frac{1}{2} + \left(n_a^0 - \frac{1}{2}\right) \exp\left[-\frac{L}{l_c} \ln\left(\frac{1}{1-2P_c}\right)\right] , \tag{A.2}$$

[2]In the situation we are considering the neutrinos are in thermodynamical equilibrium, so that their disappearance through a given reaction is balanced by their production through the inverse process.

where n_a^0 and $n_a(L)$ are the fractions of ν_a in the neutrino beam at the production time and at distance L from the production point. Here l_c is the coherence length, which represents the distance between two collisions, and P_c is the vacuum oscillation probability between two collisions: $P_c \simeq \sin^2 2\theta \sin^2(\pi l_c/l_v)$. From eq. (A.2) we see that, if $P_c \neq 0$, with the increase of L (i.e. of the number of collisions) the interplay of oscillations and collisions leads to the equilibration of the flavour densities: $n_a(L \to \infty) = n_b(L \to \infty) = 1/2$. The convergence to this limit is determined by the equilibration length $l_{eq} \equiv l_c/\ln(1/|1-2P_c|)$. For small conversion probability, $P_c \ll 1$, the length l_{eq} is much larger than l_c: $l_{eq} \simeq l_c/(2P_c) \gg l_c$. This is the case if the vacuum mixing is small and/or the collisions are much more efficient than oscillations, $l_c \ll l_v$, so that the vacuum oscillation phase $\Phi = 2\pi l_c/l_v$ is small. Thus, equilibration of the flavour densities can be obtained only after a large number of collisions: $n_{coll} = L/l_c \gtrsim 1/(2P_c)$. Conversely, if $P_c \sim 1$ equilibration is achieved rapidly after few collisions: $n_{coll} \gtrsim L/l_c$. This circumstance is realized if $l_c \gtrsim l_v$ and the mixing is large, $\sin^2 2\theta \sim 1$.

Let us consider the coherence length, l_c, in more detail. According to refs. [149, 150] l_c can be written as:

$$l_c(a,b)^{-1} = \frac{1}{2}\left[\Gamma^{abs}(a) + \Gamma^{abs}(b) + \Gamma^{fs}(a,b)\right] , \qquad (A.3)$$

where $\Gamma^{abs}(x)$ is the rate of absorption processes for the neutrino of flavour x and $\Gamma^{fs}(a,b)$ is the contribution of the flavour sensitive scatterings $\nu X \to \nu X$. This quantity is determined by the square of the difference of the ν_a-X and ν_b-X scattering amplitudes [149, 150]. In terms of the total scattering rates $\Gamma(a)$ and $\Gamma(b)$ one gets [149]:

$$\Gamma^{fs}(a,b) \simeq \Gamma(a) + \Gamma(b) - 2\sqrt{\Gamma(a)\Gamma(b)} . \qquad (A.4)$$

From eqs. (A.3)-(A.4), using the rates given in ref.[152] we find:

$$l_c(a,b) = \left[k(a,b) G_F^2 \alpha^2 \beta^5 T^5\right]^{-1} , \qquad (A.5)$$

where, for $T \gtrsim 0.5$ MeV:

$$k(e,\mu) \simeq 6.5 \cdot 10^{-3}\left[16 + 0.5\left(r(\xi_e) + r(\xi_\mu)\right) + 5.3 r(-\xi_e) + 3.5 r(-\xi_\mu)\right] , \qquad (A.6)$$

$$k(\mu,\tau) \simeq 6.5 \cdot 10^{-3}\left[0.5(r(\xi_\mu) + r(\xi_\tau)) + 3.5(r(-\xi_\mu) + r(-\xi_\tau))\right] . \qquad (A.7)$$

Here $r(\xi) \equiv I(\xi)/I(0)$ and $I(\xi) \equiv \int_0^\infty x^2 dx/(1+\exp(x-\xi))$. We define $\xi \equiv \mu/T$ with μ the chemical potential of the neutrino gas[3]. At $T \simeq 0.5$ MeV electrons

[3]Let us recall the relation between the quantity ξ and the CP-asymmetry η: $\eta = (\xi^3 + \pi^2\xi)\beta^3/(12\zeta(3))$. In eqs. (A.5)-(A.9) we considered the factor α to have the same value for all the particle species (neutrinos, electrons, positrons). We checked that this is a good approximation even for the large asymmetries we are considering.

and positrons annihilate, so that for $T < 0.5$ MeV their contribution to the scattering and absorption rates becomes negligibly small and we get:

$$k(e,\mu) \simeq 6.5 \cdot 10^{-3} \left[0.5\left(r(\xi_e) + r(\xi_\mu)\right) + 3(r(-\xi_e) + r(-\xi_\mu))\right], \quad \text{(A.8)}$$

$$k(\mu,\tau) \simeq 6.5 \cdot 10^{-3} \left[0.5(r(\xi_\mu) + r(\xi_\tau)) + 3(r(-\xi_\mu) + r(-\xi_\tau))\right] . \quad \text{(A.9)}$$

Numerically, eq. (A.5) gives:

$$l_c(a,b) \simeq 1.45 \cdot 10^{11} \text{ cm } \frac{1}{k(a,b)\alpha^2\beta^5} \left(\frac{1\text{MeV}}{T}\right)^5 . \quad \text{(A.10)}$$

- The expansion of the universe. Oscillations and collisions are ineffective if their scale lengths, l_v and l_c, are larger than the inverse expansion rate of the universe, l_H. In the radiation-dominating regime l_H is expressed as:

$$\begin{aligned} l_H &\simeq \frac{M_p}{1.66\sqrt{g}T^2} , \\ &\simeq 1.45 \cdot 10^{11} \text{ cm} \frac{1}{\sqrt{g}} \left(\frac{1\text{MeV}}{T}\right)^2 , \end{aligned} \quad \text{(A.11)}$$

where M_p is the Planck mass and g represents the number of relativistic degrees of freedom. We have $g = 10.75$ for 1 MeV $\lesssim T \lesssim$ 100 MeV and $g = 3.36$ for $T \ll 1$ MeV.

The figure A.1 shows the lengths l_v, l_c and l_H as functions of the temperature T for $\eta_\mu \simeq 1$, $\eta_e \simeq \eta_\tau \simeq 0$ and various values of Δm^2.

According to the fig. A.1 for $\Delta m^2 \simeq 10^{-7}$ eV^2 we have $l_v \sim l_c \sim l_H$ at $T \sim 2$ MeV. Before this epoch $l_c \lesssim l_H \lesssim l_v$, so that collisions are much more efficient than oscillations. The inequality $l_c \ll l_v$ implies that the vacuum oscillation probability, P_c, is suppressed by collisions, as we discussed in this section. As a consequence, for small mixings, $\sin^2 2\theta \ll 1$, the flavour composition of the background remains unchanged until $T \sim 2$ MeV; a partial equilibration of the flavours can be realized for large mixings: $\sin^2 2\theta \gtrsim 0.5$. For $T < 2$ MeV collisions are ineffective, since $l_c \gtrsim l_H$, and vacuum oscillations develop.

With the decrease of Δm^2, $\Delta m^2 \ll 10^{-7}$ eV^2, the oscillation length l_v increases and, in consequence, for $T \gtrsim 2$ MeV the suppression of oscillations due to collisions is stronger. Even for large mixings the flavour densities are preserved until the neutrino decoupling, $T \sim 2$ MeV. After this epoch oscillations are still suppressed by the expansion rate of the universe and become effective, thus changing the flavour composition of the background, only when the oscillation length is smaller than the horizon, $l_v \lesssim l_H$.

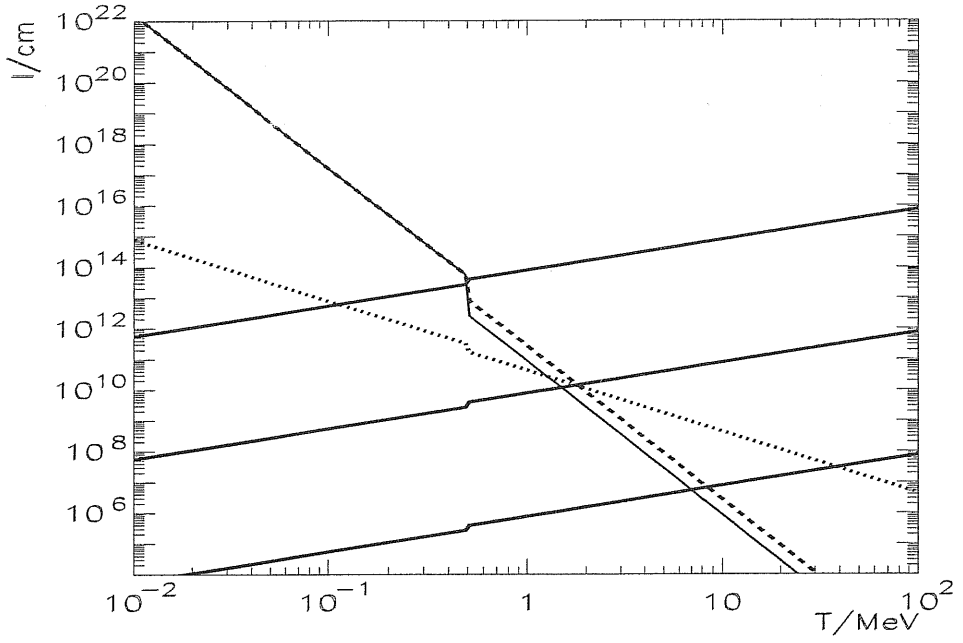

Figure A.1: The length scales l_v, l_c and l_H as functions of the temperature T of the electromagnetic radiation in the universe. The three thick solid lines represent the vacuum oscillation length l_v and correspond, from the upper to the lower, to $\Delta m^2 = 10^{-11}, 10^{-7}, 10^{-3}$ eV^2 respectively. The narrow solid line and the dashed line represent the coherence length, l_c, for the $\nu_e - \nu_\mu$ and the $\nu_\mu - \nu_\tau$ channels respectively. We have taken $\eta_\mu \simeq 1$, $\eta_e \simeq \eta_\tau \simeq 0$. The dotted line represents the inverse expansion rate of the universe, l_H.

For $\Delta m^2 \gtrsim 10^{-7}$ eV^2 the inequality $l_v \lesssim l_c \lesssim l_H$ is realized before the decoupling. In this circumstance the conversion probability, P_c, is not suppressed, in contrast with the case $\Delta m^2 \gtrsim 10^{-7}$ eV^2. Collisions are effective, thus leading to the equilibration of the flavour densities even for small mixing angles. Taking, for instance, $\Delta m^2 \simeq 10^{-3}$ eV^2 we find that equilibration can be achieved for $\sin^2 2\theta \gtrsim 10^{-3}$. Again, after neutrino decoupling the conversion is determined by vacuum oscillations.

For a different choice of the asymmetries at production, e.g. $\eta_\mu \simeq \eta_\tau \simeq 1$ and $\eta_e \simeq 0$, the results are similar to those in fig. A.1 and we come to analogous conclusions.

Let us now find the present flavour asymmetries, η_e^0, η_μ^0, η_τ^0, for specific neutrino mixings and mass spectra motivated by the oscillation interpretation of the solar and atmospheric neutrino anomalies.

We consider the mixing matrix:

$$U = \begin{pmatrix} c_\theta & -s_\theta & 0 \\ s_\theta c_\Theta & c_\theta c_\Theta & -s_\Theta \\ s_\theta s_\Theta & c_\theta s_\Theta & c_\Theta \end{pmatrix} , \tag{A.12}$$

where $c_\theta \equiv \cos\theta$ and $s_\theta \equiv \sin\theta$ and analogous definitions hold for s_Θ and c_Θ. The mass eigenstates ν_1, ν_2 and ν_3 are related to the flavour ones by the rotation: $\nu_\alpha = \sum_i U_{\alpha,i}\nu_i$. The mass squared differences $\Delta m_{ji}^2 \equiv m_j^2 - m_i^2$ are taken to be $\Delta m_{32}^2 = \Delta m_{atm}^2 \sim 10^{-3}$ eV^2 and $\Delta m_{21}^2 = \Delta m_\odot^2 \lesssim 10^{-5}$ eV^2 according to the currently favoured solutions of the solar neutrino problem. Let us first consider $\Delta m_{21}^2 < 10^{-7}$ eV^2, as predicted by the LOW and VO solutions. This range of Δm_{21}^2 is the most relevant to the conversion of ultra-energetic neutrinos (see chapter. 3).

According to the results of this section, we identify the following scenario:

Suppose that before the neutrino decoupling epoch, at $T > 2$ MeV, a large asymmetry has been produced in one flavour while the other asymmetries are initially small: e.g. $\eta_\mu = 2\eta$ and $\eta_e \simeq \eta_\tau \simeq 0$, with $\eta \sim 1$. As the universe evolves down to $T \sim 2$ MeV, the muon and tau asymmetries will be equilibrated by the combined effect of oscillations and collisions. In the same epochs ν_e oscillations are still suppressed by collisions. Therefore, the electron neutrino asymmetry, η_e, remains unchanged and, at $T \simeq T_{BBN}$, we have $\eta_\mu \simeq \eta_\tau = \eta$ and $\eta_e \simeq 0$. After this epoch neutrinos decouple from the thermal bath; collisions become ineffective and the system evolves according to vacuum oscillations. During the evolution decoherence occurs due to the spread of the wavepackets. Therefore at the present epoch the background neutrinos are in mass eigenstates. With the mixing (A.12) we find the present asymmetries η_i^0 for these states:

$$\eta_1^0 \simeq \eta \sin^2\theta , \qquad \eta_2^0 \simeq \eta\cos^2\theta , \qquad \eta_3^0 \simeq \eta . \tag{A.13}$$

The corresponding flavour asymmetries equal:

$$\begin{aligned} \eta_e^0 &\simeq \eta\frac{1}{2}\sin^2 2\theta , \\ \eta_\mu^0 &\simeq \eta\left(1 - \frac{1}{2}\sin^2 2\theta\cos^2\Theta\right) , \\ \eta_\tau^0 &\simeq \eta\left(1 - \frac{1}{2}\sin^2 2\theta\sin^2\Theta\right) . \end{aligned} \tag{A.14}$$

One can see that a large asymmetry is produced in the electron flavour provided that the mixing of the electron neutrino is large: $\sin^2 2\theta \sim 1$. Thus, the electron

neutrino asymmetry at the present epoch can be much larger than the upper bound given by the Big Bang Nucleosynthesis (see chapter 3, eq. 3.2). Notice also that $\eta_\mu^0 \simeq \eta_\tau^0$ for $\Theta \simeq \pi/4$.

If equally large asymmetries are initially produced in the muon and tau flavours, $\eta_\mu = \eta_\tau = \eta \sim 1$ and $\eta_e \simeq 0$, the equality $\eta_\mu = \eta_\tau$ is preserved until the decoupling epoch, $T \sim 2$ MeV, due to the combined effect of oscillations and collisions. The evolution of η_e is blocked by collisions for $T \gtrsim 2$ MeV. After the neutrino decoupling vacuum oscillations take place; with the mixing matrix (A.12) we get the same results as in eqs. (A.13)-(A.14).

For $\Delta m_{21}^2 \simeq 10^{-6}$ eV^2 and small mixing, $\sin^2 2\theta \simeq 10^{-4} - 10^{-3}$, according to the SMA solution of the solar neutrino problem, the equilibration length l_{eq} is very large. Therefore the electron asymmetry η_e is not equilibrated with the muon and tau asymmetries. Again, the present asymmetries are determined by vacuum oscillations which occur after the neutrino decoupling and lead to the result (A.14).

Conversely, for large mixing angle, $\sin^2 2\theta \sim 1$ and $\Delta m_{21}^2 \simeq 10^{-7} - 10^{-5}$ eV^2, as given by part of the LOW solution and by the LMA solution regions, equilibration is rapidly realized and one gets:

$$\eta_e^0 \simeq \eta_\mu^0 \simeq \eta_\tau^0 \simeq \frac{2}{3}\eta \ . \tag{A.15}$$

Notice, however, that the results (A.13)-(A.15) depend on the epoch we considered for the production of the large CP-asymmetry η: the equilibration effect of collisions does not take place if the neutrino asymmetries are generated at epochs close to the neutrino decoupling epoch, at $T \sim 1$ MeV.

A.0.2 Evolution in presence of a sterile state

If a sterile state, ν_s, is mixed with the three active ones, a general description of the evolution of the neutrino gas is complicated and would deserve a detailed study.

We consider here the specific case in which the sterile neutrino is mixed mainly with one active state only, e.g. ν_e, and the admixture of ν_s with ν_μ and ν_τ is negligible. In other words, we consider the mass states $\nu_0 \simeq \cos\theta\nu_e + \sin\theta\nu_s$ and the orthogonal combination $\nu_1 \simeq -\sin\theta\nu_e + \cos\theta\nu_s$. Similarly, we take $\nu_2 \simeq \cos\varphi\nu_\mu + \sin\varphi\nu_\tau$ and $\nu_3 \simeq -\sin\varphi\nu_\mu + \cos\varphi\nu_\tau$. This would correspond to $\nu_e - \nu_s$ solution of the solar neutrino problem and $\nu_\mu - \nu_\tau$ solution of the atmospheric neutrino anomaly.

Let us consider the evolution of the $\nu_e - \nu_s$ system. The effective mixing angle in matter, θ_m, can be written as:

$$\tan 2\theta_m = \frac{\sin 2\theta}{\cos 2\theta - 2EV/\Delta m^2} \ , \tag{A.16}$$

where V is effective neutrino-neutrino potential, $V = F\eta_\nu\sqrt{2}G_F n_\gamma$ (eq. (3.7) of chapter 3), and E is the average thermal energy of the neutrinos: $E \simeq \alpha\beta T$. Numerically, from eqs. (3.7) and (A.16) we get:

$$\tan 2\theta_m = \frac{\sin 2\theta}{\cos 2\theta - 0.8 \cdot 10^4 \alpha\beta F\eta_\nu \, (T/1 \text{ MeV})^4 \, (10^{-3} \text{ eV}^2/\Delta m^2)} \ , \qquad \text{(A.17)}$$

where we used the expression $n_\gamma(T) = 2\zeta(3)T^3/\pi^2$ for the concentration of photons at the temperature T, with the value $\zeta(3) \simeq 1.202$ for the Riemann zeta function.

From eq. (A.17) it follows that, for $\eta_\nu \gtrsim 1$, $T \gtrsim T_{BBN}$ and $\Delta m^2 \lesssim 1$ eV^2 the mixing is strongly suppressed, $\tan 2\theta_m \ll 1$, corresponding to $\theta \simeq \pi/2$ ($\theta \simeq 0$) if $F\eta_\nu > 0$ ($F\eta_\nu < 0$). Thus, no level crossing is realized before the BBN epoch. At $T \gtrsim 2$ MeV collisions are effective (see fig. A.1); however they do not modify η_e significantly due to the very small value of the mixing and consequently of the conversion probability P_c (see section A.0.1, eq. (A.2)). Thus, we conclude that no significant flavour conversion occurs and the original value of η_e is preserved at least until the BBN epoch, even in the case of large vacuum mixing angles.

As the temperature decreases, $T < T_{BBN}$, the mixing angle θ_m approaches rapidly its vacuum value. Taking $\eta_\nu \simeq 1$, $F = 2$ and $\Delta m^2 \simeq 10^{-3}$ eV^2 we get $\tan 2\theta_m - \tan 2\theta \lesssim 10^{-2}$ for $T \lesssim 10$ KeV.

Considering that the propagation of the neutrino states is adiabatic [54] (see also chapter 3, section 3.3.2), we find the present concentrations of ν_e and ν_s in terms of the initial density n_e[4]:

$$n_s^0 = n_e \cos^2\theta \ , \qquad n_e^0 = n_e \sin^2\theta \ , \qquad \text{if } F\eta_\nu > 0 \qquad \text{(A.18)}$$

$$n_s^0 = n_e \sin^2\theta \ , \qquad n_e^0 = n_e \cos^2\theta \ , \qquad \text{if } F\eta_\nu < 0. \qquad \text{(A.19)}$$

If $n_e \gg n_{\bar{e}}$, the concentrations of $\bar{\nu}_e$ can be neglected and relations analogous to (A.18)-(A.19) hold for the CP-asymmetries η_e^0 and η_e.

The present ν_μ and ν_τ asymmetries can be found according to the discussion in section A.0.1. The effect of collisions leads to equilibration of η_μ and η_τ at $T \simeq T_{BBN}$: $\eta_\mu \simeq \eta_\tau = \eta$. At later epochs vacuum oscillations develop, leaving this equality unchanged. Thus, we can summarize the present CP-symmetries for the four flavours as follows:

$$\eta_s^0 = \eta_e \cos^2\theta \ , \qquad \eta_e^0 = \eta_e \sin^2\theta \ , \qquad \text{if } F\eta_\nu > 0 \ , \qquad \text{(A.20)}$$

$$\eta_s^0 = \eta_e \sin^2\theta \ , \qquad \eta_e^0 = \eta_e \cos^2\theta \ , \qquad \text{if } F\eta_\nu < 0 \ , \qquad \text{(A.21)}$$

$$\eta_\mu^0 \simeq \eta_\tau^0 \simeq \eta \ . \qquad \text{(A.22)}$$

Having neglected any mixing between ν_e and the other (active) flavours, we find that the present value of the electron neutrino asymmetry is smaller than the one at the BBN epoch, $\eta_e^0 \leq \eta_e$, thus remaining within the bound given in chapter 3 (eq. 3.2).

[4]We assume that only active states are initially produced before the BBN epoch, thus $n_s = 0$.

Appendix B

The regeneration factor: step-like and realistic Earth profile

The analytical expressions for the regeneration factors (4.23) and (4.13) can be obtained in the two layers approximation of the Earth density profile. In this approximation the mantle and the core of the Earth are considered as layers with constant densities. Therefore the neutrinos experience a constant matter potential along trajectories in the mantle and a step-like profile mantle-core-mantle along core crossing trajectories. In what follows we summarize the analytical results obtained in the two-layers approximation, which correctly describe the general features of the Earth matter effects. The comparison with exact numerical calculations will be given at the end of this appendix.

For ν_e propagating in the mantle only the regeneration factor, f_{reg}, eq. (4.23), has the form:

$$f_{reg} = D(E, \theta, \theta_n, \rho_m) \sin^2 \left(\pi \frac{d}{l_m} \right) , \tag{B.1}$$

where $d = 2R_\oplus \cos\theta_n$ is the length of the trajectory in the Earth, $R_\oplus \simeq 6400$ Km is the radius of the Earth and ρ_m the matter density in the mantle. The depth D of oscillations equals [22]:

$$D = \sin 2\theta_m \sin(2\theta_m - 2\theta) , \tag{B.2}$$

with θ_m and l_m being the mixing angle and the oscillation length in matter and θ the mixing angle in vacuum.

Since the mixing is enhanced in matter, $\theta_m > \theta$, the depth D is positive as well as the whole regeneration factor (B.1). From eq. (B.2) one gets:

$$D = x \frac{\sin^2 2\theta}{(x - \cos 2\theta)^2 + \sin^2 2\theta} , \tag{B.3}$$

where

$$x = \frac{2EV}{\Delta m^2}$$

and V is the matter potential. The expression (B.3) vanishes in the limits of low ($x \ll 1$) and high ($x \gg 1$) energies. It reaches the maximum

$$D_{max} = \cos^2\theta \ , \tag{B.4}$$

at $x = 1$, which corresponds to the energy:

$$E_R = \frac{\Delta m^2}{2\sqrt{2}G_F n_e} \ . \tag{B.5}$$

Here G_F is the Fermi constant and n_e the electron number density in the medium.

Thus, the depth of oscillations, D, has a resonant character with $E = E_R$ being the resonance condition. The width of the resonance is given by the interval $E_- \div E_+$ in which $D \geq D_{max}/2$. One finds:

$$\frac{E_\pm}{E_R} = 2 - \cos 2\theta \pm \sqrt{(1 - \cos 2\theta)(3 - \cos 2\theta)} \ , \tag{B.6}$$

which shows that the peak at $E \sim E_R$ is wide for LMA oscillation parameters and gets narrower as θ decreases. Notice that in the limit $\theta \to 0$ the maximal depth increases, $D_{max} \to 1$, but the oscillations disappear due to the decrease of the oscillation phase and the vanishing of the resonance width (see eq. (B.6)).

For antineutrinos, and trajectory in the mantle only, the regeneration factor $\bar{f}_{reg}$, eq. (4.13), has the same form as in eq. (B.1), with the oscillation depth

$$\begin{aligned} \bar{D} &= -\sin 2\theta_m \sin(2\theta_m - 2\theta) \ , \\ &= x\frac{\sin^2 2\theta}{(x + \cos 2\theta)^2 + \sin^2 2\theta} \ , \end{aligned} \tag{B.7}$$

where we defined

$$x \equiv \frac{2E|V|}{\Delta m^2} \ .$$

Similarly to the case of ν_e the depth $\bar{D}$, and therefore the regeneration factor $\bar{f}_{reg}$, is positive, since $\theta_m < \theta$; moreover it has a similar resonant behaviour with maximum

$$\bar{D}_{max} = \sin^2\theta \ , \tag{B.8}$$

and the same resonance energy, eq. (B.5). The borders E_-, E_+ of the resonance interval are given by eq. (B.6) with the replacement $\cos 2\theta \to -\cos 2\theta$. In the limit

$\theta \to 0$ the Earth effect disappears due to the vanishing of the oscillation depth (B.8). For maximal mixing, $\cos 2\theta = 0$, we get

$$D = \bar{D} = \frac{x}{x^2 + 1} \, .$$

If the neutrino trajectory crosses both the mantle and the core the analytical treatment of the regeneration factors, $\bar{f}_{reg}$ and f_{reg}, is more complicated [65]. The interplay of oscillations in the mantle and in the core determine irregular oscillations of the factors with energy. The depth of oscillations is larger in the region of the energy spectrum close to the resonance energies in the mantle and in the core; for SMA oscillation parameters parametric effects appear (see fig. 4.14). In contrast to the propagation in the mantle only (i.e. in uniform medium), the regeneration factors have negative sign in some intervals of energy.

Once a realistic density profile of the Earth is considered, the calculation of the regeneration factors requires a numerical treatment. The results are presented in fig. B.1 together with the analytical curves obtained with the two-layers approximation. The figure shows the factors $\bar{f}_{reg}$ and f_{reg} as functions of the neutrino (antineutrino) energy for $\Delta m^2 = 5 \cdot 10^{-5}$ eV^2, $\sin^2 2\theta = 0.75$ and $\theta_n = 0°$. We used the realistic profile in ref. [112] and chose a step-like (two-layers) profile with densities $\rho_m = 4.51$ and $\rho_c = 11.95$, corresponding to the average densities of the profile of ref. [112] in the mantle and in the core along the diameter of the Earth.

From the figure B.1 it follows that the position of the oscillation maxima and minima on the energy axis are well reproduced by the step profile. This good approximation of the oscillation phase is ascribed to the choice of ρ_m and ρ_c to be the average densities of the two layers along the trajectory of the neutrinos.

In contrast, the depth of oscillations given by the numerical calculation deviates significantly, up to $\sim 50\%$, from the result of the analytical (two-layers) approximation. As a general tendency, the depth of oscillations in the realistic density profile appears smaller with respect to the case of the two-layers profile. If the density jumps along the trajectory are not very large (e.g. for trajectories in the mantle only) this feature can be interpreted, qualitatively, by considering the density as smoothly varying along the path of the neutrinos. In this case the neutrino conversion occurs adiabatically and the depth of oscillations is determined by the matter density at the surface of the Earth. Since the surface density is smaller than the average density along the trajectory and the latter in turn is smaller than the resonance density ρ_R in the relevant range of energies, a smaller depth of oscillations is expected.

A better approximation of the numerical results can be obtained by using the average density in the determination of the oscillation phase and the surface density

in the determination of the depth of oscillations.

For SMA parameters the adiabaticity is broken and the two layers model gives a good approximation of the numerical results.

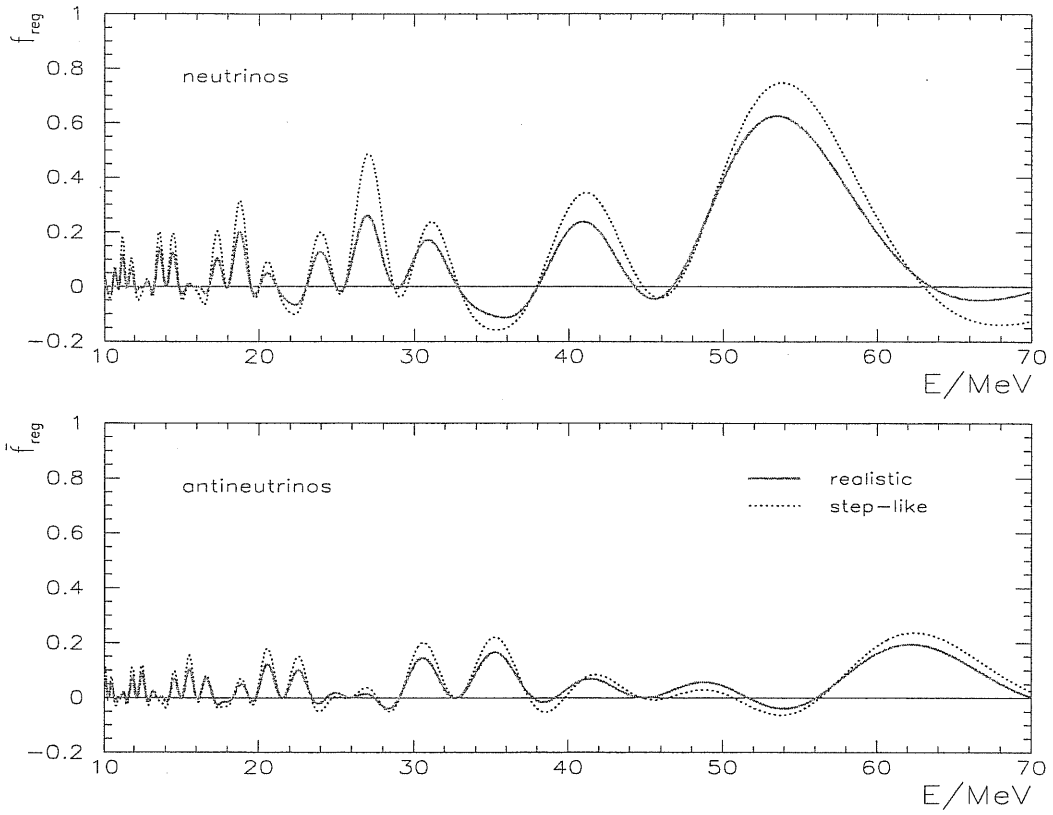

Figure B.1: The regeneration factors for neutrinos, f_{reg}, and antineutrinos, $\bar{f}_{reg}$, calculated with step-like (two layers) and realistic profiles. We have taken $\Delta m^2 = 5 \cdot 10^{-5}$ eV^2, $\sin^2 2\theta = 0.75$, $\theta_n = 0°$ and the densities $\rho_m = 4.51$ and $\rho_c = 11.95$ for the two-layers profile.

Appendix C

Parameters of detectors

We summarize here some relevant characteristics of the detectors that have been considered in the analyses of chapters 5 and 6. These detectors are Kamiokande-2 (K2) and IMB for the observation of SN1987A neutrino signal (chapter 5) and SuperKamiokande (SK), SNO and LVD for future supernova observations (chapter 6).

For each of these experiments we consider:

1. The position of the detector on the Earth, which is relevant for determining the trajectory of the observed neutrinos inside the Earth (see sect. 6.1). The locations of the three experiments are given in Table C.1 in terms of northern latitude, δ, and eastern longitude α.

2. The material which the detector is made of and its fiducial mass. These quantities are quoted in Table C.1.

3. The detection efficiency $\mathcal{E}(E'_e)$ (see eq. (5.8)); the efficiencies of the detectors under considerations are shown in fig. C.1 as functions of the charged lepton energy E'_e.

The efficiency of the K2 detector [154] rises sharply with energy, reaching $\sim 95\%$ for $E'_e \gtrsim 15 - 20$ MeV. Conversely the IMB efficiency [13] increases slowly, being $\sim 60\%$ at $E'_e \simeq 40$ MeV and $\sim 95\%$ at $E'_e \simeq 70$ MeV.

The SNO efficiency is high, so that the shape of the energy spectrum and the total number of events are determined by the detection cross section [153]. Therefore, we have taken $\mathcal{E} = 1$ in eq. (5.8).

The efficiency of the LVD detector has been provided by the dedicated collaboration [155]. For $E_{th} \leq 10$ MeV, it is given by the gaussian integral function:

$$\mathcal{E}(E_e, E_{th}) = \frac{1}{\sqrt{2\pi}} \int_{-\infty}^{x} e^{-\frac{y^2}{2}} dy \ , \tag{C.1}$$

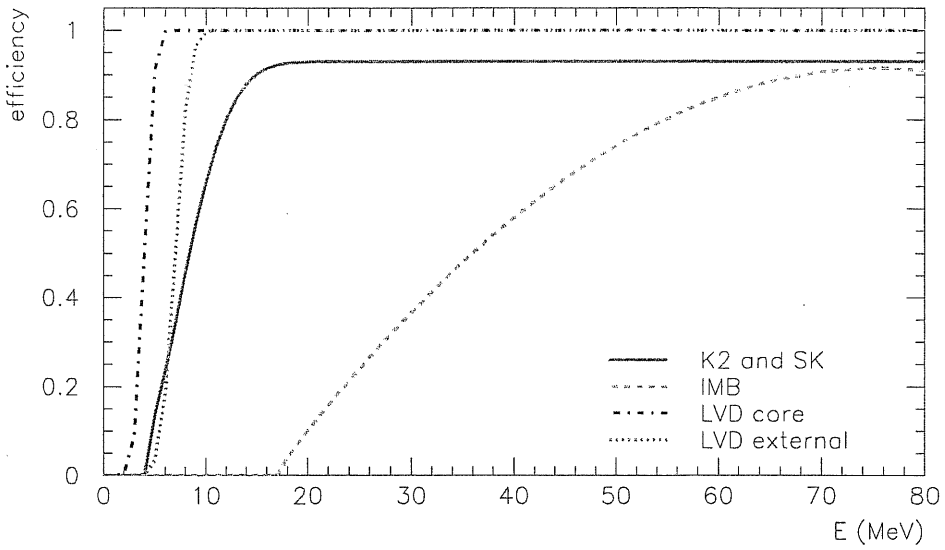

Figure C.1: The detection efficiencies $\mathcal{E}(E'_e)$ of K2, IMB, and LVD as functions of the energy E'_e of the lepton. For SK we assumed the same efficiency as the K2 detector; both the efficiencies of the core and of the external counters of LVD are shown. The SNO efficiency is not represented since it can be assumed to be close to 1 in all the relevant energy interval [153].

where $x \equiv (E_e - E_{th})/\sigma_{th}$ and E_e is the measured energy of the lepton. The values of the parameters E_{th} and σ_{th} are: $E_{th} = 4$ MeV and $\sigma_{th} = 0.74$ MeV for the core counters (mass $M = 0.57$ ktons); $E_{th} = 7$ MeV and $\sigma_{th} = 1.1$ MeV for the external counters (mass $M = 0.43$ ktons).

For SK we adopted the efficiency published for the Kamiokande-2 experiment [154].

4. The energy resolution Δ, which appears in the resolution function (5.9). We followed ref. [23] for K2 and IMB experiments, ref. [156] for SK and SNO and refs. [157, 155] for LVD. The parameter Δ depends on energy as follows:

$$\frac{\Delta}{\text{MeV}} = A\frac{E_e}{\text{MeV}} + B\sqrt{\frac{E_e}{\text{MeV}}}\,. \tag{C.2}$$

The values of the coefficients A and B are given in Table C.1.

detector	δ	α	material	mass (ktons)	A	B
IMB	$41°42'$	$-81°18'$	H_2O	6.80	0	1.16
K2	$36°21'$	$137°18'$	H_2O	2.14	0	0.87
SK	$36°21'$	$137°18'$	H_2O	32	0	0.5
SNO	$46°30'$	$-81°01'$	H_2O	1.4	0	0.35
			D_2O	1.0		
LVD	$42°25'$	$13°31'$	$(CH_2)_{10}$	1.0	0.07	0.23

Table C.1: Summary of the characteristics of the detectors we consider, in particular their locations on the Earth (in terms of northern latitude δ and eastern longitude α), the fiducial masses and the coefficients A and B which appear in the expression of the energy resolution, eq. (C.2).

Bibliography

[1] B. Pontecorvo, Sov. Phys. JETP **6**, 429 (1957) [Zh. Eksp. Teor. Fiz. **33**, 549 (1957)].

[2] G. Danby, J. M. Gaillard, K. Goulianos, L. M. Lederman, N. Mistry, M. Schwartz and J. Steinberger, Phys. Rev. Lett. **9** (1962) 36.

[3] Z. Maki, M. Nakagawa and S. Sakata, Prog. Theor. Phys. **28**, 870 (1962).

[4] B. Pontecorvo, Sov. Phys. JETP 26 (1968) 984, see also V.N. Gribov and B. Pontecorvo, Phys. Lett. B28 (1969) 493.

[5] An historical account is given in the reviews: S.M. Bilenkii and B. Pontecorvo, Phys. Rept. 41 (1978) 225, B.M. Pontecorvo, Sov. Phys. Usp. 26 (1983) 1087, J. N. Bahcall *et al.*, *"Solar Neutrinos: the first thirty years"*, Reading, USA: Addison-Wesley (1995) 440 p.

[6] R. Davis, D. Harmer and K. Hoffman, Phys. Rev. Lett. **20** (1968) 1205; recent results are reported in K. Lande et al., Astrophys. J. 496 (1998) 505.

[7] L. Wolfenstein, Phys. Rev. **D17** (1978) 2369.

[8] S.P. Mikheev and A.Y. Smirnov, Nuovo Cim. **9C** (1986) 17. Yad. Fyz. **42** (1985) 1441 [Sov.J. Nucl. Phys. **42** (1986) 913].

[9] S. P. Mikheev and A. Y. Smirnov, Sov. Phys. JETP **64** (1986) 4.

[10] Y. Fukuda *et al.* [Super-Kamiokande Collaboration], Phys. Rev. Lett. **81**, 1562 (1998) [hep-ex/9807003].

[11] Q.R. Ahmad et al. [SNO Collaboration], nucl-ex/0106015.

[12] K. Hirata *et al.* [KAMIOKANDE-II Collaboration], Phys. Rev. Lett. **58** (1987) 1490.

[13] R. M. Bionta *et al.*, Phys. Rev. Lett. **58** (1987) 1494.

[14] L. Wolfenstein, Phys. Lett. **B194** (1987) 197.

[15] S.P. Rosen, Phys. Rev. D37 (1988) 1682.

[16] T.K. Kuo and J. Pantaleone, Phys. Rev. D37 (1988) 298.

[17] H. Minakata and H. Nunokawa, Phys. Rev. D38 (1988) 3605.

[18] J. Arafune et al., Phys. Rev. Lett. 59 (1987) 1864.

[19] H. Minakata et al., Mod. Phys. Lett. A2 (1987) 827.

[20] P.O. Lagage et al., Phys. Lett. B193 (1987) 127.

[21] D. Notzold, Phys. Lett. B196 (1987) 315.

[22] A. Y. Smirnov, D. N. Spergel and J. N. Bahcall, Phys. Rev. **D49** (1994) 1389 [hep-ph/9305204].

[23] B. Jegerlehner, F. Neubig and G. Raffelt, Phys. Rev. **D54** (1996) 1194 [astro-ph/9601111].

[24] A. Y. Smirnov, talk given at the *Twentieth International Cosmic Ray Conference*, Moscow, 1987.

[25] C. Lunardini and A.Y. Smirnov, Phys. Rev. D63 (2001) 073009, hep-ph/0009356.

[26] H. Minakata and H. Nunokawa, Phys. Lett. B504 (2001) 301, hep-ph/0010240.

[27] M. Kachelriess, R. Tomas and J.W.F. Valle, JHEP 01 (2001) 030, hep-ph/0012134.

[28] M. Kachelriess et al., hep-ph/0108100.

[29] A. Burrows, D. Klein and R. Gandhi, Phys. Rev. D45 (1992) 3361.

[30] See the review T. Piran, Phys. Rept. 314 (1999) 575, astro-ph/9810256.

[31] The subject is reviewed in P. Bhattacharjee and G. Sigl, Phys. Rept. 327 (2000) 109, astro-ph/9811011; X. Bertou, M. Boratav and A. Letessier-Selvon, Int. J. Mod. Phys. A15 (2000) 2181, astro-ph/0001516.

[32] F.W. Stecker et al., Phys. Rev. Lett. 66 (1991) 2697,

[33] L. Nellen, K. Mannheim and P.L. Biermann, Phys. Rev. **D47** (1993) 5270 [hep-ph/9211257].

[34] A.P. Szabo and R.J. Protheroe, Astropart. Phys. **2** (1994) 375 [astro-ph/9405020].

[35] K. Mannheim, Astropart. Phys. 3 (1995) 295,

[36] R.J. Protheroe, (1996), astro-ph/9607165,

[37] C.T. Hill, Nucl. Phys. B224 (1983) 469,

[38] F.A. Aharonian, P. Bahttacharjee and D.N. Schramm, Phys. Rev. D46 (1992) 4188.

[39] P. Bhattacharjee, C.T. Hill and D.N. Schramm, Phys. Rev. Lett. 69 (1992) 567.

[40] A.J. Gill and T.W.B. Kibble, Phys. Rev. D50 (1994) 3660, hep-ph/9403395.

[41] E. Waxman and J.N. Bahcall, Phys. Rev. Lett. 78 (1997) 2292, astro-ph/9701231.

[42] J.P. Rachen and P. Meszaros, Phys. Rev. D58 (1998) 123005, astro-ph/9802280.

[43] E. Waxman and J.N. Bahcall, Phys. Rev. D59 (1999) 023002, hep-ph/9807282.

[44] W. Fulgione [LVD Collaboration] Nucl. Phys. Proc. Suppl. 70 (1999) 469.

[45] G.C. Hill [AMANDA Collaboration], (2001), astro-ph/0106064.

[46] L.F. Thompson [ANTARES Collaboration], Nucl. Phys. Proc. Suppl. 91 (2001) 431.

[47] P.K.F. Grieder [NESTOR Collaboration], Nucl. Phys. Proc. Suppl. 97 (2001) 105.

[48] D. Zavrtanik [AUGER Collaboration], Nucl. Phys. Proc. Suppl. 85 (2000) 324.

[49] See e.g. T. Miller *et al.*, in proceedings of Baltimore 1999, "Neutrinos in the new millennium",Edited by G. Domokos, S. Kovesi-Domokos. Singapore, World Scientific, 2000. 390p.

[50] C.K. Jung, hep-ex/0005046.

[51] The recent National Underground Science Laboratory (NUSL) proposal is available at http://www.sns.ias.edu/jnb/.

[52] Astropart. Phys. 3 (1995) 267, [hep-ph/9405296]; F. Halzen and D. Saltzberg, Phys. Rev. Lett. 81 (1998) 4305, [hep-ph/9804354]; H. Athar, Astropart. Phys. 14 (2000) 217, [hep-ph/0004191]; S.I. Dutta, M.H. Reno and I. Sarcevic, Phys. Rev. D62 (2000) 123001, [hep-ph/0005310]; J. Alvarez-Muniz, F. Halzen and D.W. Hooper, Phys. Rev. D62 (2000) 093015, [astro-ph/0006027]; H. Athar, G. Parente and E. Zas, Phys. Rev. D62 (2000) 093010, [hep-ph/0006123].

[53] L. Bento, P. Keranen and J. Maalampi, Phys. Lett. B476 (2000) 205, [hep-ph/9912240]; H. Athar, M. Jezabek and O. Yasuda, (2000), [hep-ph/0005104].

[54] C. Lunardini and A.Y. Smirnov, (2000), hep-ph/0012056.

[55] C. Lunardini and A.Y. Smirnov, Phys. Rev. D63 (2001) 073009, hep-ph/0009356.

[56] C. Lunardini and A.Y. Smirnov, (2001), hep-ph/0106149.

[57] S.P. Mikheev and A.Y. Smirnov, "Resonant Neutrino Oscillations in Matter" Prog. Part. Nucl. Phys. **23** (1989) 41.

[58] T.K. Kuo and J. Pantaleone, Rev. Mod. Phys. 61 (1989) 937.

[59] S.M. Bilenkii and S.T. Petcov, Rev. Mod. Phys. 59 (1987) 671.

[60] E.K. Akhmedov, hep-ph/0001264.

[61] See H. Nunokawa et al., Nucl. Phys. B501 (1997) 17, hep-ph/9701420, and references therein.

[62] D. Notzold and G. Raffelt, Nucl. Phys. B307 (1988) 924.

[63] S.J. Parke, Phys. Rev. Lett. 57 (1986) 1275.

[64] W.C. Haxton, Phys. Rev. Lett. 57 (1986) 1271.

[65] See e.g. E.K. Akhmedov, Pramana 54 (2000) 47, hep-ph/9907435, and references therein.

[66] A.Y. Smirnov and S.P. Mikheev, Proceedings of the 6th Moriond Workshop *Massive Neutrinos in Astrophysics and in Particle Physics*, 1986, edited by O. Fackler and J. Tran Than Van (Editions Frontières, Gif-sur-Yvette, France, 1986), p. 355.

[67] J. Bouchez et al., Z. Phys. C32 (1986) 499.

[68] V.K. Ermilova, V.A. Tsarev and V.A. Chechin, JETP Lett. 43 (1986) 453.

[69] A.Y. Smirnov, hep-ph/9811296.

[70] C. Giunti, C.W. Kim and M. Monteno, Nucl. Phys. B521 (1998) 3, hep-ph/9709439.

[71] See e.g. the recent analysis J.N. Bahcall, M.C. Gonzalez-Garcia and C. Pena-Garay, JHEP 08 (2001) 014, hep-ph/0106258.

[72] P.I. Krastev and A.Y. Smirnov, (2001), hep-ph/0108177.

[73] C. S. Lim, preprint BNL-39675, 1987.

[74] E. K. Akhmedov, Nucl. Phys. **B538** (1999) 25 [hep-ph/9805272].

[75] P. I. Krastev and A. Y. Smirnov, Phys. Lett. **B226** (1989) 341.

[76] E.K. Akhmedov, Yad. Fiz. **47** (1988) 475.

[77] J.N. Bahcall, *"Neutrino Astrophysics "* Cambridge University Press, 1989.

[78] V.L. Ginzburg, V.A. Dogiel, V.S. Berezinsky, S.V. Bulanov and V.S. Ptuskin, *"Astrophysics Of Cosmic Rays,"* Amsterdam, Netherlands: North-Holland (1990) 534 p.

[79] R.F. Mushotzky, Astrophys. J. **256** (1982) 92.

[80] T.J. Turner and K.A. Pounds, Mon. Not. Roy. Astron. Soc. **240** (1989) 833.

[81] R.M. Sambruna, M. Eracleous and R.F. Mushotzky, [astro-ph/9905365].

[82] H. Minakata and A.Y. Smirnov, Phys. Rev. **D54** (1996) 3698 [hep-ph/9601311].

[83] P. Meszaros and M. Rees, Mon. Not. Roy. Astron. Soc. **269** (1994) 41P.

[84] H. Kang and G. Steigman, Nucl. Phys. B372 (1992) 494; G.B. Larsen and J. Madsen, Phys. Rev. D52 (1995) 4282.

[85] J.A. Adams and S. Sarkar, preprint OUTP-98-70P, and talk presented at the workshop *The Physics of Relic Neutrinos*, Trieste, September 1998; W.H. Kinney and A. Riotto, Phys. Rev. Lett. 83 (1999) 3366, [hep-ph/9903459]; J. Lesgourgues and S. Pastor, Phys. Rev. D60 (1999) 103521 [hep-ph/9904411].

[86] P. de Bernardis et al., Nature 404 (2000) 955, [astro-ph/0004404]; A.E. Lange et al., (2000), astro-ph/0005004; S. Hanany et al., (2000), astro-ph/0005123; A. Balbi et al., (2000), astro-ph/0005124; A. T. Lee *et al.*, astro-ph/0104459; C. B. Netterfield *et al.*, astro-ph/0104460.

[87] J. Lesgourgues and M. Peloso, Phys. Rev. D62 (2000) 081301, (2000), [astro-ph/0004412].

[88] S. Hannestad, Phys. Rev. Lett. 85 (2000) 4203, astro-ph/0005018.

[89] M. Orito, T. Kajino, G. J. Mathews and R. N. Boyd, astro-ph/0005446.

[90] S. H. Hansen, G. Mangano, A. Melchiorri, G. Miele and O. Pisanti, astro-ph/0105385.

[91] M.J.S. Levine, Nuovo Cim. 48A (1967) 67.

[92] D.A. Dicus and W.W. Repko, Phys. Rev. Lett. 79 (1997) 569, hep-ph/9703210.

[93] G.G. Raffelt, "Stars as Laboratories for Fundamental Physics" The University of Chicago Press, 1996.

[94] J. Pantaleone, Phys. Lett. B287 (1992) 128.

[95] M.C. Gonzalez-Garcia et al., Phys. Rev. D63 (2001) 013007, hep-ph/0007227.

[96] M. Krumholz, S.E. Thorsett and F.A. Harrison, Ap. J. 506 (1998) L81, [astro-ph/9807117]; D.W. Hogg and A.S. Fruchter, Ap. J. 520 (1999) 54; IASSNS-AST-98-32. M. Schmidt, Ap. J. 523 (1999) L117, [astro-ph/9908206]; H.J.M. S. Mao, Astron. and Astrophys. 339 (1998) L1, [astro-ph/9908342]; see also E. E. Fenimore and E. Ramirez-Ruiz, (2000), astro-ph/9906125.

[97] T. Miyaji, G. Hasinger and M. Schmidt, MPE-478 [astro-ph/9910410].

[98] F. W. Stecker and M. H. Salamon, Space Sci. Rev. **75**, 341 (1996) [astro-ph/9501064].

[99] See the review P. Bhattacharjee, astro-ph/9803029.

[100] P. Bhattacharjee and N.C. Rana, Phys. Lett. B246 (1990) 365; P. Bhattacharjee and G. Sigl, Phys. Rev. D51 (1995) 4079, [astro-ph/9412053].

[101] U.F. Wichoski, J.H. MacGibbon and R.H. Brandenberger. (1998), hep-ph/9805419,

[102] E. Roulet, Phys. Rev. D47 (1993) 5247.

[103] See e.g. J.N. Bahcall, P.I. Krastev and A.Y. Smirnov, JHEP 05 (2001) 015, hep-ph/0103179.

[104] A. Burrows, T. Young, P. Pinto, R. Eastman and T. Thompson, astro-ph/9905132.

[105] G. E. Brown, H. A. Bethe and G. Baym, , Nucl. Phys. A **375** (1982) 481.

[106] H. T. Janka and W. Hillebrandt, Astron. Astroph. Suppl. **78** (1989) 375; Astron. Astrophys. **224** (1989) 49.

[107] Super-Kamiokande, S. Fukuda et al., Phys. Rev. Lett. 85 (2000) 3999, hep-ex/0009001.

[108] CHOOZ collaboration, M. Apollonio *et al.*, Phys. Lett. **B466** (1999) 415 [hep-ex/9907037]; Phys. Lett. **B420** (1998) 397 [hep-ex/9711002].

[109] F. Boehm et al., Phys. Rev. D62 (2000) 072002, hep-ex/0003022.

[110] A. S. Dighe and A. Y. Smirnov, Phys. Rev. **D62** (2000) 033007 [hep-ph/9907423].

[111] A discussion of adiabaticity in the context of supernova is given in M. Kachelriess and R. Tomas, hep-ph/0104021; see also references therein.

[112] A. M. Dzewonski and D. L. Anderson, Phys. Earth. Planet. Inter. **25** (1981) 297.

[113] M.C. Gonzalez-Garcia, C. Pena-Garay and A.Y. Smirnov, Phys. Rev. D63 (2001) 113004, hep-ph/0012313.

[114] P. Vogel, Phys. Rev. D29 (1984) 1918.

[115] S.A. Fayans, Sov. J. Nucl. Phys. 42 (1985) 590.

[116] P. Vogel and J.F. Beacom, Phys. Rev. D60 (1999) 053003, hep-ph/9903554.

[117] S. Nakamura et al., Phys. Rev. C63 (2001) 034617, nucl-th/0009012.

[118] E.N. Alekseev et al., JETP Lett. 45 (1987) 589.

[119] E.N. Alekseev et al., Phys. Lett. B205 (1988) 209.

[120] M. Aglietta et al., Europhys. Lett. 3 (1987) 1315.

[121] V.L. Dadykin et al., JETP Lett. 45 (1987) 593.

[122] E. Amaldi et al., Europhys. Lett. 3 (1987) 1325.

[123] M. Aglietta et al., Nuovo Cim. C12 (1989) 75.

[124] M. Aglietta et al., Nuovo Cim. B106 (1991) 1257.

[125] M. Aglietta et al., Nuovo Cim. C14 (1991) 171.

[126] See e.g. C.A. Dickson and B.F. Schutz, Phys. Rev. D51 (1995) 2644, and references therein.

[127] J. Arafune and M. Fukugita, Phys. Rev. Lett. 59 (1987) 367.

[128] For analyses of K2 and IMB signals see e.g. L. M. Krauss, Nature **329** (1987) 689; A. Burrows, Astrophys. J. **334** (1988) 891; H. T. Janka and W. Hillebrandt, Astron. Astrophys. **224** (1989) 49; see also [93] for a discussion, and the recent detailed study by T.J. Loredo and D.Q. Lamb, (2001), astro-ph/0107260.

[129] See e.g. G. L. Fogli, E. Lisi, D. Montanino and A. Palazzo, hep-ph/0008012; M. C. Gonzalez-Garcia and C. Peña-Garay, hep-ph/0009041.

[130] For a review on supernova neutrino experiments see K. Scholberg, Nucl. Phys. Proc. Suppl. 91 (2000) 331 [hep-ex/0008044].

[131] See C.J. Virtue for the SNO collaboration, Nucl. Phys. Proc. Suppl. 100 (2001) 326 [astro-ph/0103324], and references therein.

[132] The Super-Kamiokande collaboration, Y. Fukuda et al., Phys. Rev. Lett. 81 (1998) 1158 [hep-ex/9805021].

[133] See J.F. Beacom and P. Vogel, Phys. Rev. D60 (1999) 033007 [astro-ph/9811350], and references therein.

[134] A study was presented by the CHOOZ collaboration, M. Apollonio et al., Phys. Rev. D61 (2000) 012001 [hep-ex/9906011].

[135] For review, see e.g. C. Spiering, Annalen Phys. 10 (2001) 131.

[136] F. Halzen, J.E. Jacobsen and E. Zas, Phys. Rev. D53 (1996) 7359, astro-ph/9512080.

[137] The AMANDA collaboration, J. Ahrens et al., (2001), astro-ph/0105460.

[138] A. Bouchta and C. De Los Heros for the AMANDA collaboration, private communication.

[139] A similar criterion was proposed in K. Takahashi et al., (2001), hep-ph/0105204.

[140] V. Barger, D. Marfatia and B.P. Wood, Phys. Lett. B498 (2001) 53, hep-ph/0011251.

[141] R. Barbieri and A. Strumia, JHEP 12 (2000) 016, hep-ph/0011307.

[142] H. Murayama and A. Pierce, (2000), hep-ph/0012075.

[143] For an experimental review see e.g. A. Piepke for the KamLAND collaboration, Nucl. Phys. Proc. Suppl. 91 (2001) 99.

[144] S.G. Wojcicki, Nucl. Phys. Proc. Suppl. 91 (2001) 216.

[145] A comprehensive review is given in C. Albright et al., (2000), hep-ex/0008064.

[146] S. Samuel, Phys. Rev. D48 (1993) 1462.

[147] G. Sigl and G. Raffelt, Nucl. Phys. **B406** (1993) 423.

[148] V.A. Kostelecky and S. Samuel, Phys. Rev. D52 (1995) 621, hep-ph/9506262.

[149] L. Stodolsky, Phys. Rev. **D36** (1987) 2273.

[150] G. Raffelt, G. Sigl and L. Stodolsky, Phys. Rev. Lett. **70** (1993) 2363 [hep-ph/9209276].

[151] The interplay of collisions and refraction is discussed also in A.Y. Smirnov, "New aspects of neutrino oscillations in matter", in *Les Arcs 1987, Proceedings, New and Exotic Phenomena"* , 275-289.

[152] X. Shi, D.N. Schramm and B.D. Fields, Phys. Rev. D48 (1993) 2563, astro-ph/9307027.

[153] H. Robertson for SNO collaboration, private communication.

[154] K.S. Hirata et al., Phys. Rev. D38 (1988) 448.

[155] P. Antonioli and W. Fulgione for LVD collaboration, private communication.

[156] J.N. Bahcall, P.I. Krastev and E. Lisi, Phys. Rev. C55 (1997) 494, nucl-ex/9610010.

[157] P. Antonioli et al., Nucl. Instrum. Meth. A309 (1991) 569.